STUDY OF THE OSCILLATION OF VAPOUR BUBBLE FORMED BY THE RADIATION INDUCED PHASE TRANSITION OF SUPERHEATED LIQUID

THESIS SUBMITTED TO THE

JADAVPUR UNIVERSITY

FOR THE DEGREE OF

DOCTOR OF PHILOSOPHY (SCIENCE)

By

SURAJ ALI

DEPARTMENT OF PHYSICS
JADAVPUR UNIVERSITY
JADAVPUR, KOLKATA - 700 032, INDIA

2025

Date: 11/04/2025

CERTIFICATE FROM THE SUPERVISOR(S)

This is to certify that the thesis entitled "**STUDY OF THE OSCILLATION OF VAPOUR BUBBLE FORMED BY THE RADIATION INDUCED PHASE TRANSITION OF SUPERHEATED LIQUID**" submitted by Suraj Ali who got his name registered on 18/11/2021 (Index No: 96/21/Phys./27) for the award of Ph.D. (Science) Degree of Jadavpur University, is absolutely based upon his own work under the supervision of Prof. Pabitra Kumar Paul, Department of Physics, Jadavpur University, Kolkata- 700032 and co-supervision of Prof. Mala Das, High Energy Nuclear & Particle Physics Division, Saha Institute of Nuclear Physics, Kolkata - 700064 and that neither this thesis nor any part of it has been submitted for any degree/ diploma or any other academic award anywhere before.

Pabitra Kumar Paul
11/04/2025

Prof. (Dr.) Pabitra Kumar Paul
Professor
Department of Physics
Jadavpur University
Kolkata - 700032

(Signature of the Supervisor date with official seal)

Mala Das 11/04/2025

(Signature of the Co-supervisor date with official seal)

डा. माला दास / DR. MALA DAS
प्रोफेसर / Professor
उच्च उर्जा परमाणु एवं कण भौतिकी प्रभाग
High Energy Nuclear & Particle Physics Division
साहा इंस्टिटयूट ऑफ न्यूक्लियर फिजिक्स
SAHA INSTITUTE OF NUCLEAR PHYSICS
1/ए एफ, विधाननगर, कोलकाता-700 064
1/AF, Bidhan Nagar, Kolkata-700 064

Dedicated to my Parents

Acknowledgement

I would like to praise Allah the supreme Almighty and most Merciful for his showers of blessings throughout my research journey, enabling me to complete my research.

It is a pleasure to thank and gratitude to my supervisor, Prof. Pabitra Kumar Paul, Department of Physics, Jadavpur University, Kolkata, India and my co-supervisor Prof. Mala Das, High Energy Nuclear & Particle Physics Division, Saha Institute of Nuclear Physics, Kolkata, India, for their persistent motivation, immense knowledge and timely support in completing my work. They guided me in a novice like way to explore countless possibilities and carry out research with a free mind and undying spirit. It was a great experience to complete the research under their guidance.

I am grateful to my research advisory committee members for their advice and encouragement: Head of the Department of Physics, Jadavpur University, Kolkata, India, and Prof. Sankar De, Saha Institute of Nuclear Physics, Kolkata, India. I would like to express special thanks to Prof. A. N. Sekar Iyengar, for his valuable discussions and inputs on the nonlinear analysis technique. My sincere thanks also go to Mr. Nilanjan Biswas, Scientific Assistant, Saha Institute of Nuclear Physics, Kolkata, India for his unending support during the experiment and his hands-on training in the fabrication of the Superheated Emulsion Detector. I am thankful to Dr. Sunita Sahoo, Mr. Vimal Kumar and Mr. Alapan Pal for their help in the experiments and analysis. I extend my sincere thanks to Prof. Maitreyee Nandy and the Health Physics Unit, Variable Energy Cyclotron Centre (VECC), Kolkata, India for providing the neutron

source for my research work. I would like to thank workshop members of the Saha Institute of Nuclear Physics, especially Dr. Jisnu Basu and Mr. Sudipta Barman, for their help in my many developmental works related to the detector.

I would like to thank the Department of Physics, Jadavpur University, and Saha Institute of Nuclear Physics for providing the research facilities. I extend my gratitude to all the faculty members, non-teaching staff and research scholars for their cooperation. Deeply thankful to my fellow research colleagues at Saha Institute of Nuclear Physics, Jadavpur University and colleagues of Muralidhar Girls' College for the insightful discussions. Heartfelt thanks to my family and relatives, especially my mother for her endless love, faith, constant encouragement and support. I would like to offer heartfelt gratitude to my father, even though he is no longer with me. Thanks to my wife Tania Yasmin for her constant motivation and support.

Date: (Suraj Ali)

Place: Jadavpur, Kolkata Research Scholar

. Department of Physics

. Jadavpur University

List of Publications

Research paper publications related to my Ph.D. thesis

1. Characterization of homogeneous nucleation of superheated liquid droplets by nonlinear analysis, **Suraj Ali**, Mala Das, A. N. Sekar Iyengar, Pabitra Kumar Paul, Nuclear Instruments and Methods in Physics Research A, 2023, **1057**, 168777.

2. Discrimination of neutron and gamma ray induced nucleation events at high frequency in R-134a superheated emulsion, **Suraj Ali**, Mala Das, Nuclear Instruments and Methods in Physics Research A, 2022, **1025**, 166186.

3. The Study of the Frequency of Bubble Oscillation in R-12 Superheated Emulsion for Neutron - Gamma Discrimination, **Suraj Ali**, Mala Das, Pabitra Kumar Paul, Book - Advanced Radiation Detectors and Instrumentation in Nuclear and Particle Physics, Springer Proceeding in Physics, 2023, **282**, 33 - 38.

Paper under communication to journal

1. Advances in identification of neutron and gamma-ray induced events in SED using Empirical Mode Decomposition, **Suraj Ali**, Mala Das, Pabitra Kumar Paul.

Research paper publications where I have substantial contribution

1. The background study at 555 m deep underground with superheated emulsion detector, Sunita Sahoo, **Suraj Ali**, Mala Das, Nilanjan Biswas, Piyush Pallav, Jisnu Basu, Nuclear Instruments and Methods in Physics Research A, 2021, **1008**, 165450.

Conference/ workshop attended and presented

1. "Advanced Workshop On The Applications Of Nuclear Security: Detection Equipment And Methodologies", organised by Amity University, Noida, India from 19th to 22nd June 2023. Role: Attended.

2. "Advances in Astroparticle Physics and Cosmology (AAPCOS-2023)", organised by Saha Institute of Nuclear Physics, Kolkata, India, from 23rd to 27th January 2023. Role: Oral presentation.

3. "Workshop on Practical Application of Nuclear Security", organised by Amity University, Noida, India from 15th to 17th June, 2022. Role: Attended.

4. "High-Performance Computing (HPC) for Computational Fluid Dynamics (CFD) Applications", organised by IIT Bombay, India, C-DAC under NSM, from 17th to 20th May 2022. Role: Attended.

5. "Advanced Radiation Detector and Instrumentation in Nuclear and Particle Physics (RAPID2021)", organised by the Department of Physics, University of Jammu, India, from 25th to 29th October 2021. Role: Oral presentation.

6. "Nonlinear And Complex Phenomena (NCP -2020)", organised by Centre for Plasma Studies, in collaboration with the Department of Mathematics, Jadavpur University, and Advance Centre for Nonlinear and Complex Phenomena (ACNCP), Kolkata, India from 18th to 19th February 2020. Role: Poster presentation.

7. "Advances in Astroparticle Physics and Cosmology (AAPCOS -2020)", organised by Saha Institute of Nuclear Physics, Kolkata from 6th to 10th January 2020. Role: Attended.

Synopsis

A liquid is said to be superheated when it is in a liquid state at temperature and pressure values corresponding to the vapour region. This represents a metastable state of the liquid and serves as the seed of nucleation site of the homogeneous phase transition. Superheated Emulsion Detector (SED) mainly contains a large number of droplets of the superheated liquid inside the gel matrix. The homogeneous nucleation can be started inside the SED by deposition of energy in the medium. When an energetic particle passes through the droplet, it deposits energy and causes a phase transition from the metastable liquid state to the stable vapour state. If the particle deposits the energy within the critical length and the energy is larger than the critical value, the vapour bubble grows and the whole liquid is converted into vapour state. An acoustical signal is produced in the phase transition of the superheated liquid droplets which is recorded by a piezoelectric sensor. Nowadays, SEDs are useful detectors in neutron dosimetry, neutron spectrometry, gamma-ray, heavy ion detection and dark matter detection. The mechanism of SED is similar to bubble chamber [1] but complete physics of nucleation is not yet known. The process of bubble growth is a complex phenomenon involving many nonlinear thermodynamic processes [47]. In the thesis a detailed study of the nucleated acoustical signals from SEDs using neutrons and gamma-rays are presented. Complexity of the nucleation has been studied using the nonlinear analyses and the chaotic behaviour has been identified. The coherent mode in the nucleated signal have also been studied by empirical mode decomposition technique. New parameters have been developed for better understanding and discrimination of the neutron and gamma-ray induced signals. Ultraviolet Visible

absorption and Fluorescence spectroscopy of the gel matrix of the SEDs have been studied for fabricating the stable SED. Finally, the SEDs have been applied to study the variation of neutron flux during a solar eclipse day. A Bel-Jar type SED and a pressurization system have been developed and initial testing have been carried out and the results have been described.

This thesis is divided into seven chapters. Chapter 1 and 2 discusses the general introduction of the superheated state, SED, the oscillation of the bubble after nucleation and its nonlinearity. Chapters 3 describes the chaotic nature of the generated acoustical signals and the bubble nucleation using nonlinear analysis. The different discrimination techniques of the signal from neutron and gamma-ray induced nucleation using two types of SEDs with different liquids ($R-134a$ and $R-12$) are covered in Chapter 4. Ultraviolet-Visible absorption and Fluorescence spectroscopy of the gel matrix of SED are described in Chapter 5. The application of the discrimination technique and the development of a new generation of Bell-Jar type SED are described in Chapters 6. Finally, Chapter 7 devotes the conclusion of the work and future plan. The contents of each chapter are described below in brief.

Chapter 1: Introduction of superheated liquid

In this chapter, mainly the details of the superheated state of a liquid are described. It also covers the principle and the physics of nucleation of superheated liquid droplets inside SEDs. Impurities present in the gel matrix of SED and random temperature fluctuations can cause heterogeneous nucleation inside SED. The homogeneous nucleation by the neutrons and gamma-rays are our prime interest of study and here the homogeneous nucleation mechanism by neutrons and gamma-rays are described. The present use of SEDs in the detection of particles and dark matter are described in this chapter.

Chapter 2: Introduction of nonlinear nature of bubble oscillation during nucleation

The proto-bubble after nucleation grows very fast and the time scale approximately equal to 10^{-8} ms and becomes a vapour bubble. The growth process can be divided into three regimes and known as surface tension controlled regime, inertia controlled regime and heat diffusion controlled regime. The growth of the bubble and the three stages are elaborately described in this chapter. After the growth stages the bubble oscillates and the details of the frequency of oscillation are also addressed here. The oscillation of a bubble is considered as a nonlinear, complex and chaotic process. Previous nonlinear chaotic dynamics are addressed which has the potential tools to classify the underlying physical process. This chapter also summarises the recent and past research on the nonlinear behaviour and the presence of chaos in bubble oscillations after nucleation.

Chapter 3: Nonlinear behaviour of the homogeneous nucleation

Boiling is a common phenomenon but the complete mechanism of boiling is not fully understood because of the nonlinearity and complexity of the process. The complexity occurs due to the presence of interacting sub-process in nucleation and this type of process under selected conditions show chaos. The homogeneous nucleation of superheated liquid droplets is nonlinear and complex like normal boiling. Normal boiling is referred to as heterogeneous nucleation. It occurs in the presence of any discontinuity and homogeneous nucleation occurs inside the bulk liquid. This chapter describes the nonlinear analysis that has been carried out on the acoustical signals from homogeneous nucleation of superheated liquid droplets. The analysis shows the existence of chaos and also differences have been observed in the acoustical signals from neutron and gamma-ray induced nucleation.

Chapter 4: Discrimination techniques

4.A: Discrimination techniques of neutron and gamma-ray induced bubble nucleated signals

High ionizing particles can induce bubble nucleation at even low temperature and low ionizing particles can induce nucleation at only high temperature. The bubble nucleation by high ionizing particles like neutrons and low ionizing particles such as gamma-rays has been investigated here. The experiments with neutrons and gamma-rays have been performed in temperatures ranging from 32 ^oC to 50 ^oC for $R-134a$ and in temperatures ranging from 35 ^oC to 55 ^oC for $R-12$ in the presence of $^{241}Am-Be$ and ^{137}Cs source. All the experiments have been done with two kinds of superheated liquids droplets these are $R-134a$ and $R-12$. Two different sizes

of superheated droplets have been used. The SEDs have been fabricated at the laboratory of SINP. The signals from bubble nucleation have been analysed by using different kinds of parameters like Pvar, Fundamental Frequency (F.F.), Duration of the signal and Number of Peaks. These parameters of the signals have been obtained from bubble nucleation of $R-134a$ and $R-12$ superheated liquid droplets and tried to discriminate the neutrons and gamma-rays induced signals.

4.B: Advanced discrimination techniques of bubble nucleated signals by nonlinear analysis

A chaotic bubble nucleated signals are highly fluctuating, non-stationary and intermittent. It has broadband features and may consist superposition of many localized structures. Noise is present in almost all experimental signals and coherent features may present in a signal after denoising it. The coherent structure is considered as the mode of the signal with the highest energy concentration. A signals may have more than one coherent mode. The detection of coherent mode in a bubble nucleated signal is important because it is the primary part of the whole signal which contains the major energy and fundamental frequency of the signal. Analysis was done on the experimental bubble nucleated signals from a non-standard point of view to understand the nucleation process. The present study extends the nonlinear studies on the signals and tries to discriminate the bubble nucleated signals by focusing on the new parameters of signals.

Chapter 5: Spectroscopic characterization of the gel matrix for the fabrication of a stable SED

The transition process of electrically excited molecules from excited singlet states to the ground state is called Fluorescence. Molecular properties like associations, dynamics or any complex photochemical reaction can be studied using Fluorescence emission. In this chapter, the Fluorescence analysis and Ultraviolet-Visible (UV-Vis) of the gel matrix are described. The stability of a SED depends on the properties of the gel matrix, where the droplets of the superheated liquid are distributed. A stable SED can be fabricated using a gel matrix that should be clean and free from all kinds of impurities inside it. Ultraviolet-Visible (UV-Vis) absorption spectroscopy and Fluorescence spectroscopy have been done on the gel matrix to detect the impurity or contaminant substance present in the gel matrix and to check the best combination ratio of the constituents of the gel matrix.

Chapter 6: Application of SED and few R & D

An experiment has been done at the laboratory on an annual solar eclipse day to measure the variation of neutron flux. The measurement shows an enhancement of neutron flux during solar eclipse relative to a normal day. A large size Bell-Jar type of SED is constructed with four AE sensors. The volume of the SED is one litre and out of four AE sensors three are symmetrically placed at the side of the Bell-Jar and the fourth one is placed at the bottom. In the present chapter, the construction and the test run of this Bell-Jar type of detector are presented. A pressurization system convert the nucleated bubbles back to the liquid state to reuse the same detector in multiple experiment. Details, testing and improvement of a pressurization system

have been presented.

Chapter 7: Conclusion and future plan

The existence of chaos and the nonlinearity in the bubble nucleation are discussed. A summary of the different parameters extracted from the signals for the discrimination of neutron and gamma-rays are discussed. The importance of the characterization of the gel matrix of the SED is summarised. Finally, the summary of the applications of SED and the R & D works on detector have been presented here.

Contents

List of Tables

List of Figures

Chapter 1

Introduction of superheated liquid

1.1 Inroduction

The principle of a superheated detector is based on the nucleation of superheated liquids and it has been extensively used as a radiation detector. Superheated Emulsion Detector (SED) is made up of microscopic droplets of superheated liquids and the droplets are suspended inside a visco-elastic degassed gel matrix. The process of nucleation of superheated droplets are very similar to bubble chamber [1] but the complete physics of each step of nucleation is not yet completely known to us. SED is a threshold detector because it can detect heavy ionizing particles like neutrons while remaining insensitive to low ionizing radiation like gamma-rays and muons [2, 3]. In SED, the liquid remain in superheated state which is the state of a liquid when it remains in the liquid state even at temperatures exceeding its boiling point. In this state the chemical potential energy is high compared to its vapour state. This is a relative minimum state and the state exists without violating the thermal or mechanical stability of the system [3]. The typical phase diagram of a liquid in terms of pressure (P) and temperature (T) parameters is shown in Figure 1.1 and the superheated state can be explained by using this phase diagram. The point P in Figure 1.1 is the point where all the three phases of a matter (solid, liquid and vapour or gas) coexist and is known as the "Triple point". The "Critical point" is the end of the phase equilibrium curve represented by point Q. In the diagram the three phases

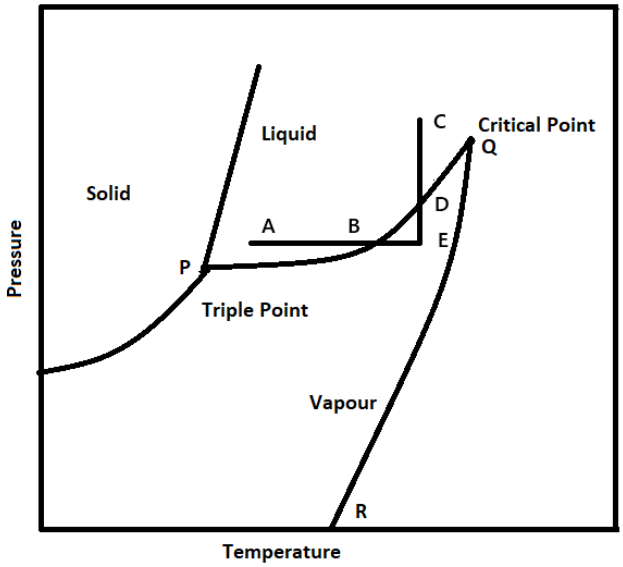

Figure 1.1: Typical phase diagram of a substance.

of the matter are separated by three distinct lines. The lines are known as solid-liquid, liquid-vapour and solid-vapour phase boundaries. The solid and liquid state of matter coexists at the solid-liquid phase boundary whereas the liquid and vapour state of matter coexists at the liquid-vapour phase boundary. The solid-vapour phase boundary is the line where the solid and vapour state of matter coexists. If a liquid at the point "E" in the purely vapour state maintains its liquid state at the same position then it will be a superheated state. The two ways to reach the superheated state of a liquid are isobaric heating and isothermal decompression. The isobaric heating is the process where the temperature of the liquid increases very slowly above the boiling point starting from a low temperature at constant pressure. In the case of isothermal decompression, the pressure of the liquid is reduced very slowly and reaches the ambient pressure starting from comparatively high pressure at constant temperature.

The temperature by which a liquid exceeds its boiling point at constant pressure is called the degree of superheat. At a constant temperature, the degree of superheat is defined as the difference between the vapour pressure and the ambient pressure [4]. Critical temperature (T_c) is the theoretical maximum limit of superheated state. It is difficult to reach at this critical temperature in the laboratory [5].

The superheated state is a metastable state of the liquid, and to maintain the state, liquid should be free from any kind of perturbation. The most common form of perturbation is the presence of any kind of discontinuity in the liquid which causes the normal boiling starting from heterogeneous nucleation sites. This type of boiling can be prevented by removing the discontinuity like interfaces of liquid-solid, liquid-liquid and liquid-gas. The superheated state of a liquid can be understood in detail by using the phase diagram shown in Figure 1.2 which is represented in pressure-volume space [2]. Two Venders Waals curves are shown in the Figure 1.2 which represent the variation of pressure as a function of volume at a constant temperature. Among the two curves, the temperature of one is below the critical temperature (T_c) and the other curve is at the critical temperature (T_c). A substance in the stable liquid state expands beyond the point "b", it reaches the stable vapour state by following the path "a-b-d-f-g". A substance at "b" in liquid under special conditions enters into the metastable region "c", the substance can stay in this meta-stable state for a long time in the absence of any disturbances. It will reach the next stable vapour state in the presence of any small fluctuations. In Figure 1.2 the point "c" is the minima of the curve as $\frac{dP}{dV} = 0$ at this point and this point represents the maximum limit of superheat at a constant temperature. The superheated liquid will vaporize more

easily as the temperature of the liquid increases at constant pressure till it reaches the point "c". Beyond the point "c", $\frac{dP}{dV} > 0$ and lowering the pressure the liquid enters in this unstable state, the curve between the metastable and unstable state is known as the spinodal curve. The primary cause of the transmission from the vapour state to the liquid state is the variation of the density of the liquid and radiation interaction at the molecular level. The variation of the liquid's density and the energy deposition by radiation are sufficient to overcome the energy barrier of producing the new phase which leads to the phase transition from liquid to vapour state [6]. The limit of superheat is maximum at temperature below the critical point with constant pressure and the liquid can maintain its superheated state without undergoing phase transition. The energy barrier like surface tension sustains the superheated liquid in a metastable state. The energy barrier is defined as the energy for unit surface area at the interface of the liquid and vapour phase [7]. The phase transition can also be triggered by the presence of trapped air bubbles, gas pockets at the solid-liquid interface of the container, impurities and random fluctuation of the temperature of the liquid, etc.

1.2 Superheated Emulsion Detector (SED)

"Robert Apfel" 1979 developed a Superheated Droplet Detector (SDD) by refining the concept of bubble chamber [1]. Bubble chamber was developed by D. A. Glaser at the time when he observed that ionizing radiation could initiate boiling in a container of superheated solution; this invention earned him the Nobel Prize in 1960. Hydrogen,

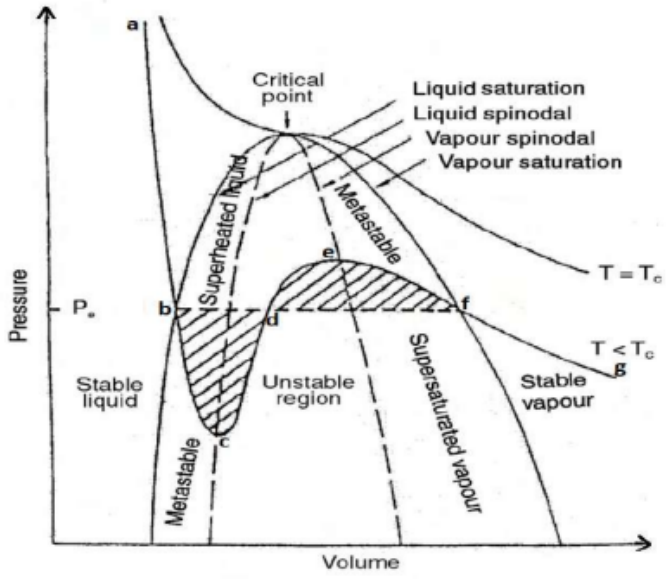

Figure 1.2: Schematic representation of pressure-volume isotherms for a pure substance [2].

deuterium, helium, propen, freon, and xenon have been used in the bubble chamber and many elementary particles were first discovered by this technique. An energetic practice when passes through a liquid kept in a chamber produces bubbles along its track. The process consumes the whole liquid and re-pressurization is required every time before using it and the faster bubble chamber does not work beyond 20 cycles per second. The another form of this type of detector is known as a "Superheated Droplet Detector (SDD)" and "Bubble Detector (BD)", where superheated minute droplets of halocarbon or hydrocarbons are suspended in an aqueous gel like medium [4] or the superheated droplets are suspended in a polymer matrix [9]. The re-pressurization is not necessary in SDD as when a liquid drop vaporizes it keeps the other drops unaffected. SDD can be used as a continuously sensitive miniature bubble chamber. International Commission on Radiation Units and Measurements

(ICRU) and the International Organisation for Standardization (ISO) adopted the common denomination of "Superheated Emulsion". The superheated drop detector manufactured by Apfel Enterprise Inc., USA, and Bubble Technology Industries Inc., Canada considers SDD and BD respectively as their trade name. In the last few decades, extensive research on this detector has established this as a useful neutron detector and it has made its important place in many branches of physics. In a "Superheated Emulsion Detector (SED)", small size droplets of superheated liquid can remain in a superheated state for long time by fractioning them into small sizes and suspending in another liquid medium. The superheated droplets are suspended in viscous immiscible liquid and they should be stored in perfectly smooth containers. The isothermal decompression method has been used in the preparation of SED. The presence of any imperfections at the surfaces of the container or the presence of air bubbles in the suspending medium of the superheated droplets acts as a heterogeneous nucleation site and can cause heterogeneous nucleation [2]. The formation of the nucleus of a new phase is known as "nucleation", here the vapour state is formed from the superheated liquid droplets. The formation of stable vapour bubbles takes place by the process of nucleation, and this nucleation may arise from small perturbations like mechanical vibration and thermal fluctuation. Heterogeneous and homogeneous nucleation are the primary two types of nucleation processes. In the SED, heterogeneous nucleation predominantly occurs at the interface of two phases, like solid-liquid, liquid-liquid or liquid-gas and homogeneous nucleation occurs within the bulk of the superheated liquid. Normal boiling is an example of heterogeneous nucleation and the temperature of this nucleation is much below the homogeneous nucleation temperature. Typically the refrigerant liquids of low boiling point are uti-

Liquid	R-12	R-21	R-22	R-115	R-114	R-134a
Chemical Formula	CCl_2F_2	$CHCl_2F$	$CHClF_2$	C_2ClF_5	$C_2Cl_2F_4$	$C_2H_2F_4$
Molecular Weight	120.91	102.92	80.47	154.47	170.93	102.03
Boiling Point (T_b ^oC)	-29.79	8.92	-40.75	-38.70	3.77	-26.3

Table 1.1: Physical properties of some liquids used in SED.

lized in constructing SED, making them sensitive to ionizing particles even at room temperature [3]. Some of the liquids and their physical properties are listed in Table 1.1 used in the fabrication of SED. An energetic particle while passing SED, interact with the droplets and can cause nucleation, this type of nucleation is known as radiation induced nucleation. The interacting energetic particle must deposit the required energy while passing through the SED within a critical length to initiate the bubble nucleation. The minimum amount of required energy for the bubble nucleation is known as threshold energy or critical energy, its value relies the detector's working temperature and pressure. The SEDs are sensitive to the heavy ions [10–13], neutrons [14,15] when the degree of superheat is moderate. SEDs are also sensitive to low ionizing particle like electron, beta particle and gamma-rays [16–18] when it is highly superheated. The SED can be made sensitive to neutrons while it remains insensitive to gamma-rays at a particular threshold energy of the detector. The threshold energy can be changed only by changing the working temperature and pressure of the SED. This threshold nature is useful in the detection of neutrons in the mix field of neurons and gamma-rays. Typically SED is a good neutron detector and well established for neutron spectrometry and dosimetry [19–27], it was also made to detect gamma-rays and other charged particles [28–32]. International Commission on Radiological

Protection (ICRP)- 60 recommendations are considered for the accuracy of the measurements, real time response, low minimum detection threshold and dose equivalent response [60]. SED was developed for the position sensitive neutron spectrometer or dosimeter for the application of radiotherapy [61], angle-differential neutron fluence measurements [62] and response enhancement to high energy neutrons [63]. The information of a neutron is provided by the differential angle and energy distributions. Correlating physical quantities such as absorbed dose, as well as non-isotropic protection quantities like organ doses and effective dose, or operational quantities such as personal dose equivalent and directional dose equivalent, is made possible by understanding the angle and energy differential fluence distributions. The photo neutron in high energy radiotherapy X-ray beams [33] can be measured by SED. It is useful in three dimensional dosimetry [34, 35]. The very important properties of SEDs are low cost, easily available, easy to fabricate and threshold nature. These properties make it useful in different research fields like radiation physics [36, 37], high energy physics [38], health physics [39], space physics [40], nuclear astrophysics [41], etc. The bubbles are nucleated from the superheated droplets inside the SED due to the energy deposited by the particles and the deposited energy inside the SED depends upon the stopping power of the particle. The nucleation of the superheated droplets produces an acoustic signal or shock wave during the vaporization. A condenser microphone or piezoelectric sensor has been used to detect produced acoustic signals [42–44]. These acoustic signals contain information about the particle that deposits the energy. The droplet after nucleation becomes a stable and visible bubble but before reaching to a stable condition it has to go through a different growth regime [45, 46]. The bubble oscillates in different frequency regions and emits acoustical signals of different

amplitude [47] in different growth regions. Many parameters have been defined from the acoustical signals and also from the frequency spectrum of the signal to understand the complete process of nucleation but the complete picture of the nucleation is not clear to us. Among the disadvantages of SED, the major one is the destructive blast waves that propagate into surroundings due to sudden de-pressurization of the container containing the superheated liquid [48–50]. Other weak points of the SED are the refrigerants used in this detector are chlorofluorocarbons which are controlled substances due to the depletion of the ozone layer.

The nucleation of superheated droplets inside SED and its sensitivity or efficiency depends on various factors like the operating temperature, pressure, type of liquid, number of droplets inside SED, the size of the droplets and geometry of the SED, etc. Presently many extensive researches have been done using SED for the identification of particle induced nucleations to identify the neutron, gamma-rays and alpha particles individually [51–57]. Numerous indirect observations from both astronomy and cosmology show that the significant portion of matter of the universe is Dark Matter (DM). Weakly Interacting Massive Particles (WIMPs) is a favoured undiscovered candidate for the dark matter having very low cross-section, many international collaborations (SIMPLE, PICASSO, COUPP, PICO and MOSCAB) are working on the detection of WIMPs using the SED [58, 59].

1.3 Nucleation of superheated droplets

The droplets of SEDs remain in a metastable state inside the gel matrix and it converts into a stable vapour state. In the beginning, it forms a seed of a vapour bubble, it grows and reaches into the vapour state. Initially, σA amount of energy is needed for production of a free gas cavity, where σ and A are the surface tension and area of the cavity respectively. The amount of energy for expanding the cavity at constant pressure is $P\Delta V$, where P is the pressure and ΔV is the change in volume. According to the universally accepted theory, during the passage of a particle or radiation through the liquid droplet, it deposits energy along the track. Different sized vapour bubbles are created along the particle's path. Gibb's [8] using classical thermodynamics define the free energy (W) required to form a vapour bubble of radius R as the difference between the two terms as follows,

$$W = 4\pi R^2 \sigma(T) - \frac{4\pi}{3} R^3 [P_v(T) - P_l(T)], \tag{1.1}$$

Here, $\sigma(T)$ represents the liquid-vapour interfacial surface tension at temperature T, $P_v(T)$ is the equilibrium vapour pressure and $P_l(T)$ is ambient pressure of the superheated liquid at temperature T. The quantity $P_v(T) - P_l(T)$ is defined as the "degree of superheat" of the liquid. The first term in Equation 1.1 is the energy needed to create the surface of the vapour bubble against the surface tension at the liquid-vapour interface is known as the surface energy term. The second term represents the energy needed to create the volume of the vapour bubble due to the excess vapour pressure which is known as the volume energy term. Gibb's free energy

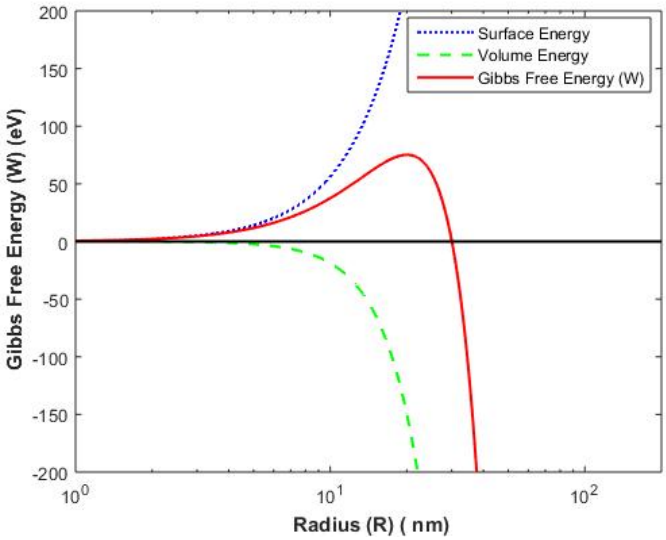

Figure 1.3: The calculated surface energy, volume energy terms and Gibb's free energy for a vapour bubble.

(W) becomes a maximum at some certain value of radius and this radius is known as the critical radius (R_c), it is represented by Equation 1.2.

$$R_c = \frac{2\sigma(T)}{(P_v - P_l)} \tag{1.2}$$

The surface energy and volume energy terms and the Gibb's free energy of $C_2H_2F_4$ liquid at 32 ^oC temperature are plotted as shown in Figure 1.3. The variation of W shows that the value of the Gibb's free energy reaches a maximum value and then decreases again. The bubbles will become thermodynamically unstable after reaching to the critical radius and grows very fast and form a stable vapour bubble. The minimum thermodynamic energy required to form a critical size vapour bubble is

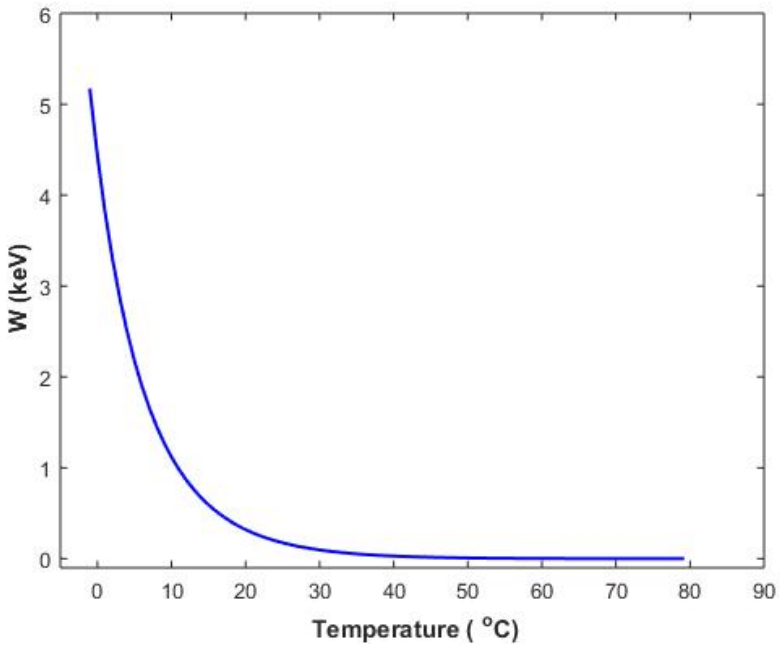

Figure 1.4: The variation of calculated Gibb's free energy as a function of temperature.

given by the following Equation 1.3.

$$W_{min} = \frac{16\pi\sigma^3(T)}{3[P_v(T) - P_l(T)]^2} \tag{1.3}$$

The value of the minimum energy decreases due to the rising temperature, the degree of superheat increases $(P_v - P_l)$ increases and surface tension $(\sigma(T))$ decreases with increase in temperature, the Figure 1.4 shows the variation the W_{min} for $C_2H_2F_4$ liquid. In the expression of energy, only the reversible thermodynamic work has been considered. The energy can also be calculated by considering the reversible work done by bubble surface. Also calculated by evaporation of the liquid growth counteracting the pressure exerted by the liquid, and other irreversible work. The acoustic wave emission, action of the viscous forces at the time of bubble growth and heat energy

lost during bubble expansion are the irreversible work considered in the expression of energy. The expression of the energy by introducing all other terms as mentioned above is represented by E_c and is described below [64–67]. Bell et. al. [68] gave the more accurate expression by considering the kinetic energy and viscous energy and represented by Equation 1.4.

$$E_c = W + H + E_{wall} + F \tag{1.4}$$

The other terms like H, E_{wall}, and F represent the vaporization energy, kinetic energy of the liquid and energy by the activity of the viscous forces respectively. The contribution of the third term is negligible and D. V. Bugg [70] defines the critical energy (E_c) by defining only the vaporization and surface energy terms. The expression of the critical energy (E_c) is given by Equation 1.5,

$$E_c = 4\pi R_c^2(\sigma - T(\frac{\partial\sigma}{\partial T})) + \frac{4\pi}{3}R_c^3\rho_v(h_v - h_l), \tag{1.5}$$

where, ρ_v is the vapour density, and h_v and h_l are the specific enthalpies of the vapour bubble and liquid respectively [69]. The first term of the Equation 1.5 is represented by the free energy which is known as the surface energy term. The second term is related to the energy of for the vaporization. There is a difference between the work done at vapour pressure P_v and liquid pressure P_l, so a corrective factor has been introduced in the vaporization term as we have considered that the vapour bubble grows from zero to critical radius. Considering the correction terms, the final

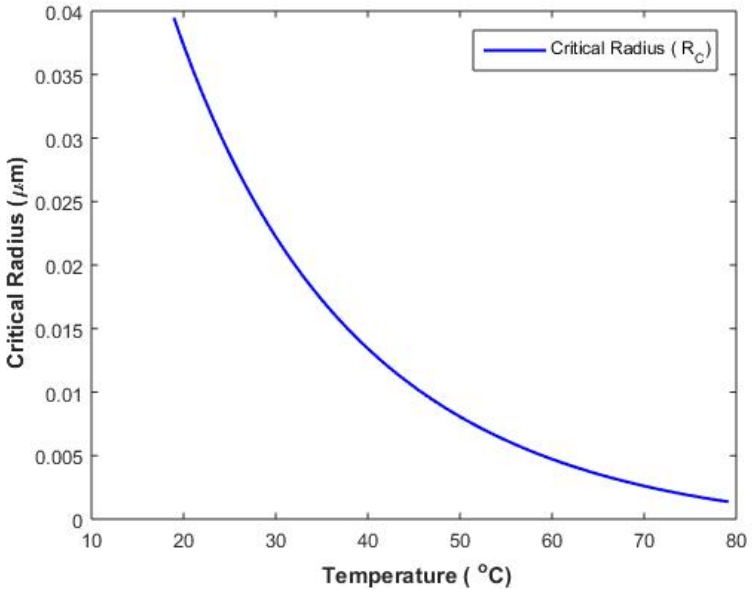

Figure 1.5: The variation of calculated critical radius (R_c) with the temperature of $C_2H_2F_4$ superheated liquid.

expression of the E_c becomes,

$$E_c = 4\pi R_c^2(\sigma - T(\frac{\partial\sigma}{\partial T})) + \frac{4\pi}{3}R_c^3\rho_v(h_v - h_l) - \frac{4\pi}{3}R_c^3(P_v - P_l) \tag{1.6}$$

Some irreversible work has to be considered in the expression of E_c and represented by W_{irr}. This term has been neglected because the calculations show that only 1 % of total energy is lost by the irreversible work. The expression of the critical radius (R_c) and critical energy (E_c) as represented by Equation 1.2 and 1.6 respectively have been calculated for $C_2H_2F_4$ liquid at different temperatures. The variation of the R_c and E_c are presented in Figure 1.5 and Figure 1.6 respectively.

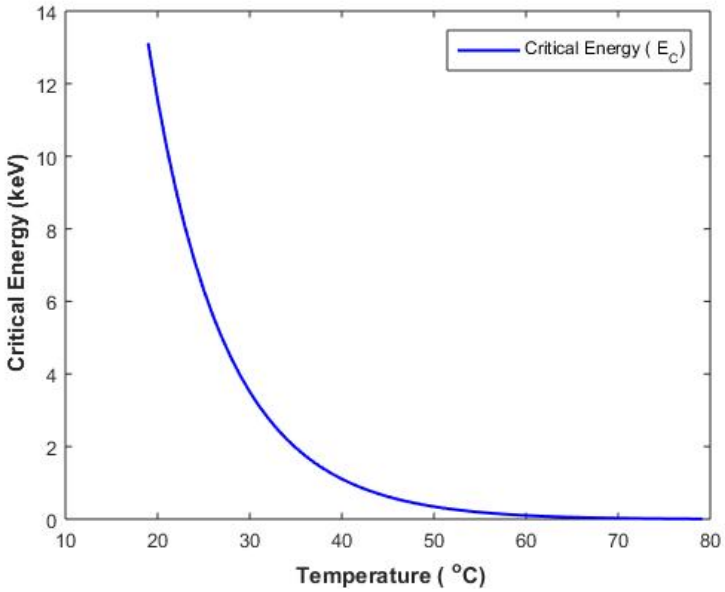

Figure 1.6: The variation of calculated critical energy (E_c) with the temperature of $C_2H_2F_4$ superheated liquid.

1.3.1 Nucleation by neutron

The superheated droplets inside SED nucleate due to the passage of energetic particles. The interaction mechanism of the energetic particle or radiation with the detector material and the deposited energy is a key factor in the nucleation of the superheated droplets. The charged particles like electrons or heavy ions interact with the detector medium by coulomb interaction and the interaction depends upon the nature of both the particle and the medium of the detector. The stopping power of these particles are designated as the deposited energy in the detector medium and it is represented by the Linear Energy Transfer (LET) of the particle. Neutrons, X-rays, and gamma-rays are uncharged particles and these particles interact with the target by producing charged particles. The bubbles are nucleated by the energy deposited

by these charged particles inside the medium. According to "Seitz's thermal spike model" [69], the energetic particles produce thermal spikes by depositing energy in a very localized way inside the droplets. The bubbles of different radii form but the bubbles having a radius greater than R_c become vapour bubble by the evaporation of the superheated liquid. The energetic particle should deposit the energy over an effective path of the particle inside the liquid. The particle should have energy greater than the threshold energy. The energy deposited by the particle should satisfy the following condition represented by Equation 1.7 for the bubble nucleation,

$$E_{dip}^{L_{eff}}(T) = \int_0^{L_{eff}} \left(\frac{dE}{dx}\right) dx \geq \frac{E_c}{\eta_T} \tag{1.7}$$

L_{eff} is the effective length over which the particle deposits the energy. It can be expressed as below Equation 1.8,

$$L_{eff} = bR_c \tag{1.8}$$

Here, $\frac{dE}{dx}$ is known as the stopping power, and the quantity "b" is the nucleation parameter. The value of critical radius or diameter plays an important role because the value of $b = 2$ is considered [69]. The dynamical theory of bubble nucleation has been established [71]. The molecular dynamical simulation of bubble nucleation of superheated liquid droplets shows the value of "L_{eff}" should be equal to "$4R_c$". For the bubble nucleation [72] the value of $b = 2$ lies in the range of 2 to 2π [72–74]. The term η_T in the Equation 1.7 is the thermodynamic efficiency in the process of bubble nucleation and its value is less than one. The value of η_T represents the fraction of energy used in the process of bubble nucleation.

The neutron creates the recoil nucleus by interacting with the target nucleus of the constituent elements of the detector material and this recoil nucleus deposits the energy inside the medium. The recoil nucleus starts moving inside the liquid and loses its energy by coulomb interaction and finally comes to rest. Elastic scattering, inelastic scattering and nuclear reaction are the main three processes by which the neutrons interact with the target nucleus of the detector material. On elastic scattering the maximum amount of energy is transferred to the target nucleus. The threshold energy for a fast neutron can be calculated by considering the elastic scattering. In the Equation 1.9, E_i represents the energy transferred to the i^{th} nucleus when a neutron having energy E_n interacts with the i^{th} target nucleus and scattered elastically with it [2].

$$E_i = \frac{4A_i E_n \cos^2\theta}{(A_i+1)^2}, \tag{1.9}$$

Where θ and A_i are the recoil angle and the atomic number of the target nucleus. The target nucleus gains the maximum amount of energy for the headon elastic collision. The Equation 1.9 shows that the amount of energy received by the different recoil nucleus is different. The electron density of the material and the stopping power $\frac{dE}{dx}$ of the liquid to the recoil nucleus decides the deposited energy inside the liquid by the recoil nucleus. As mentioned previously the energy must be deposited within an effective path length L_{eff} of the recoil nucleus in a localized way. The possibility of nucleation is greater for the nuclei having a high value of stopping power. The value of the deposited energy at a particular operating temperature and pressure of the detector must reach or exceed the critical energy (E_c). In the case of $C_2H_2F_4$ liquid the recoil nuclei ^1H, ^{12}C and ^{19}F will receive different amounts of energy depending upon the atomic number of the nucleus. The Figure 1.7, the stopping power of the

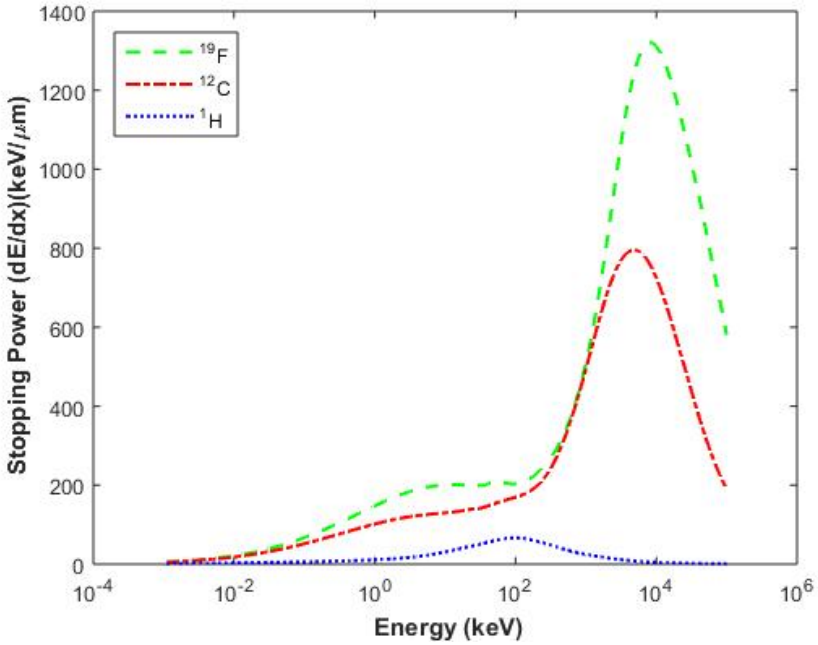

Figure 1.7: Stopping power of ^{1}H, ^{12}C, and ^{19}F nuclei in $C_2H_2F_4$ liquid.

nuclei (^{1}H, ^{12}C, and ^{19}F) for the $C_2H_2F_4$ liquid are shown. The stopping power of the ^{19}F nucleus is more than ^{1}H and ^{12}C. SRIM-2008 software package [75] has been used for the calculation of the stopping powers of the nuclei. Earlier workers on superheated liquid show that the chlorine atom in CCl_2F_2 at a very high superheated state became sensitive to the thermal neutrons by the production of an exotic capture reaction [76, 77]. As Cl is absent in $C_2H_2F_4$, it is not sensitive to thermal neutrons.

1.3.2 Nucleation by gamma-ray

The gamma-rays interact with the electrons and transfer their energy to the orbital electron. The electron deposits the energy and nucleates the bubble after satisfy-

ing the bubble nucleation conditions. The secondary particle like electrons from the gamma-ray are produced through coulomb interaction and these electrons deposit energy in the detector medium. The gamma-rays primarily interact with the detector medium by three processes as photoelectric effect, compton effect, and pair production. Photoelectric and compton effects are mainly dominant effects for gamma-ray energies within the keV to MeV range. Pair production is dominant if the energy of the gamma-rays is above 1.2 MeV. The electrons from gamma-rays gain the energy of the gamma-rays. The energy deposited by the electron depends on the value of dE/dx and the dE/dx of the electron is very small because of the low mass and large range. The electron nucleates more than one droplet after satisfying the nucleation conditions as the range of the electron is large. Bethe Equation 1.10 has been employed to determine the stopping power of the electron inside the detector medium.

$$-\frac{dE}{dx} = \frac{4\pi k_o^2 e^4 n}{mc^2\beta^2}\left[\ln\frac{mc^2\xi(\xi+2)}{\sqrt{2}I} + F^-(\beta)\right], \tag{1.10}$$

$$F^-(\beta) = \frac{1-\beta^2}{2}\left[1 - \frac{\xi^2}{8} - (2\xi+1)\ln 2\right], \tag{1.11}$$

$$\beta = \frac{v}{c}, \tag{1.12}$$

$$\xi = \frac{E}{mc^2}, \tag{1.13}$$

Where, $k_o = 8.99X10^9\ Nn^2/C^2$, e is the charge of the electron and n is the number density of the electron in the liquid. v and E are the velocity and energy of the

electron. The average excitation energy of the liquid molecule is represented by I.

$$n \ln I = \Sigma N_i Z_i \ln I_i, \tag{1.14}$$

where n and Z_i are the total numbers of electrons in the liquid and the atomic number of the individual elements in the liquid respectively. The basic additive rule has been used in Equation 1.14 for the calculation of the average excitation energy of the molecules of the liquid.

1.4 Detector efficiency

The efficiency of a particle detector is a important parameter that determines its performance in various applications. Several factors affect this efficiency, mainly three different types of efficiencies are taken into account i) detection efficiency, ii) thermodynamic efficiency and iii) nucleation efficiency [78–80].

First the detection efficiency is the ability of the detector material and design to detect a particle or radiation when it passes through or interacts with the detector. It includes the nature of interaction of a particle that causing a detectable event. Such as ionization in a gaseous detector, scintillation in a scintillator detector or nucleation of superheated droplets in SED. The detection efficiency, which is similar for all kinds of detectors, is defined as the ratio of the number of events detected to the number of energetic particles falling on the detector [80]. The second one is the thermody-

namic efficiency of SED, which involves understanding how these detectors uses the energy to detect particles. The efficiency depends on the degree of superheat, energy deposition by particles and the nucleation of bubbles. The last one is the nucleation efficiency in SED, which refers to the ability of the detector to form bubbles when exposed to energetic particle or ionizing radiation. Nucleation efficiency is a important in determining the overall performance and sensitivity of the detector.

As mentioned the efficiencies of SED is influenced by several factors and the primary factor determining the efficiency is the threshold energy required for nucleation. The particles that only deposit sufficient energy to overcome the threshold energy will be detected. Different particles have different processes of interacting with the superheated liquid and deposits their energy. The efficiency varies with the type and energy of the particles that passes through the detector. It also changes on the type of the liquid in the SED, the common superheated liquids like freons, hydrocarbons and chlorine. The choice of liquid is based on its degree of superheat and its sensitivity to different types of radiation. The degree of superheat is controlled by the temperature and pressure of the SED and it directly affect the threshold energy. At higher degree of superheat the threshold energy is low and it thereby increases the efficiency of the detector. The efficiency is also affected by the dynamics of bubble growth and the ability of the sensor to detect these nucleations. The geometric design of the detector, including the volume of the superheated liquid impacts the efficiency. The efficiencies of superheated liquid detectors is determined by the amount of energy deposited by the incident particles. The efficiency of neutrons and gamma-rays using various

referents liquid has been calculated [53, 78, 79]. Apfel calculated the thermodynamic efficiency of two liquids $C_2Cl_2F_4$ and C_4F_{10}, and the values are in the range of 3% to 5% [76]. Recent results from the PICASSO experiment, which are based on extensive neutron irradiations and Monte Carlo simulations, along with a refined reanalysis from SIMPLE, have indicated a nucleation efficiency of the form [80].

$$\dot{\eta}(E) = 1 - \exp\left[- \Gamma\left(\frac{E}{E_c} - 1\right)\right] \tag{1.15}$$

Where Γ is a detector-dependent parameter and its value is 2.5 ± 0.2, it essentially characterizes the slope of the curve above the threshold energy.

1.5 Application of SED

1.5.1 Neutron spectrometry

The principle of neutron spectrometer lies on property of the liquid which shows that a superheated liquid becomes more superheated and SED become sensitive to the low energy neutrons. The degree of superheat, as mentioned earlier is calculated as the difference between the ambient temperature and the boiling point of the liquid. SED using liquids having low boiling points are become more sensitive to low energy neutron at higher degree of superheat and at a high temperature. The primary methods used in neutron spectrometry involves using multiple superheated liquids with different boiling points to create varying threshold energies [40]. In another method employs two liquids at four different temperatures and produce eight distinct thresh-

old energies [81]. Das et. al. developed a more precise technique by continuously adjusted the temperature of a R-12 liquid over a broad range and demonstrated its effectiveness as a neutron spectrometer [22]. Neutron detection efficiency was also measured using a passive device using superheated liquid [23].

1.5.2 Neutron dosimetry

The energy spectrum of neuron is broad and accurate neutron dosimetry is challenging. The superheated drop detector (SDD) has been shown to closely match the ICRP curve and an ideal dosimeter should align with the ICRP equivalent curve. Apfel and Lo reported that the 40% of neutron energies above 100 keV with SDD response follows the ideal ICRP dose equivalent curve [20]. The unique characteristics like photon insensitivity, passive operation, tissue equivalent composition, isotropic response, compact size and affordability of SDD reaches it a valuable tool in neutron dosimetry.

1.5.3 Gamma-ray detection

SDD is well established detector in neutron dosimetry and spectrometry. The Use of SDD in the detection of photon has also become popular. A superheated liquid can detect neutrons because of high LET of neutron. It does not detect gamma-rays at a given temperature because of low LET of the electron from gamma-rays. The electron from gamma-rays do not able to transfer enough energy for nucleation. Therefore, most liquids suitable for neutron detection at room temperature and it

can detect gamma-rays at higher temperatures. D'Errico et. al. observed that a superheated liquid becomes sensitive to photon at a mean temperature of its boiling and critical points [35]. Experiments by Roy et. al. suggested that gamma-ray sensitive temperature varies with energy and temperature and it indicate a more complex relationship [17].

1.5.4 Dark Matter search

An important unresolved question in the fields of cosmology and particle physics today is uncovering the true nature of dark matter. Compelling gravitational evidence for its existence spans scales from individual galaxies to the entire cosmos. While this evidence strongly supports the presence of dark matter, its precise composition remains a mystery [82, 83]. A leading theoretical candidate is the Weakly Interacting Massive Particles (WIMPs). WIMPs interact only through gravity and weak nuclear forces as a result its detection is extremely difficult [84, 85]. Direct detection experiments aim to observe WIMPs scattering off nuclei within detectors, which are perpetrated at underground laboratory to shield them from cosmic ray interference. The use of superheated liquid techniques for detecting WIMPs induced nuclear recoils have several significant advantages. This technique rejects the minimum ionizing particles like gamma-ray and electron backgrounds or beta decay. This detectors are mechanically simple, cost-effective to construct and allow to use of different target materials. These detectors are discussed in the next section and the experiments were conducted by the PICASSO [86] collaboration and the COUPP [87, 88] collaboration. The merged effort of these two groups under the PICO collaboration has been

explored [89]. MOSCAB [90] a new European initiative aimed at developing a superheated liquid detector utilizing the innovative geyser technique for WIMP nuclear recoil detection. The primary distinction between COUPP/PICO and MOSCAB detectors lies in the operational technique. MOSCAB utilizes the geyser method. A notable feature common to these detectors is the acoustic system. This acrostic sensor which plays a crucial role in background rejection. The deep underground locations like SNOLAB minimize environmental backgrounds. Additional mechanism is necessary to discriminate the alpha and other cosmic particles.

PICASSO

The PICASSO experiment (Project in Canada to Search for Supersymmetric Objects) focuses on direct WIMP detection through the scattering of superheated liquid droplets of C_4F_{10}. The droplets of the liquid dispersed within a polymerized and water saturated matrix [86]. The detector is largely insensitive to cosmic muons, gamma-rays and beta radiation below 50 ^oC [86]. The detector is sensitive to alpha particle across the WIMP sensitivity range which is the dominant background. PICASSO developed an event-by-event discrimination technique based on acoustic signal to address this issue.

COUPP

The Chicagoland Observatory for Underground Particle Physics (COUPP) employs a detection technique similar to PICASSO. It uses a single vessel filled with active liquid

which is operated as a bubble chamber [87, 88] and it is located in SNOLAB. Four piezoelectric transducers record acoustic emissions and two CCD cameras capture 3D spatial coordinates of bubbles with a 20 ^oC stereo angle at 100 frames per second.

PICO

The PICO collaboration was established in 2013 through the merger of the PICASSO and COUPP collaboration [89]. This collaboration combines the bubble chamber technique of COUPP with the fluid handling expertise of PICASSO. The first prototype PICO-2L was constructed which contains 2.9 kg of C_3F_8. Results demonstrate that superheated liquid detectors are excellent in the detection of both spin-dependent and spin-independent WIMP interactions at low WIMP masses.

MOSCAB

MOSCAB (Materia OSCura A Bolle) is a European initiative led by the University of Milano-Bicocca. Its goal is to develop a bubble chamber capable of detecting WIMP nuclear recoils [90]. These detectors collectively highlight the advancements in superheated liquid chamber technology for Dark Matter searches.

Chapter 2

Introduction of nonlinear nature of bubble oscillation during nucleation

Nucleation is a primary process in phase transitions and after nucleation a new phase of a system emerges. In the case of superheated liquid, nucleation refers to the formation of vapour bubbles from the superheated liquid droplets. The present chapter describes the bubble growth, its dynamics and the associated sound emission from the nucleation of superheated liquid droplets. The complex phenomena involving nonlinear thermodynamic processes of the nucleation are discussed in this chapter. The phenomenon of particle-triggered acoustic emission in superheated liquids was first introduced by Yu. N. Martynyuk [91]. A general and non-quantitative description can be given about the mechanisms responsible for the nucleation and acoustic signals. Theoretical works of Rayleigh and Plesset-Zwick [92, 93] were based on an approximate solution of the Navier–Stokes equation. It shows that bubble grows, following the formation of the critical bubble from a liquid drop. The whole process occurs in three stages described below [92].

1. Surface tension control state: in this stage the growth process is dominated by surface tension.

2. Inertial growth stage (sometimes referred to as Rayleigh growth): in this growth stage the bubble expands with a constant velocity. The velocity of the bubble growth is driven by the internal energy of the bubble, contributed by vapour pressure and surface tension of the liquid.

3. Thermal growth stage (asymptotic stage): this growth is controlled by heat transfer from the liquid. The bubble growth is decelerating in this stage.

The first stage starts when the bubble reaches to the critical radius. The bubble expands by the energy stored inside it and its surrounding liquid. At the beginning of this stage, the surface tension affects the radial velocity of growth. The effect of surface tension decreases as the bubble radius increases with time. The influence of viscosity and surface tension diminishes and the inertia of the liquid imposes a constraint on bubble growth. These growth stages can be described by the Rayleigh–Plesset equation [92]. The solution of Rayleigh–Plesset equation [92] indicates that the radius increases linearly with time (Equation 2.1). The growth speed in this stage is proportional to the square root of the superheat (Equation 2.2).

$$R_{in}(t) = A(T)t \tag{2.1}$$

$$A(T) = \sqrt{\frac{2}{3\rho_l}\Delta P} \tag{2.2}$$

Where, $A(T)$ is the speed of bubble growth in an inertia-controlled regime and ΔP is defined as the superheat and ρ_l is the density of the liquid. ΔP increases with increasing temperature as a result the speed of the bubble growth increases. When the volume of the bubble increases, the vapour inside and the liquid near the bubble walls cool down and reach the boiling temperature. The further growth requires energy and it is supplied by the heat transfer from the different liquid layers. Growth slows down as it becomes governed by thermal diffusion and the rate continuously

decreases. This behaviour is described by the Plesset-Zwick equation [93]. It predicts a much slower increase in the bubble radius and the radius scales with the square root of time in this regime (Equation 2.3).

$$R_{th}(t) = B(T)\sqrt{t} \tag{2.3}$$

$$B(T) = \sqrt{\frac{12}{\pi}\kappa\rho_l C_l}\frac{T - T_b}{h_{lv}\rho_v} \tag{2.4}$$

Here $B(T)$ is the speed of bubble growth at that temperature (T) in the thermal growth regime, κ is the thermal conductivity of the liquid, C_l is its specific heat, ρ_v is the density of the vapour, T_b is the boiling point and h_{lv} is the latent heat of evaporation of the liquid. These growth rates have been predicted by the classical model. The experiments with superheated liquids revealed that the growth rates were significantly lower than the forecaster by inertial growth. Whereas the linear growth rates are still faster than thermal growth [94].

2.1 Growth of bubble

The complete time evolution of the radius of the bubble through the three stages as described by Robinson and Judd [47] is represented by the Equation 2.5.

$$R(t) = R_c + \frac{2}{3}C_o((t + 4C)^{\frac{2}{3}} - t^{\frac{2}{3}} - (4C)^{\frac{2}{3}}) \tag{2.5}$$

The expressions of the constants C_o, C and J_a are represented by Equations 2.6, 2.7, 2.8 [47].

$$C_o = \sqrt{\frac{\pi}{27\alpha_l}}\left(\frac{\Delta P}{\rho_l J_l}\right) \tag{2.6}$$

$$C = \frac{9\rho_l \alpha_l J_a^2}{2\pi \Delta P} \tag{2.7}$$

$$J_a = \frac{\rho_l C_l \Delta T}{\rho_v h_{lv}} \tag{2.8}$$

Where, α_l is the thermal diffusivity of the superheated liquid at constant pressure and , J_a is the Jakob number. The pressure $(P(t,r))$ of the sound emitted in the liquid by an expanding or oscillating spherical bubble of radius $R(t)$ is proportional to the acceleration of its volume $V(t)$ [46]:

$$P(r,t) = \frac{\rho_l}{4\pi}\frac{\ddot{V}(t-\frac{r}{c})}{r} \tag{2.9}$$

$$P(r,t) = \frac{\rho_l}{r}(2R\dot{R}^2 + R^2\ddot{R}) \tag{2.10}$$

The Equations 2.9 and 2.10 are the pressure $(P(t,r))$ generated in the liquid at some distance r. Where, c is the velocity of sound and an overdot on V and R means differentiation with respect to time.

2.2 Oscillation of the bubble

One can model a bubble in a liquid as a system capable of oscillations. For the formulation of the model equations for this bubble oscillator, it is necessary to specify

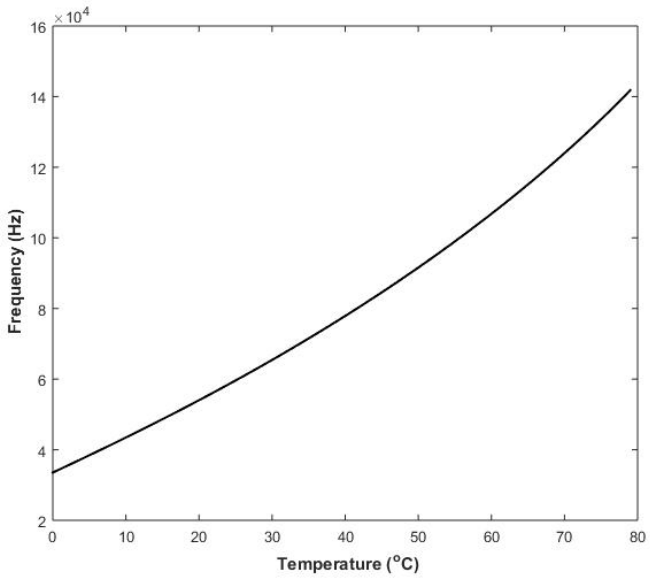

Figure 2.1: The resonance frequency of bubble with the change of the temperature of the detector.

various features of the liquid medium surrounding the bubble. The complete description of the gas and vapour contents are also important. The size and shape of a spherical bubble was simplified by the radius R. The primary part is to determine the radius and how this radius changes over time. After the growth stages, the bubble enters into a final phase. In this phase the bubble performs a free harmonic oscillation of radius (R) with a resonant frequency known as the Minnaert frequency [95]. The expression of the resonance frequency given by Equation 2.11 [95].

$$f = \frac{1}{2\pi R}\sqrt{\frac{3kp_o}{\rho_l}} \tag{2.11}$$

Where R is the radius of the bubble, k is the polytropic coefficient of the gas and p_o is the equilibrium ambient pressure. The resonance frequency represented by Equation 2.12 is also calculated from the Gilmore model, Keller-Miksis model, Rayleigh-Plesset

model [92] and represented by Equation 2.12.

$$f = \frac{1}{2\pi R\sqrt{\rho_l}}\sqrt{3k(p_o + \frac{2\sigma}{R} - p_v) - \frac{2\sigma}{R} - \frac{4\mu^2}{\rho_l R^2}} \tag{2.12}$$

Where, μ is the viscosity, σ is the coefficient of surface tension of the liquid and ρ_v is the vapour pressure of the superheated liquid. The resonance frequency of the oscillation of R-134a bubble of radius 100 μm is shown in Figure 2.1. Oscillations of nucleated bubbles from superheated droplets, particularly in a superheated liquid involve complex thermodynamic and fluid dynamic processes. However, the detected acoustical signals after nucleation and their temperature dependence were studied. It allow some conclusions to be drawn and these studies describe the information about the bubble growth, its oscillation and acoustic signal production.

2.3 Experimental studies on bubble oscillation

Experiments related to the initial stages and primary features of boiling or nucleation are limited. Few of the experiments and nonlinear studies on the experimental only predicted some initial stages before and after oscillation. The experiments of laser light and electric spark discharge are two common processes that produce a tiny single bubble. The bubbles were captured in an acoustic trap using intense laser light after producing it [96–99]. In the case of an electric spark discharge, the bubble can be produced between two submerged electrodes by focusing a laser light [100]. The electrodes limit the exploration of the bubble as the electrodes constitute a

perturbation to the flow. The common and popular technique for studying the bubble oscillation properties is the levitation of bubbles in an acoustical trap [101–105]. Some of the experiments on the production of bubbles and the nonlinear oscillation of the surface of the bubble is described briefly in this section 2.3. The experiment of the oscillation of a bubble in a acoustical trap, bubble by laser light and bubble from radiation are discussed.

2.3.1 Bubble in acoustical trap

The bubble oscillation and shock wave emission have been studied in detail by a trapped single bubble in a stationary acoustic field [106, 107]. The experimental arrangement is composed of a rectangular glass cuvette equipped with a single piezoelectric transducer. The transducer placed at the bottom and it produces the sound field. A thin platinum wire at the upper right side of the cuvette produces bubbles. The current pulses have been introduced through the platinum wire. The oscillating behaviour of the bubble is continuous and each acoustic cycle being highly precise [108, 109]. A long distance microscope was used and high resolution images of the bubble in both time and space can be captured [107]. During the capture the bubble remains stationary. Light directed at the bubble surface is deflected and it causes the spherical bubble to appear dark against a brighter background. A rapid collapse with several subsequent rebounds is observed, along with a slow expansion. Experimental observations of single spherically oscillating bubbles within a bubble trap show the theoretical model of the bubble oscillation. The steep collapse predicted by calculations is not fully explained in the experiment. The light except the

scattering at the bubble wall, it also compress water surrounding the collapsed bubble. The Rayleigh–Plesset theory shows a sufficient agreement with the experiment. More advanced models are needed to explain more the rebounds of the bubble. The experiments by Matula [110] validated the entire stages of the bubble oscillations.

2.3.2 Bubble induced by laser light

The short pulses of laser light into a liquid can produce spherical bubbles [99,111–114]. A controlled way with a large range of parameters related to the bubbles can be studied by this method. The darkness of the bubble is caused by the motion at its core and the light being refracted by its curved edges. The process of bubble collapse is very fast and after bounce it is not spherical in shape. The Keller-Miksis mode is comparable to the oscillation and transient decay of the bubble. The fast collapse can be demonstrated by the high value of the bubble dimensions. The Gilmore model can be used to calculate the radius of the spherical bubble which is comparable to validate the experimental radius of the bubble. The origin of the shock waves radiated upon collapse is lies in the sharp decrease of the size of the bubble. The shock wave which is emitted that propagates a large portion of the energy. Furthermore, the shock wave also alters the path of the light which does not allow to obtaining the radius near collapse. The damping is observed in high viscosity oil than in water that has low viscosity. The experiment is a fairly good agreement with the Rayleigh–Plesset model.

2.3.3 Bubble induced by radiation

Bubble chambers using the superheated liquids are able to detect the tracks of elementary particles. The radiation with sufficient energy that will form bubbles can be studied. A large number of experiments with different thresholds for photon induced nucleations in organic liquids and water were performed. The fast neutrons will change the threshold to a few atm for some organic liquids. The pressure threshold drops to only about 50 atm for water [115]. In a work the droplets of R-12 liquid in an aqueous gel at ambient temperature are superheated to 50 ^oC to produce bubbles when exposed to neutrons [115]. The bubbles can experience a oscillation ranging from low to high amplitude. The amplitude depends on the nature and type of the liquid, the radius of bubbles and the acoustical parameters. In this thesis all the experiments have been done using this nucleation mechanism.

2.4 Interior dynamics of bubble

There are many interior dynamics besides the dynamics of the bubble and its oscillation. Internal dynamics can be described by the equation of state of the bubble contents. These equations are described by the time dependent pressure and temperature. Shock waves propagating in the interior of the bubble centre may lead to a sufficiently and sudden pressure change at the bubble. Many rigorous descriptions of bubble oscillation addressed the inhomogeneous dynamics of the interior of the bubble. The first theoretical work started by Trilling [116] and many approximations

were taken for considering the acoustic approximation during the pressure change. All the approximation were done at the bubble wall and the internal acoustic shocks were calculated. Micro shocks occur inside a collapsing bubble which are observed by Jarman [117]. The intense temperatures are considered as the starting point of sonoluminescence and micro shocks. Pressure as well as temperature measurements inside a bubble are impossible to understand the interior dynamics of bubbles at collapse. The expected phenomena and observed outside effects can be explained by extending the numerical calculations. The major two possible approaches are continuous approach and molar dynamics simulations. In a continuous approach the trapped gases and vapours are treated in continuum form. The radius from the spherical bubble, time of oscillations, instantaneous pressure and temperature of the bubble are considered as the descriptive variables. The governing equations were formulated using these variables and the equations were solved. In the second approach the high temperatures exceeding a million Kelvin with converging shocks in the interior was explained. All the expiation was done by restricted fluid dynamics models [118, 119]. The diffusive processes of heat and transfer of mass between the gaseous and liquid phases relaxed the shocks. As a result, the temperatures reduced to the order of tens from thousands of Kelvin [121, 122]. There are several limitations and a few limitations in these considerations are unknown. The capture of steep pressure gradients, phase boundaries, special algorithms were identified [123]. An alternative numerical approach as molecular dynamics (MD) simulations were explored. In this approach one can overcome the difficulties and limitations with the continuum formulation molecular dynamics [120, 124–127]. A three dimensional Lennard-Jones fluid was taken by Matsumoto et. al. and represented as an empty space with embedded soft-

core particles to model the bubble [127]. Many significant condensation of molecules during collapse was observed in this Lennard-Jones fluid. The bubbles obeying the Rayleigh–Plesset equation were considered as continuum carries of liquid by Metten et. al. [120]. The gas and vapour molecules inside the bubble bounce around and inside the bubble. These molecules are colliding with other particles and the bubble wall. These were treated as hard spheres. The imposed pressure on the wall by these particle impacts and the interior dynamics was coupled to the bubble wall dynamics. The general problem of bubble oscillation was explained by these fine details. The temperature in the centre reached to 10^5 K when energy consuming effects are not introduced. In the continuum calculations without diffusion processes the observed temperature was million Kelvin. The temperature is expected to drop significantly by introducing the water vapour [128]. Evolution of vapour and radial oscillation of the bubble interior have been modelled by the molecular dynamics calculations.

2.5 Interaction of oscillating bubble

The bubbles oscillation is not free, it is interrupted by many interactions like interaction with the boundary of the container known as boundary interaction. Two oscillating bubbles are also interrupted by each other known as interaction between the two bubbles. These interactions are described below in details.

2.5.1 Boundary interaction

Bubbles cannot oscillate spherically due to the boundaries. The boundary interrupts the necessary symmetry conditions of the bubble oscillations [26]. The shape and elastic properties of boundaries are different. The interface of liquid with air and solids which may be ductile or brittle. Large numbers experiments were conducted to investigate the bubbles at different distances from the plane rigid boundary [129–131]. These investigations have been done by placing the bubbles at a free surface [132,133]. In some experiments the bubbles were placed across the boundary of a free and solid surface [134] and in front of a convex or concave solid wall [135, 136]. Also few investigations have been done by considering an elastic boundary [137, 138]. In these experiments the bubble have been pleased near an elastic membrane [139, 140].

2.5.2 Interaction of two bubbles

An oscillating bubble will impact the oscillatory and translational motion of surrounding bubbles in its neighbourhood. The reason is the presence of some bubble-bubble interaction force. The bubble-bubble force of interaction can be described in terms of the oscillatory behaviour of spherical bubbles like the normalized inter-bubble spacing. The oscillating bubbles will remain spherical if the bubbles stay at a far distance from one another. The bubble-bubble interaction force will be weak in this situation. An experiment has been done on the interaction of two laser induced bubbles by Testud-Giovanneschi et. al.. The experiment showed that the shape deformations and translations motion [141]. The interaction will become strong and complicated

if the oscillating bubbles come close together and they will lose spherical shape. The oscillation bubbles additionally acts as a free surface except from emission of sound. More observations will be given Testud-Giovanneschi et. al. considering weak and strong bubble-bubble interaction [141].

2.6 Shock waves from oscillating bubbles

A bubble oscillates and a sequence of shock waves produced by the bubbles on a solid layer in a characteristic way. As an example a toroidal shock wave is produced in an experiment when the water hits a bubble wall at its lower inside in a ring. Many studies have been performed on the oscillation periods of laser induced bubbles near a solid wall and in a free liquid. These studies compare oscillation periods of a bubble in a liquid. These studies conclude that oscillation periods were more for a bubble generated by laser irradiation oscillates [142]. The pressure pulse has been studied and shows that the first pressure pulse is more significant in the spherical bubble relative to the distorted bubble. The studies also conclude that more than 70% energy radiated as a first shock wave [143]. The bubbles from underwater explosion induced by spark and laser, this 70% of its energy has been lost at first collapse as observed in the calculations. Series of measurements have been done to estimate the first collapse time of a collapsing bubble. In this case the bubbles were considered which are not spherical in shape vicinity of a solid boundary, compared to the spherical case. The oscillation frequency of a spherical bubble adjacent to a solid and a free boundary has been given by Strasberg [144]. The calculation of the frequency was done by considering

the capacitance of two neighbouring spheres. Where the oscillations being driven by a sound field and the vales have been calculated numerically by Sato et. al. [145]. The results show that the resonance frequency curve shifts towards the lower driving frequencies. Here a bubble in infinite fluid was considered because the oscillation periods increase for bubbles near a solid wall. Johnsen and Colonius have studied contraction of a spherical bubble close to a solid boundary [146]. They considered both spontaneous (Rayleigh) and externally driven (shock-induced) collapses and also included the emission of shock waves. Laser induced bubbles in a silicone tube have been done by Vogel et. al. and reported a time dependent radius of a bubble confined in an elastic tube [147] this curve can show the oscillation of the bubble.

2.7 Nonlinear bubble oscillation

The boiling in liquid or nucleation referred to as heterogeneous nucleation is a common phenomenon. The underlying mechanism of nucleation is still not fully understood because of the complexity of the process. Boiling inside liquid, maintained in a superheated state is known as homogeneous nucleation. In homogeneous nucleation the phase transition occurs inside the bulk liquid and the bubbles can experience a oscillatory radial motion covering both low and high amplitude regimes. The oscillations of a gas bubble in a liquid or the oscillation of a bubble after nucleation of superheated liquid droplets (homogeneous boiling) is a difficult mathematical problem. Because all the processes are of a highly nonlinear nature which may generate complex governing equations. The existing studies are based either on linearised anal-

ysis or numerical computation [95,148–150]. A model that can describe the nonlinear oscillations consists of one ordinary differential equation. The equations governing the motion of the bubble radius over time can be solved once initial conditions are known. These initial conditions are related to both the radius and the speed of the bubble interface. The solution of the differential equation describes a nonlinear oscillator. This approach has been applied only across a significant portion of the parameter space. The primary parameters of interest for acoustic signal are the amplitude and frequency. Except for empty bubble, closed analytical solutions to the above bubble models remain unknown. On the other hand, numerical solutions can be obtained. The bubbles produce the acoustical signal starting from some initial condition. Finally it reaches a steady state condition as determined by damping of the medium. Apart from steady state oscillation the bubbles may produce many sub-harmonics [151]. The period of a sinusoidally driven bubble can become infinitely long. The resulting oscillations become in never repeating oscillations known as deterministically chaotic oscillations. This chaotic oscillation raises many question about the oscillations. Like, how a deterministic oscillator subjected to periodic force can produce such non-repeating behaviour. This phenomenon is explored in dynamical systems theory. This theory also offers methods for effectively visualizing deterministically chaotic oscillations [152]. The main question is the origin of the chaotic oscillations, which can be explained by the dynamical theory of the system. The common feature of the dynamical system is the period doubling or frequency halving. At this time the control parameters characterizing the system are varied. For a linear system, the amplitude of the steady state oscillation shows only one maxima at the resonance when the damping is sufficiently low. The main resonance of the

nonlinear oscillator begins to shift toward higher or lower resonance frequencies. For infinitely small oscillations, the bubble resonates at some frequency known as the linear resonance frequency and the most simple one is represented by Equation 2.11 calculated by Minnaert [95]. The more accurate one shown in Equation 2.12 has been calculated from the Rayleigh-Plesset, Gilmore and Keller-Miksis model. The properties of bubble oscillation are not fully explored because of the effect of a large number of parameters and their combined effect. The oscillation of a bubble can be studied by different ways. Few of them are pure oscillation or with damping from heat conduction, mass diffusion, and sound radiation. The nonlinear oscillations of gas bubbles in liquids have been studied with different parameters space by Prosperetti and co-worker [153–159]. The theoretical steady state solution and stability have also been studied in this literatures. Investigation of bubble dynamics in boiling liquids are associated with many complex process. The origin of the complexity lies in the nonlinear growth of bubbles and also the nonlinear processes involved in nucleation and boiling. Many experimental and numerical studies on bubble dynamics are carried out. These studies offer multiple empirical and semi-empirical relationships for the estimation of bubble dynamics parameters. As most of the processes of nucleation are fundamentally nonlinear. The nonlinear chaos dynamics provides valuable insights into the underlying mechanisms through detailed analysis. This allows an understanding of the dynamics of the phenomena and to quantify their complex characteristics measure using this new form of dynamics. This approach helps us to find the nonlinear parameters associated with nucleation and clarifies the dynamic process of bubble oscillation that gives the observable behaviours.

2.7.1 Response curves

The response curve describes the peak value oscillations as governed by driving frequency. In a linear system, the amplitude response curve of the steady state oscillations is plotted by the amplitude of the oscillations and driving frequency. For a small damping condition at resonance the response shows one maxima. In the case of nonlinear oscillators the primary resonance shifts toward higher or lower frequencies. There exists a more steady state solution at the same driving frequencies with different initial conditions. These steady state solutions are known as attractor. The other resonances frequencies are the multiple of some linear frequency. The number may be a rational or near rational number. These frequencies are known as harmonic resonances, sub-harmonic resonances and ultra-harmonic [151], these phenomena is known as period doubling and may originate chaos [160]. The bubble radius acts as a reference to understand the oscillatory behaviour of the bubble by a radius response curve. In radius response curves, the radius has been plotted instead of frequency response curves [161, 162]. Similar response diagram is obtained with harmonic, sub-harmonic and ultra-harmonic resonances. This is because Minnaert's linear resonance frequency is inversely proportional to the corresponding bubble radius at rest.

2.7.2 Chaos in bubble oscillations

The bubble oscillation repeats many features like, two periods for same driving frequency are known as period doubled oscillations. The period doubled oscillations are present besides the steady state oscillations. Never repeating oscillations and the pe-

riod of a sinusoidal driven bubble can increase indefinitely. This may be considered as deterministically chaotic oscillations. The deterministic oscillator with periodic force is the origin of never repeating oscillation. Visualizing the essential characteristics of chaotic oscillations by the radial oscillations of a bubble is difficult. The dynamical system theory investigates this type of questions and provides for best visualizing deterministically chaotic oscillations [152]. The Poincare section through the state space in this case is the only plot that can image the chaotic oscillation called a strange or chaotic attractor. The origin of chaotic bubble oscillations can be explained by dynamical systems theory. The period doubling is the one of the simplest and common ways for this explanation. Oscillations along the period doubling are the route of chaos. The common methods to characterize a nonlinear oscillation are Poincare section plot. The power spectral density as a function of frequency is also an important tool. The Poincare section plot shows just a single point and the power spectrum represents the harmonics. The power spectrum of a chaotic oscillation must be continuous. The spectrum contains many fine lines which look like a noise spectrum. These fine lines are intrinsic noise from a deterministic system. The radius of a oscillating bubble corresponding to each driving frequency can be plotted and the plot were analysed further at a given phase of the driving oscillation and shows that period doubling is the origin of chaotic oscillations. The degree of chaotic nature of the oscillation can be quantified. The spectrum of numbers can be calculated by the Lyapunov exponent spectrum [163]. For periodic oscillations the maximum Lyapunov exponent is lower than zero. The maximum Lyapunov exponent when greater than zero, the system exhibits chaotic behaviour. An investigation has been performed using Keller–Miksis model [164], which shows that the maximum Lyapunov exponent

approaches zero. In this case the oscillation approaches to a period doubling point. There will be chaotic oscillations when the maximum Lyapunov exponent becomes positive. The sensitivity to the initial conditions can be measured by the largest Lyapunov. This analysis gives more information about the oscillations in the context of bubble dynamics [165]. The period doubling of oscillations can be directly visualized by the Fourier analysis. The Fourier spectrum contains the frequencies that indicate the sub-harmonic in the oscillation. Fourier analysis can directly confirm the steady state and chaotic oscillations [165, 166]. The complete properties of bubble oscillations are difficult to understand because of many parameters present in the system. One of the simplest approaches to understand pure oscillations is with specific sets of parameters. In this approach heat conduction, sound radiation and mass diffusion are considered as a damping mechanism. Prosperetti and co-workers have done theoretical work to understand the complete process [153–159]. Behnia et. al. computed a series of bifurcation diagrams to understand the bifurcation behaviour of spherical bubble oscillators [167]. Hydraulic oil [168], Powell–Eyring fluids [169] and polymer solutions [170,171] have been used to understand the bubble oscillations and its frequency response curves.

2.7.3 Chaos in nucleation

As we know, nucleation primarily means the formation of new phases. Heat transfer is an important process for nucleation. The initial processes of nucleation start after absorbing heat. The site interaction in the case of nucleation at the interface of liquid is the most complex process. There are many other types of interaction present in

the complete process like thermal interaction between the nucleation site and with heated walls and hydrodynamic interaction. Two types of hydrodynamic interaction are dynamic interaction between the bubble and the bulk fluid and the hydrodynamic interaction between the bubbles. Some variables may be selected that reflect the complexity of boiling. These variables are not able to give advance information about the nonlinear chaotic nature of billing. The dynamics of the system can show the information of noise in a system and it can be generated from the nonlinearity of the system [172]. The quantification of complexity and the dynamical structure can be understood by the new variable of a dynamics system. The complex behaviours come from the nonlinear elements present in the dynamical mechanism. New approaches to the system can be useful to understand complexities of the system and also give information about the process.

2.8 Experimental studies

2.8.1 Complexity from wall temperature fluctuations

The experiments on the basis of the nonlinear chaotic aspects of boiling are relatively few. The chaotic nature can be explained by temporal or spatio-temporal information of the system. The wall temperature fluctuation has been measured in many nonlinear experiments. The nonlinear analysis on the wall temperature fluctuation can clarify the dynamic mechanism of the system. This information yields the observed complex behaviours and conjugate processes of the boiling system. The complexity

of boiling has been studied in a compact and simplified setup by Shoji et. al. [173]. In this experiment a platinum wire has been used to boil water under atmospheric pressure. This wire acts as a heater and sensor for the measurement of the temperature of the boiling system. The information of the hydrodynamic features in the different regimes were observed by a high-speed video camera. The Fourier spectrum and attractor have been reconstructed using the embedding method. All the analysis was done on the temperature fluctuations to understand the nonlinear nature of the process. The fractal dimension of the attractor has been estimated by the technique of Grassberger and Procaccis [174]. The broad band power spectrum of the temperature fluctuations confirms chaotic behaviour. This chaos is involved in the boiling and the fractal dimension shows that the level of complexity is high.

The origin of these nonlinear effects and chaos are not clarified. Kenning and Yan measured the local instantaneous temperature distribution by a horizontal steel plate at atmospheric pressure [175]. The temperature was collected using a crystal thermometer and a high speed video recording was done from the back side of the heater. The wall superheat distribution at any instant of time during bubble nucleation and growth is confined in a circular region. This circular area was chosen in such a way that it corresponds to the largest visible surface area of the bubble. The evaporation of the liquid is agreement with the heat absorption from the surroundings. The rate of heat absorption considerable deviated below the expected value from the model by bulk liquid. The wall temperature fluctuations at individual sites were observed. The obtained result and site characteristic reflects that nucleation is influenced by

the instantaneous superheat at the wall.

2.8.2 Local spot characteristics

The detailed temperature information is important information for more details and extended nonlinear analysis. The time averaged temperatures have been collected from the experiment. The high resolution temperatures have been collected using micro thermocouples. This thermocouple was located on a heated surface in the experiment by Shoji et. al. [176]. The power spectrum from the Fourier series and attractor reconstructed of the time series using the embedding method confirms the nonlinear characteristics of the boiling system. Temperature fluctuations show different aspects or modes. One of the mode with small amplitudes and high frequencies and another one with large amplitudes and low frequencies was detected. The correlation dimension and the maximum Lyapunov exponent were estimated from the temperature fluctuations. The technique of Wolf et. al. [177] was used in the calculations of these parameters. The positive maximum Lyapunov exponent supports the existence of chaotic behaviours. Another experiment with a smaller heated disc by Shoji et. al. [176] also showed the similar results.

2.8.3 Radiation thermography

There are many ways to measure the wall temperature, one of the possible ways is to use a radiation thermometer. There are many difficulties to measure the details temperature and the accuracy of the data, it is compromised by the limited capability

and resolution of traditional thermometers. Some experiments have been done by Shoji and his co-workers. Satisfactorily measured the spot temperatures and line temperature distributions using the developed equipment [178,179]. The existence of low dimensional chaotic dynamics has been shown by this experiment. The results also indicate that even simple systems can exhibit rather complicated features. The complexity of the system increases with the increasing scale of the system.

2.9 Models of nonlinear nucleations

Modelling of the nonlinear nature has been attempted using a wide variety of topics. These modelling focus on the configuration of the boiling system, associated modes, and their transitional behaviour. These studies are purely based on the theoretical and qualitative measurement that can be determined. The origin of chaotic features using simplified dynamical models has been addressed in some of the models. Large numbers of models have been explored to understand the hydrodynamic behaviours of bubbles. The actual underlying processes and interactions can also be explained by modelling. Improving the understanding of the complex system is to use simplified minimal models and the fundamental nature of the phenomena. A highly idealized theoretical model like the coupled map lattice method was proposed by Yanagita [180,181]. The qualitative nature of complex spatio-temporal systems can be studied by this method. This technique can also be used for nonlinear analysis along with statistical processing techniques. In the model by Yanagita, the whole phenomena decomposed into thermal convection, bubble generation, and phase change

dynamical processes. The time varying parameters of the different processes have been successively carried out. In this model the temperature was started by a small uniform random number. The maximum Lyapunov exponent was calculated. They concluded the presence of spatio-temporal chaos in the system. Here, the mode that is considered for the modelling is a homogeneous nucleation phenomenon. In the case of homogeneous nucleation the model permits liquids to vaporize in bulk. In the case of superheated liquid the homogeneous nucleation shows the chaotic nature discussed in the next chapter 3 and these chaotic nature can be modelled in a similar way like heterogeneous nucleation.

Chapter 3

Nonlinear behaviour of the homogeneous nucleation

A research paper based on the work presented in this chapter has been published in "Nuclear Instruments and Methods in Physics Research A, 2023, **1057**, 168777".

3.1 Introduction

The boiling of liquid and nucleation are a common phenomenon through the underlying mechanism of boiling is still not fully understood because of the complexity of the process. In these cases, mutual interaction between bubbles and the heating surface and interaction with neighbouring nuclear sites play important roles. The complexity level is high because the interactions create a complex dynamical system that includes many processes like heat transfer, phase change, coalescence and their combined effects. Nonlinear dynamical systems under selected conditions are able to show chaos [176, 182]. A system is said to be chaotic where the output is not proportional to the input, and under some conditions, such systems exhibit unpredictable long-term behaviour. Irregularity of motion and sensitivity to the initial conditions are the key signatures of the chaotic system. A computer simulation with appropriate mathematical tools can confirm the experimentally observed chaotic behaviour of a system. However, the chaotic behaviour of an experiment can be directly identified from experimental data using nonlinear time series analysis. There is not enough

literature available on the nonlinear dynamical behaviour in the acoustic signature of the bubble nucleated signals and the nucleation process. In this chapter, nonlinear time series analysis methods have been used to identify the chaotic behaviour of the homogeneous nucleation of superheated liquid droplets from the acoustical signals produced during nucleation. The nonlinear analysis has been carried out on acoustical signals from the homogeneous nucleation of superheated droplets by neutrons and gamma-rays. The analysis shows the existence of chaos and the characteristic differences have been observed in the neutrons and gamma-rays induced signals. An attempt has been made to explain these observations by the nonlinearity of the energy disposition by the recoil nuclei and the electrons.

3.2 Fabrication of SED

The SEDs contain the droplets of the refrigerant liquid and the boiling point of these refrigerant liquid is very low. The sizes of the droplets are in the order of micrometers. These droplets are suspended in an immiscible visco-elastic gel medium. The gel medium holds the droplets and the gel matrix should be degassed to remove air bubbles and gas pockets. As a result the droplets of superheated liquid can stay in the metastable state and can reduce heterogeneous nucleation of the liquid droplets. The quality of the gel matrix is an essential criteria to get stable SEDs. The whole process of SED fabrication can be divided into the following steps: gel matrix preparation, degassing of the gel matrix and formation of the superheated liquid droplets. After fabrication, the radius of the droplets were measured and the

distribution of the radius of the droplets gives the quality of the SEDs. The complete processes of each step of the fabrication of SEDs have been discussed below.

3.2.1 Gel matrix preparation

The preparation of the gel matrix is the first step of the fabrication of SED. The droplets of the superheated liquid are suspended in the gel matrix. The gel matrix has been prepared by the mixture of glycerine and ultrasound gel in an appropriate proportion. The suitable proportion of the glycerine and ultrasound gel produce a smooth medium and it also reduces the possibility of heterogeneous nucleation. The mixture should provide a visco-elastic medium that allows the liquid droplets to expand and become a vapour bubble. In the present fabrication 400 ml of glycerine and 100 gm of ultrasound gel were mixed in a clean conical flask. The glycerine and ultrasound gel inside the conical flask was placed on a magnetic stirrer for 30 minutes to mix the glycerine and ultrasound gel. After the mixture it was ready for the degassing process.

3.2.2 Degassing of gel matrix

The air pockets were trapped in the gel matrix during the mixing when it was placed on a magnetic stirrer. These air pockets should be removed from the gel matrix. The conical flask that contains the gel matrix was connected to a vacuum pump to extract the trapped air pockets. This process is known as degassing of the gel matrix. This process was continued for three to four days to get a smooth and air pockets free gel

matrix. After completing one day the gal matrix was heated up to a temperature around 50 ^oC during degassing. The next two to three days the degassed process was done and after that it will be ready for the detector fabrication.

3.2.3 Preparation of superheated droplets

The degassed gel matrix was transferred inside a stainless steel autoclave and kept inside the refrigerator over the night before the fabrication of SED. Next day the autoclave was kept in pressure tight condition upto the saturation vapour pressure of the liquid. The refrigerant liquid was transferred inside the autoclave containing the degassed cold gel matrix. The amount of the active liquid in SED was 7.6 % of the total gel matrix. The percentage of active liquid of a SED is defined as the loading factor. The autoclave that contains the gel matrix and refrigerant liquid under pressure was stirred. This process was done by the stainless steel blades inside the autoclave which were connected to an electric motor. The speed of the stirring blades can be controlled and within a few minutes the speed reaches to a steady value which is 1400 rpm and it was done for a duration of 5 minutes. This produces droplets of the superheated liquid which are distributed inside the gel matrix. The distribution of the radius of the droplets depends on the speed of the stirring blades and the duration of rotation. The whole process of stirring was done by maintaining the pressure of the autoclave same as the liquid's saturation vapour pressure. The autoclave was kept for one hour inside an ice bath and the pressure was slowly released from the autoclave at a constant temperature to achieve the superheated state. Finally, the superheated droplets with the gel matrix were poured into clean borosilicate glass

vials and it was kept in the refrigerator for a few days. Several SEDs were fabricated using the $R-134a$ refrigerant liquid and these detectors have been used for all the experiments.

3.3 Experiment

The fabricated superheated emulsion detector by $R-134a$ superheated liquid has been used in the experiments. The Figure 3.1 is the schematic diagram of the present experimental setup. The actual experimental setup is shown in Figure 3.2. The Figure 3.2.A represents the experimental setup without the radioactive source. Figure 3.2.B represents the arrangement of the detector and the radioactive source. The SEDs were stored in low temperatures for the stability of the detector. The SED was removed from low temperatures and kept at room temperature for 30 minutes then the detector is placed inside a water bath which is surrounded by a heating coil. A temperature controller (METRAVI, DTC 200) with precision $\pm 1\ ^oC$ connected with the temperature sensor and a heating coil. The heating coil wound around the water and it is used to increase the temperature of the water bath and the temperature sensor is put inside the water of the water bath. The signals from the homogeneous nucleation of the superheated droplets were collected by a sensor (AE – WSα by Physical Acoustics Corporation) (frequency range few kHz to 1 MHz). The sensor was placed on the top of the detector and it was kept in such a way that it remained in contact with the gel matrix of the detector. The sensor converts the acoustical signals into electrical signals and those electrical signals having amplitude greater than 40

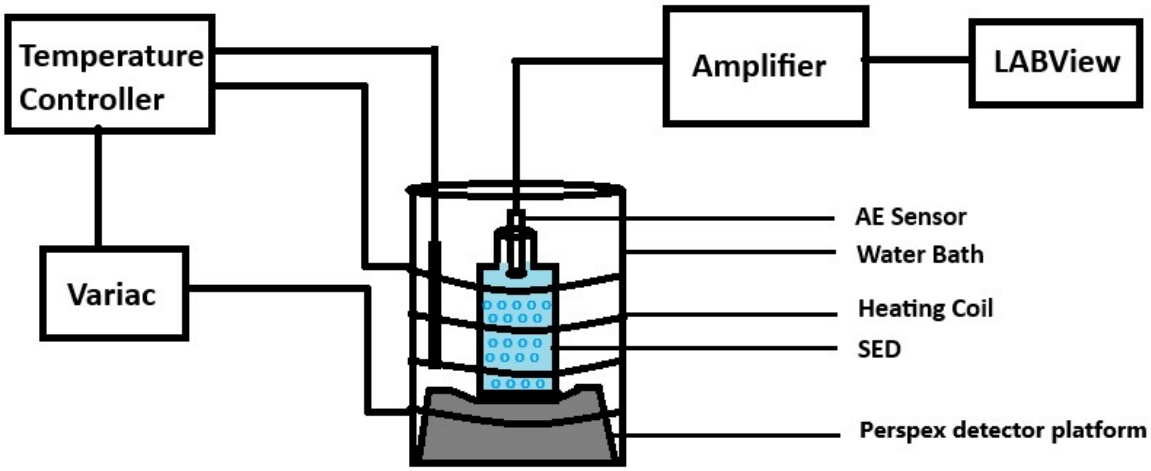

Figure 3.1: Schematic diagram of the present experimental setup.

mV were collected. The threshold voltage of 40 mV was set to minimize the electrical noises and the electrical signals were stored by LabVIEW hardware and software. The SED was irradiated separately with $^{241}Am-Be$ (10 mCi) neutrons and ^{137}Cs (5 mCi) gamma-rays sources. The responses of SEDs were studied and the signals from nucleation in the presence of $^{241}Am-Be$ (10 mCi) and ^{137}Cs (5 mCi) sources were collected at different temperatures. All the experiments in the presence of ^{137}Cs (5 mCi) were done at temperatures above $38.5^{o}C \pm 1.4\ ^{o}C$ as R-134a becomes sensitive to gamma-rays above this temperature [18].

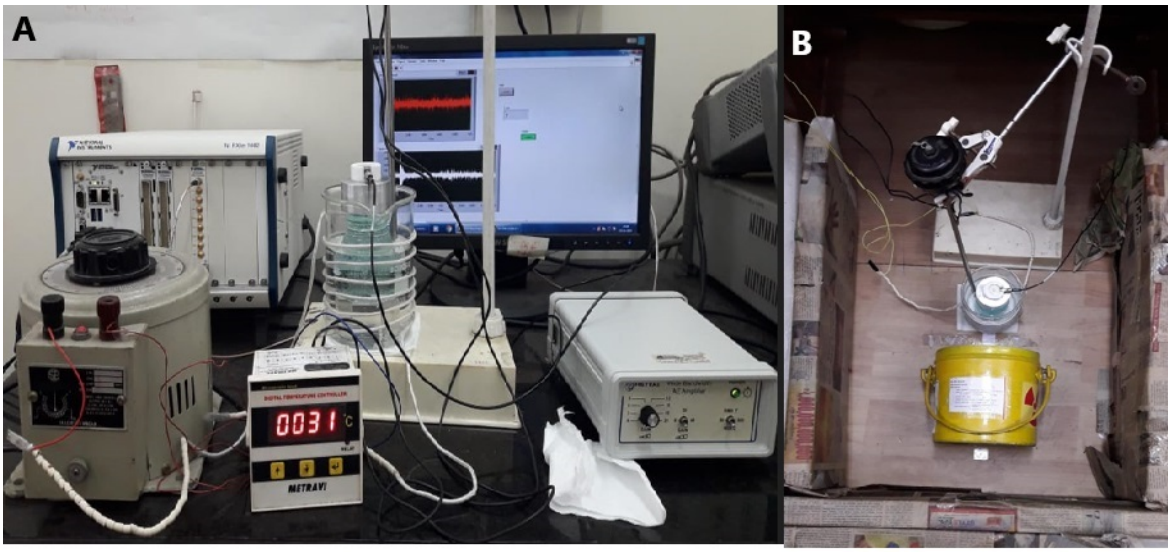

Figure 3.2: Experimental setup of the present experiments.

3.4 Nonlinear analysis techniques

The classical nucleation theory provides estimates for the energy barrier, critical bubble radius and nucleation rate. A comprehensive and exact solution is challenging due to the complex thermal and hydrodynamic interactions. These interactions are further complicated because of the existence of the nonlinear convection factors in the momentum and energy equations [183, 184]. The nucleation phenomenon can be understood experimentally by the nonlinear analysis of acoustic signals. The methods used in this analysis of the acoustical signals (see Figures. 3.3 and 3.4) are described below.

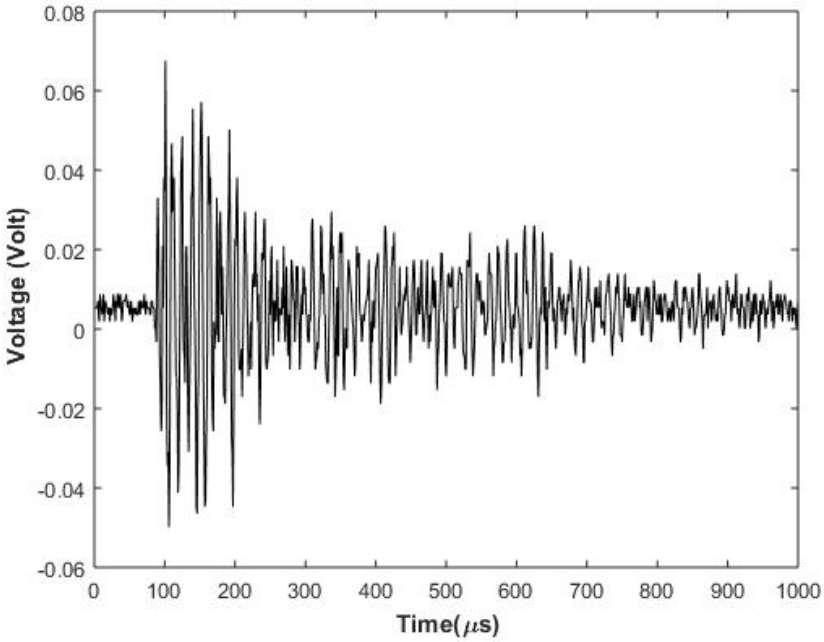

Figure 3.3: Bubble nucleated signal by neutron induced nucleation.

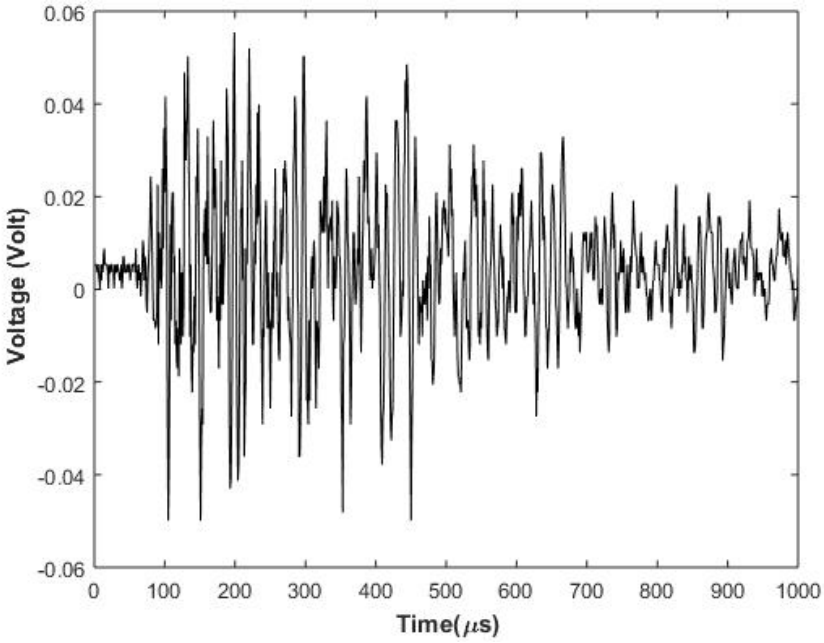

Figure 3.4: Bubble nucleated signal by gamma-ray induced nucleation.

3.4.1 Attractor Reconstruction

The state space also known as the attractor is reconstructed as a first step in nonlinear analysis. No prior information about the system was required for the estimation of the attractor. Important information of the chaotic behaviour of the time series was provided by the 3D attractor reconstruction of an experimental time series. The attractor has been constructed by the embedding theorem [185]. According to the theorem proposed by Hegger et al. [186], if x_i represents the sequence of measurements of a state of a system. The embedding vectors are formed as $x_{i+\tau}$, $x_{i+2\tau}$ and $x_{i+3\tau}$, where τ denotes the time delay of the reconstructed attractor. In the present case, the 3D attractor was reconstructed by selecting the embedding space method. Variable sets of $x(t)$, $x(t+\tau)$ and $x(t+2\tau)$ have been used. The time delay (τ) was determined as the time corresponding to the first local minimum of mutual information in the time series [187]. This mutual information has been widely utilized to find the value of τ in the experimental time series. At first, the bubble nucleated signals were filtered using a 15 kHz to 150 kHz band-pass filter. This filtration removed very low and high frequency noises. The values of τ were determined to be 3 μs and 4 μs for the neutron and gamma-ray induced signals respectively. The attractor reconstruction of these filtered acoustical signals from neutron and gamma-ray induced events is illustrated in Figures 3.5 and 3.6. The structure of the attractor indicates that the bubble nucleated signals exhibited chaotic oscillation and it shows the presence of chaos in the homogeneous nucleation of superheated liquid droplets. Comparing the 3D attractors of the neutron and gamma-ray induced signals, the differences in the line density of trajectories and the convergence patterns of the curves have been

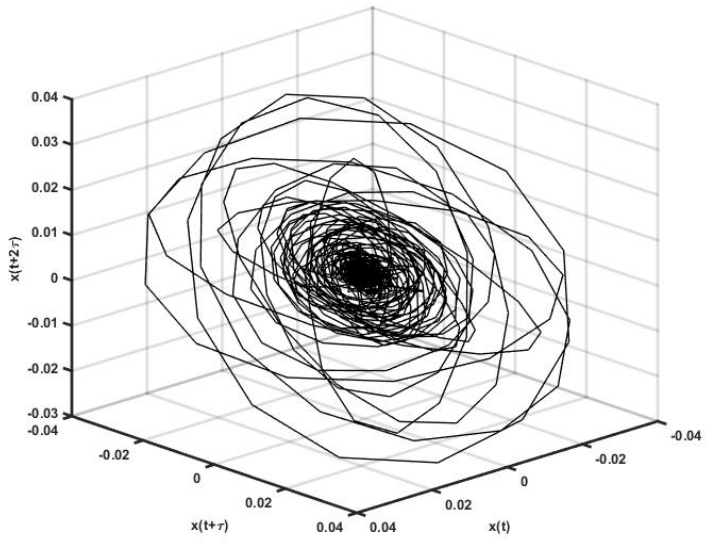

Figure 3.5: 3D attractor reconstruction of bubble nucleated signal by neutron induced nucleation.

observed. The trajectory of the gamma-ray induced signal was found to form a more complicated pattern than that of the neutron induced signal. The 3D attractor of the neutron induced signal systematically converged toward the center. The 3D attractor of the gamma-ray induced signal did not display such a converging pattern. The converging behaviour of the 3D attractor implies that neutron induced bubbles were more stable than gamma-ray induced bubbles.

3.4.2 Fast Fourier transformation

Fast Fourier Transformation (FFT) has been utilized to analyze the frequency spectrum of bubble nucleated signals. The results are represented in the Figures 3.7 and 3.8. The periodic oscillations is represented by frequency spectra displaying sharp

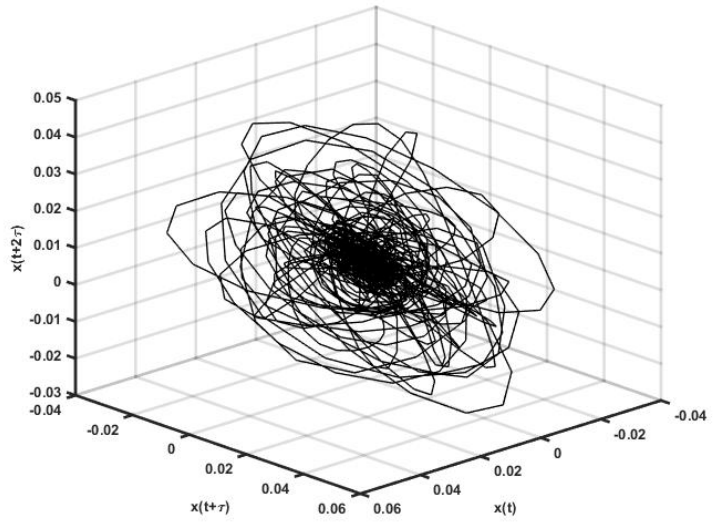

Figure 3.6: 3D attractor reconstruction of bubble nucleated signal by gamma-ray induced nucleation.

peaks indicative of specific frequency [184]. Whereas a continuous frequency spectrum indicates chaotic or quasi-periodic oscillation. In the present analysis both neutron induced and gamma-ray induced signals exhibit peaks with irregular frequency intervals. The spectrum of gamma-ray induced signal is distributed over a significantly broader frequency band. According to the analysis by Baker and Gollub, the chaotic behaviour is present within the system [184]. To establish these observations Lyapunov exponents have been calculated from the signals discussed below.

3.4.3 Lyapunov exponent

The Lyapunov exponent is a widely recognized parameter and it characterizes the nonlinear properties of attractors and serves as a critical diagnostic tool for chaotic

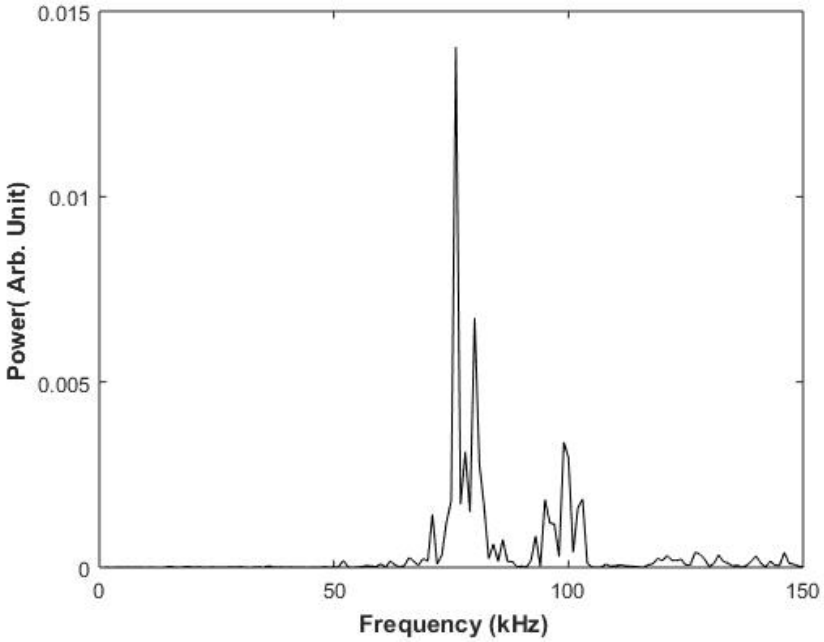

Figure 3.7: FFT of the filtered bubble nucleated signal by neutron induced nucleation.

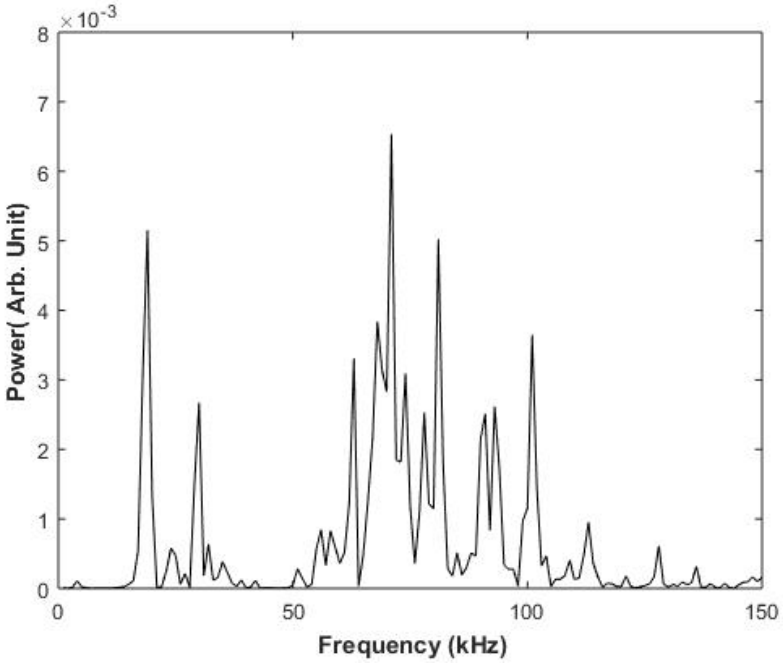

Figure 3.8: FFT of the filtered bubble nucleated signal by gamma-ray induced nucleation.

systems [188]. It provides a quantitative of the sensitivity of the system for the initial conditions. It describes how trajectories in phase space either diverge or converge over time [188]. In phase space, any two points x and x + Δ x, vary as functions of time and their separation (Δx) also depends on time. The Lyapunov exponent is formally defined as the average exponential rate at which two initially close trajectories diverge and it is expressed in Equation 3.1. The exponential divergence means the system behaves differently, whose initial differences are not able to resolve. A straight forward method exists to estimate the Lyapunov exponent for a systems with explicitly defined equations of motion but this approach can not be applied to experimental data. The one dimensional Lyapunov exponent is calculated using Equation 3.1. The sign of the Lyapunov exponent gives the information of the dynamic system. A chaotic system should have at least one positive Lyapunov exponent. In the case of the signals of the present study, the largest Lyapunov exponents were determined to be 13.60 for neutron induced signal and 8.34 for gamma-ray induced signal. The positive values of these exponents show that the presence of chaos. This finding suggests that periodicity is lost during the processes of bubble nucleation. The signal generation shows a chaotic nature present in the acoustical signals and the process of bubble nucleation.

$$\lambda = \lim_{t\to\infty} (\frac{1}{t}) \ln \frac{\Delta x(t)}{\Delta x(0)} \tag{3.1}$$

3.4.4 Rescaled Range analysis

The rescaled range denoted as R/S has been considered as a fundamental tool in fractal analysis. It has been applied in many disciplines to analyse the signals, originating

from different types of probes. The signals exhibiting self-similar scaling properties and the R/S ratio of the signal follows a power-law relationship with the window size (n) [189]. The Hurst exponent quantifies the persistent or anti-persistent behaviour of a time series and also determines whether the series has random or long-term memory characteristics. The R/S value of the time series can be estimated from Equation 3.2.

$$\frac{R(n)}{S(n)} = \frac{max(0, W_1, W_2, .., W_n) - min(0, W_1, W_2, .., W_n)}{\sqrt{S^2(n)}} \tag{3.2}$$

$$W_k = x_1 + x_2 + x_3 + ... + x_k - k\overline{X(n)}, \tag{3.3}$$

Where, $\overline{X(n)}$, $S^2(n)$ and n are mean, variance, and time lag of the signal respectively. For a periodic system the slope of R/S eventually saturates and begins to oscillate. The point of oscillation indicates the frequency of the signal. The value of the Hurst exponent for a purely random and a purely periodic time series are 0.5 and 1, respectively and for chaotic systems the Hurst exponent lies between 0.5 and 1. Hurst exponent reflects the temporally aperiodic nature of the signal. The bubble nucleated signals from neutron and gamma-ray were analysed and their Hurst exponents were calculated. The results show two different features of slopes among the neutron and gamma-ray induced signals. For the neutron induced signal (see Figure 3.9) the R/S plot shows two distinct regimes with slopes of 0.95 and 0.11. The initial slope of 0.95 indicated strong correlations and persistence (conservation of current trends) in the oscillations of the neutron induced signal. Over time the slope has decreased and reached to 0.11, which signifies anti-persistence (fluctuation or frequency reversal trends). In contrast, the slopes of the R/S plot for the gamma-ray

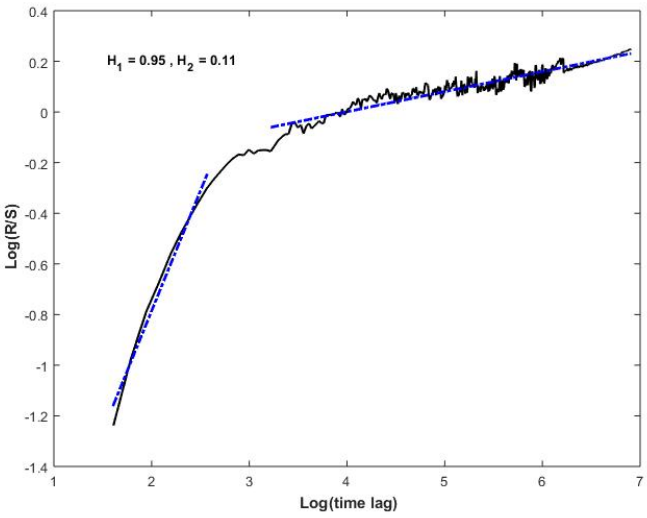

Figure 3.9: R/S analysis of bubble nucleated signal by neutron induced nucleation.

induced signal is different across different points and finally approaches zero as the time lag increases. Hence, neither persistence nor anti-persistence could be definitively identified for the gamma-ray induced signal (see Figures 3.10). The origin of the observation of the neuron and gamma-ray induced nucleation can be discussed by the origin of the nucleations mechanism. The surface temperature of the heating surface determines the nuclear boiling of a single vapour bubble. Chaotic behaviour is observed as there are local fluctuations in heat flux from the nuclear boiling of R - 114 liquid [190]. The changes in local temperature increases with rising surface temperatures. It was explained by R. Mosdorf [191] that chaos originates in pool boiling due to the nonlinearity of heat transfer. In the present analysis of homogeneous nucleation of superheated liquid droplets in both neutron and gamma-ray induced signals chaos has been identified. The nucleation of R-134a liquid droplets originates from the energy deposited by recoiling nuclei or electrons. The LET (Linear Energy

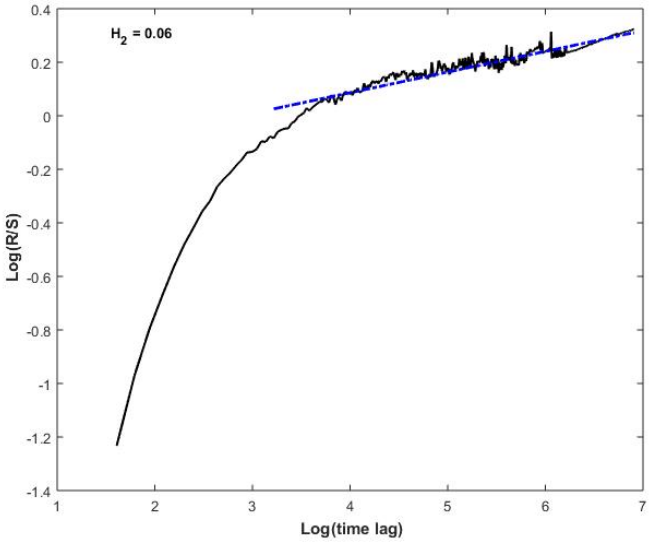

Figure 3.10: R/S analysis of bubble nucleated signal by gamma-ray induced nucleation.

Transfer) or stopping power (dE/dx) of the recoiling nucleus and the electrons from neutrons and gamma-rays in R-134a liquid droplets is shown in Figures 3.11 and 3.12 respectively. The LET of the recoil nucleus in R-134a liquid has been calculated [192] using the SRIM 2008 code. While Bethe's equation has been used to calculate the stopping power of the electron [3, 193]. The nonlinear nature of the LET or dE/dx of the recoil nuclei and electrons are observed in Figures 3.11 and 3.12. This nonlinearity contributes to chaos in neutron and gamma-ray induced nucleation. This nonlinearity that attributes the origin of chaos generated from the nonlinear nature of heat or energy transfer in homogeneous nucleation is similar to other types of boiling. Except from the presence of chaos, the differences between neutron and gamma-ray induced bubble nucleated signals have been observed in the 3D attractor reconstruction, FFT and R/S plots. These differences arise from the distinct nucleation mechanisms of neutrons and gamma-rays, as recoiling nuclei from neutrons and

electrons from gamma-rays deposit energy along their paths inside the droplets. The vapour bubbles are generated if nucleation conditions are satisfied. Approximately one droplet is nucleated along the track of recoil nuclei (H, C,and F). In other cases the electrons nucleate about 11 droplets due to the larger range [194]. A recoil nucleus generates a single bubble from a droplet along its track when nucleation conditions are satisfied. Conversely in the case of gamma-ray, the electrons can produce many bubbles when any droplet along the track satisfies the nucleation conditions and these bubbles may merge with others along the path. The bubble nucleated signals from neutrons carry information about a growing bubble originating from a single droplet. The gamma-ray induced signals give information about bubbles that merge along the track. This merging is the origin for the crowded attractor, broadband frequency spectrum, and the R/S plot without persistence in gamma-ray induced signals.

3.5 Conclusion

The nonlinearity of acoustical signals from neutron and gamma-ray induced bubble nucleation were analysed. The analysis show the chaotic behaviour in homogeneous nucleation. The chaotic behaviour is confirmed by the positive Lyapunov exponent. The differences between neutron and gamma-ray induced signals were identified through the nonlinear analysis. The R/S analysis shows that the neutron induced nucleated signals initially exhibited long-range persistence, which diminished over time. This behaviour was not detected in the gamma-ray induced signals. The merging of droplets along the track of electrons was found to cause the complex 3D

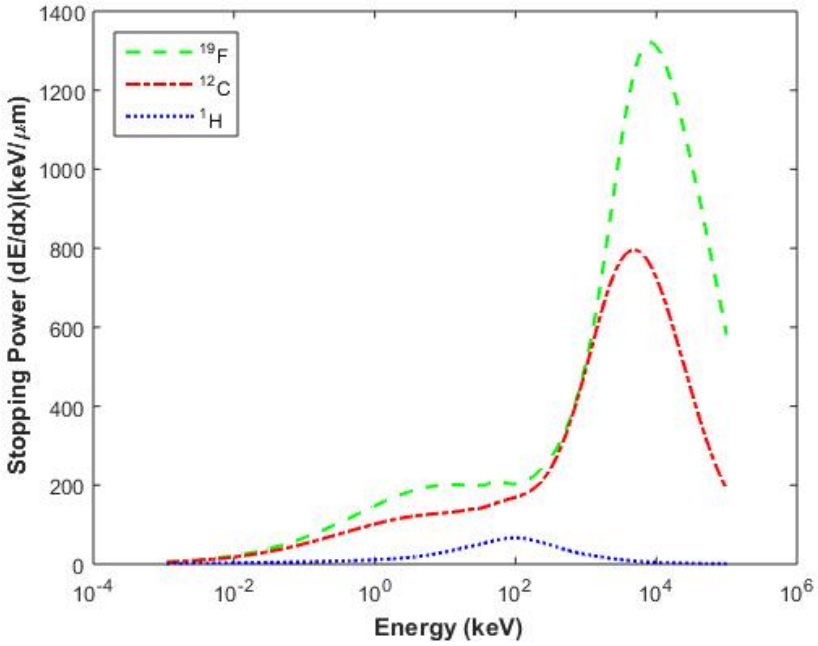

Figure 3.11: Calculated stopping power (dE/dx) of recoil nuclei in R-134a liquid.

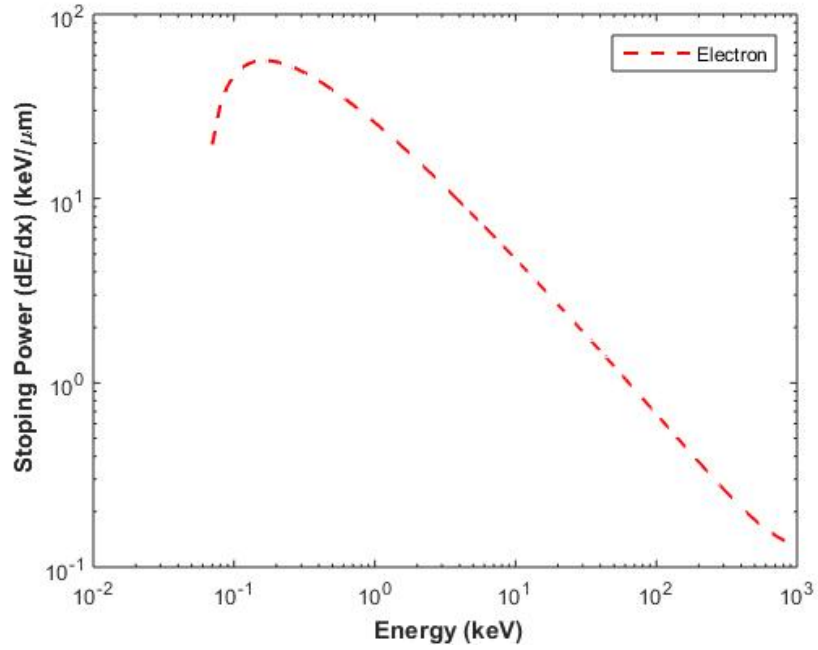

Figure 3.12: Calculated stopping power (dE/dx) of electron in R-134a liquid.

attractor reconstruction, broadband FFT spectrum, and R/S plot without persistence in gamma-ray induced signals. This study contributes to the understanding of chaos in homogeneous nucleation and it also identifies the neutron and gamma-ray induced signals in superheated droplets.

Chapter 4

Discrimination techniques

Part - A: Discrimination techniques of neutron and gamma-ray induced bubble nucleated signals

Research papers based on the work presented in this chapter have been published in "Nuclear Instruments and Methods in Physics Research A, 2022, **1025**, 166186" and "Book - Advanced Radiation Detectors and Instrumentation in Nuclear and Particle Physics, Springer Proceeding in Physics, 2023, **282**, 33 - 38"

4.1 Introduction

As already mentioned in chapter 1 the superheated emulsion detector used as a neutron detector and the active liquids are $R-12$ $(CCl_2F_2; b.p. = -29.8^oC)$, $R-114$ $(C_2Cl_2F_4; b.p. = 3.7^oC)$, $R-134a$ $(C_2H_2F_4; b.p. = -26^oC)$ etc [2, 22]. This detector is also utilized for determining the neutron dose equivalent in the presence of large background. As SED is a threshold detector and the threshold energy of the detector depends on the operating temperature, pressure of the detector and it also depends on the type of liquid inside SED. SED can detect only the neutrons in presence of a gamma-rays background if we make the detector insensitive for gamma-rays. It can be done by simply adjusting the operating temperature and pressure of the detector. d'Errico investigated the photon sensitivity of different liquids by the energy deposition by the electrons produced from gamma-rays. An empirical formula was es-

tablished by d'Errico which states that the midpoint of the boiling temperature and critical temperature would be the gamma-ray sensitive temperature. The bubbles are nucleated by the electron from gamma-ray at their peak ionization energy. SED with liquid $C_4F_{10}(b.p. = -1.9^oC)$, $C_2ClF_5(b.p. = -38.9^oC)$, CF_3I $(b.p. = -21.8^oC)$, etc. are also useful to search the Dark Matter candidate WIMPs (Weakly Interacting Massive Particles). The WIMPs induced nuclear recoils are similar to the neutron induced nuclear recoils [195]. PICO and SIMPLE are two major experiments using the superheated liquid in the detection of Dark Matter. SEDs can be useful in the low mass region of the WIMPs and it can be done by lowering the threshold energy of the detector. The major problem in the detection of low-mass WIMPs region using SED is the backgrounds like neutrons, alpha particles, gamma-rays, etc. The PICO and SIMPLE experiments use many different pulse analysis techniques to identify these backgrounds. These analysis techniques remove them the backgrounds events from the events from WIMPs [196, 197]. The major contributing background at low threshold energy is coming from gamma-rays. The identification of gamma-rays are important to use SED in low threshold condition.

In this chapter, the details of the different discrimination techniques of neutrons and gamma-rays induced nucleated signals have been discussed. The signals used in the discrimination have been collected from the experiments using the SEDs, which have been fabricated at SINP laboratory. These SEDs have been fabricated with $R-134a$ liquid and this liquid also has the ability to detect sub-GeV WIMPs at low thresholds. Also, SEDs with $R-12$ liquid have been fabricated. The experiments with these SEDs have been presented because $R-12$ is a well studied liquid and will be used in the comparative studies. The experiments were carried out in presence of neutrons

and gamma-rays to understand the neutrons and gamma-rays induced nucleated high frequency signals. Efforts have been done to detect the differences between the signals by defining new parameters from the detected bubble nucleated signals.

The complete processes of SED fabrication were described in the previous chapter 3. In the present case all the similar steps were followed to fabricate the detectors. Here two different kinds of refrigerants liquids $R-134a$ and $R-12$ have been independently used to fabricated different SED. Also, two different sets of detectors were fabricated. In the first sets of detector the stirring was carried out with a speed of 900 rpm. In the second sets of detector the stirring was carried out with a speed of 1400 rpm and the stirring was done for 5 minutes for both the rotational speed.

4.2 Experiment

The detector fabrication is the first part of the experiment and the complete processes of SED fabrication were described in the previous chapter 3. Here two different kinds of refrigerants liquids $R-134a$ and $R-12$ have been independently used to fabricate the SEDs. Also, two different sets of detectors were fabricated. In the first sets of detector the stirring was carried out with a speed of 900 rpm. In the second sets of detector the stirring was carried out with a speed of 1400 rpm. In both the sets stirring was done for 5 minutes. The fabricated detectors of R-134a and R-12 have been used in all the experiments presented in the present chapter. Figure 4.1 shows the schematic of the current experimental setup. The SEDs after fabrication were stored at low temperatures to make it stable detector. Before the experiments the

temperature SED was brought to room temperature. During experiments the SED has placed in a water bath connected with a heating coil. The temperature of the water bath was controlled by a METRAVI DTC 200 temperature controller. The accuracy of the temperature controller is $\pm 1\ ^oC$. It is connected to both a temperature sensor and the heating coil wounded around the water bath. The temperature sensor was placed within the water to monitor the temperature of the detector. Acoustic signals from the homogeneous nucleation of the superheated droplets were captured by an sensor (model - AE WSα) from Physical Acoustics Corporation. The sensor has a frequency response from few kHz to 1 MHz. It was placed on the top the detector and maintaining direct contact with the gel of the detector to efficiently capture acoustic signals. The acoustical signals were converted into electrical voltages and only those electrical signals were stored exceeding a 40 mV threshold voltage. This threshold voltage is set to reduce electrical noises. The resulting data were stored using LabVIEW hardware (Model – NI PXIe-4353) and LabView software.

During the experiments each SED was irradiated independently using ^{241}Am-Be (10 mCi) and ^{137}Cs (5 mCi) sources. ^{241}Am-Be acting as a neutron source and ^{137}Cs as a gamma-ray source. SED responses were studied by collecting the bubble nucleated signals at various temperatures for both sources. The experiments involving ^{137}Cs were conducted at temperatures above 38.5 ^oC $\pm$ 1.4 ^oC. As $R - 134a$ becomes sensitive to gamma-rays at temperatures above 38.5 ^oC $\pm$ 1.4 ^oC as reported by Sahoo et al. (2019) [18]. The critical radius and the critical energy required for bubble nucleation has been calculated. The critical radii are 20.09 nm and 8.07 nm

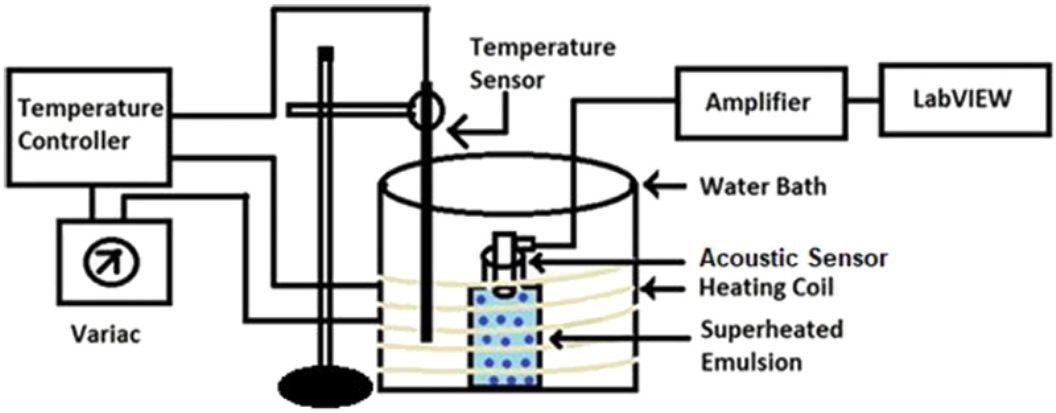

Figure 4.1: Schematic diagram of the present experimental setup.

and the critical energies are 2.87 keV and 0.34 keV at 32 ^oC and 50 ^oC temperatures respectively for R-134a liquid SED. All the parameters have been extracted from the neutrons and gamma-rays induced signals from the experiment.

4.3 Frequency and power emission from bubble nucleation

The droplets vaporize quickly after satisfying the bubble nucleation conditions. The nucleation generates a acoustical wave during the expansion of the bubble. The whole process of nucleation and generation of acoustical wave explained in details in the chapter 1. The vapour bubble oscillates after evaporation and the frequency of the bubble can be determined by Minnaert frequency [95], represented by Equation 2.11. The frequency of the oscillating bubble at any instant is inversely proportional to the radius of the bubble. The evaluation of the radius of the bubble in all the stages of bubble growth as described by Robinson and Judd [47] is represented by

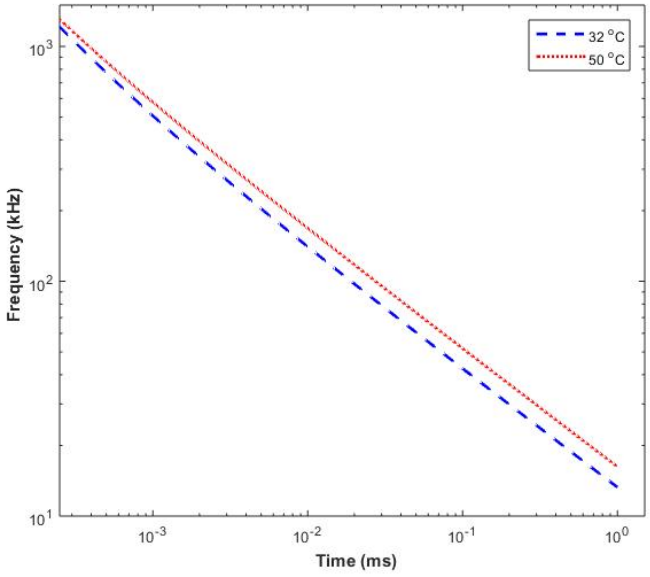

Figure 4.2: The emitted frequency of the oscillating bubble with bubble growth time.

Equation 2.5. The pressure change produced in the liquid at a distance from the growing bubbles are represented by Equations 2.9 and 2.10. The bubbles after nucleation initially produce high frequency oscillations but it starts oscillating with low frequency as it increase its radius with time. The calculated variation of the frequency of the oscillating bubbles at different time is shown in Figure 4.2 at two different temperatures. The Figure 4.2 shows that the bubble at the end of its process starts oscillating with audible frequency. The acoustical power radiated by the bubbles after nucleations is shown in Figure 4.3 as a function of the frequency of the oscillating bubbles. Figure 4.3 shows that at high frequency or at the beginning of the bubble growth, the high power is radiated from the bubble. In the present study the high frequency signals from bubble nucleation have been collected to study the initial phase of the bubble growth.

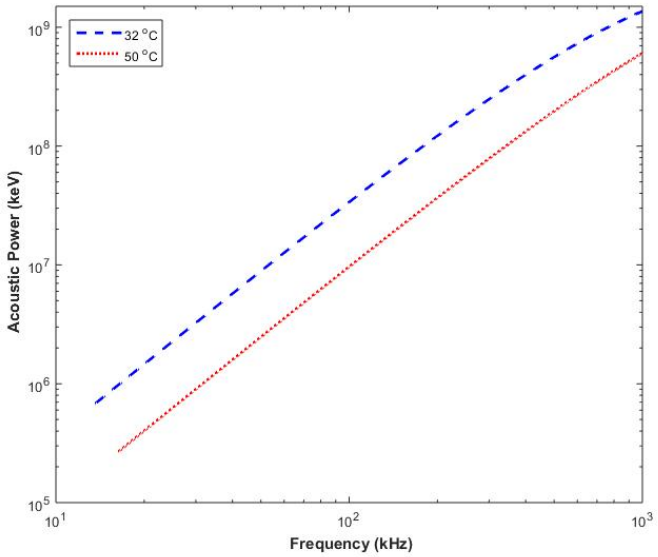

Figure 4.3: The Acoustic Power of the oscillating bubble with the frequency of the oscillation.

4.4 Analysis techniques

The analysis of the bubble nucleated signals can give information which helps to understand the steps of bubble nucleation and identify the particle that initiates the bubble nucleation. Few parameters have been extracted from the signals that are highly irregular in nature but the efforts have been given to identify parameters having some regular patterns. First, the recorded bubble nucleated signals were extracted from all the collected data after removing the noise by eye selection. The typical signals induced by neutrons and gamma-rays in R-134a are displayed in Figures 4.4 and 4.5 respectively. A typical noise is shown in Figure 4.6. Information about the nucleation can be extracted using different parameters estimated from these signals. Parameters like Maximum voltage, Pvar, Time of maximum voltage, Rise time, Fall

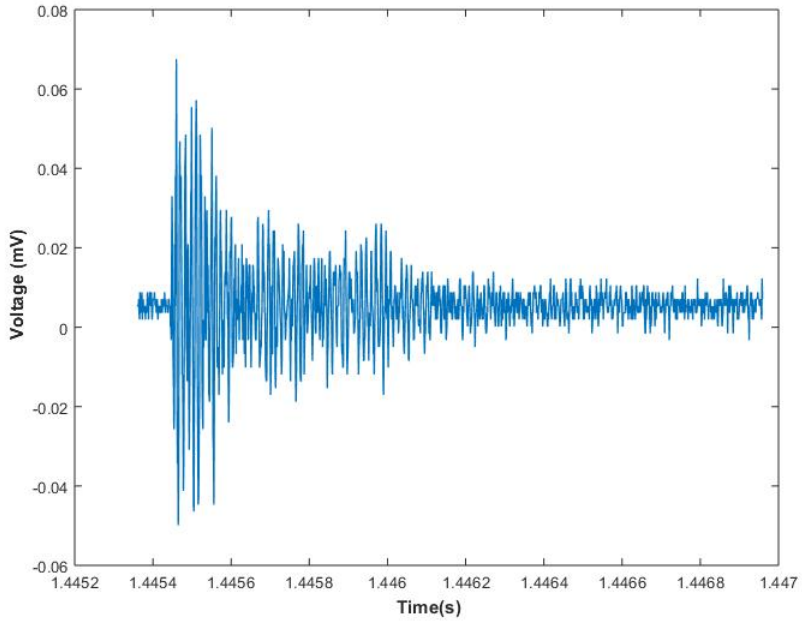

Figure 4.4: Typical neutron-induced bubble nucleated signal.

time of the signals, Duration of the signals and Number of peaks have been extracted from these signals.

The maximum voltage of a signal indicates the strength of the signal and it also represents the energy being transmitted with the signal. In the present case, the maximum voltage gives the information about the energy deposited by the particle for the nucleations. The Pvar of the signal is the more efficient way to understand the energy deposited by the particle. It is defined as the summation of the square of the voltages of the signal. The summation extends over the whole duration of the signals. The typical signals show that the amplitude of the signal after reaching the maximum value reduces and finally it becomes zero. The time when the signals reach the maximum value gives insight into the dynamic behaviour. The overshoot,

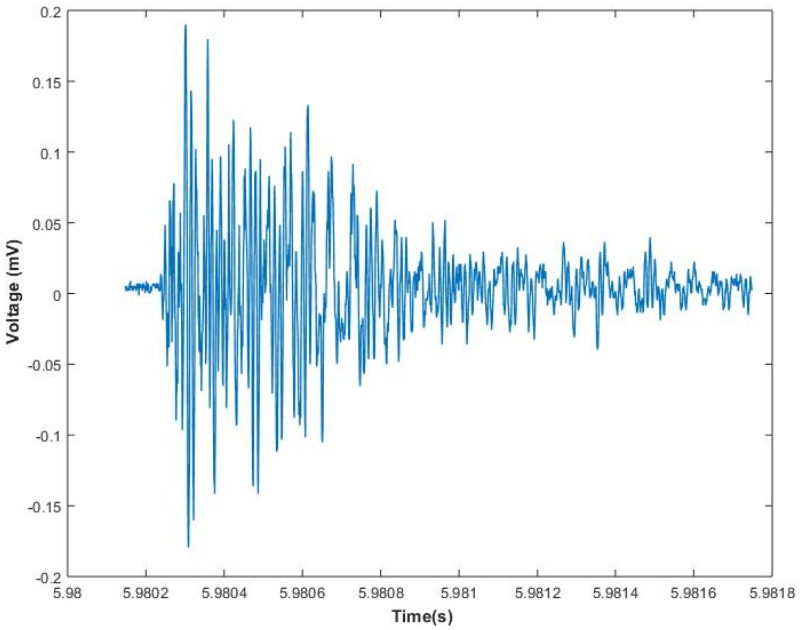

Figure 4.5: Typical gamma-ray-induced bubble nucleated signal.

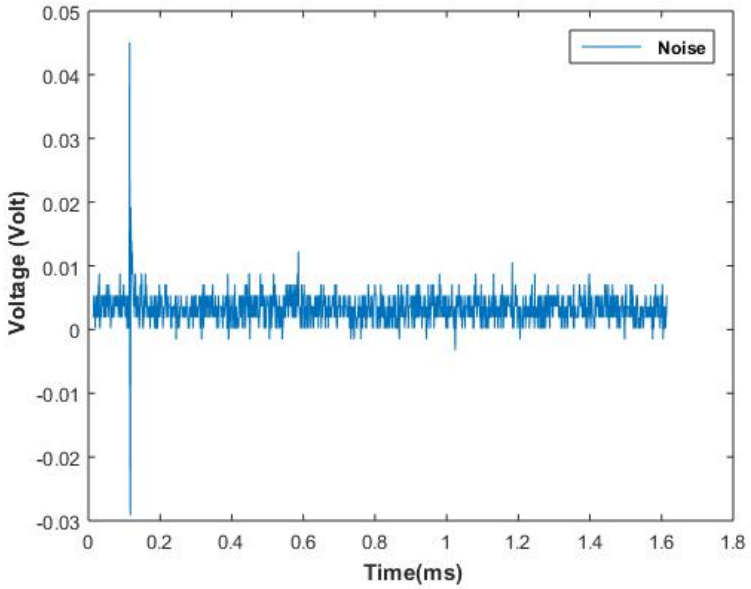

Figure 4.6: Typical noise from SED.

damping and transient performance of a signal can be understood from this time. If a signal reaches its peak value too quickly or too slowly, it may indicate lack of stability. This parameter also determines how quickly a system can respond to the changes; a shorter rise time indicates a fast response. However, excessively fast rise time can introduce high frequency noise and ringing. Fall time is defined from the opposite side of the signal; it is defined as the time after which the signal reaches zero after going through maxima. The duration of the signals has been measured by the difference between the time when it reaches greater the threshold voltage and the time when it reaches lesser the threshold voltage. The small duration may suggest a transient nature of the signal while longer durations could indicate sustained properties of the signal. The numbers of local maxima in the signals above the threshold have been defined as numbers of peaks. This is another parameter to understand the bubble nucleation and identify the particle responsible for bubble nucleation.

4.5 Frequency spectrum

The signals have been analysed in the voltage time domain and also different other parameters have been defined. In frequency spectrum the whole signal has been broken into its constituent frequencies by the Fast Fourier Transformation (FFT). FFT provides the frequency spectrum that reflects the frequency composition of a signal and their power value. The spectrum gives the insights of the signal like its fundamental frequency, harmonic structure, periodicity and other underlying patterns. FFT basically identifies the individual frequency components that combine to form

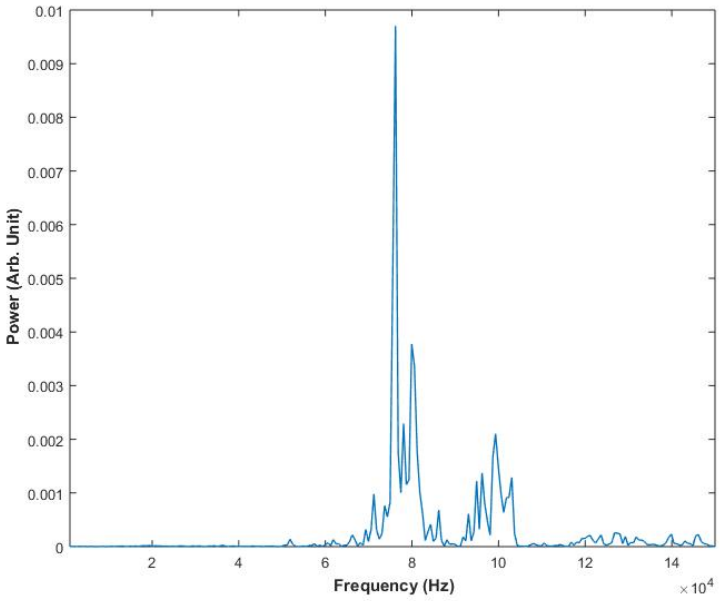

Figure 4.7: FFT of typical neutron-induced bubble nucleated signal.

the overall signal. In the spectrum the x-axis indicates the frequency, while the height of the peaks on the spectrum represents the strength or intensity of that frequency in the signal. The periodic signal will show a distinct peak in the spectrum. Harmonic frequencies which are integral multiples of a frequency are often visible and provide the harmonic content of the whole signal. The frequency with maximum power has been collected from each FFT spectrum of the signal and defined as Fundamental Frequency (F.F.). The power corresponding to the F.F. is also collected from the spectrum. The typical FFT spectrum of neutron and gamma-ray induced nucleated signals collected from the present experiment is presented in Figures 4.7 and 4.8 respectively.

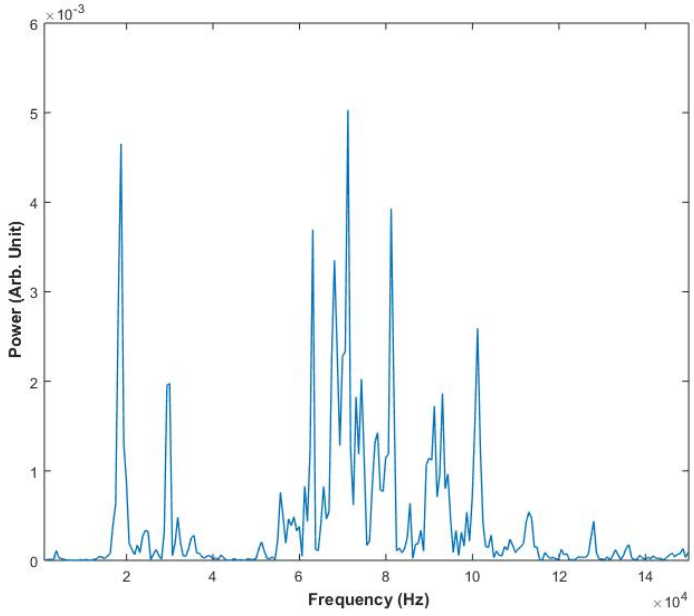

Figure 4.8: FFT of typical gamma-ray-induced bubble nucleated signal.

4.6 Results and discussion

The experiments have been done at different temperatures with different types of SED fabricated at SINP laboratory. All the collected signals of bubble nucleation have been analysed individually. Many well established and new parameters have been calculated from each collected signal. In the present section, only the parameters which are useful and give information about the discrimination of the signals and bubble nucleation are discussed below.

4.6.1 Maximum voltage and Pvar the signals

The observed distribution of the maximum voltage (V_{max}) and Pvar for the neutron and gamma-ray induced signals from R-134a liquid SED with 1400 rpm rotation are shown in Figures 4.9 and 4.10 respectively. The distributions show that the V_{max} and Pvar of the neutron induced signals lie within 0.1 $volt$ and 1 $volt^2$ respectively. The V_{max} and Pvar of gamma-ray induced signals with the same set of detectors are shifted towards higher values. The similar analysis has been done with the signals from a set of SED fabricated with R-134a liquid but the rotation was done at 900 rpm. The distribution of the maximum voltage (V_{max}) and Pvar for the neutron and gamma-ray induced signals from this SED are shown in Figures 4.11 and 4.12 respectively. The distribution of the V_{max} and Pvar of the neutron and gamma-ray induced signals are similar for the present set of SED.

The distribution of V_{max} and Pvar of neuron induced nucleation with R-134a liquid with 1400 rpm and 900 rpm rotation are localised. The localized energy deposition plays an important role in the case of neutron induced or recoil nucleus induced bubble nucleation. The recoil nuclei from the neutrons deposit the whole energy within a shorter range and bubbles resulting from such energy deposition produce signals of smaller V_{max} and Pvar compared to gamma-ray induced bubbles. In the case of gamma-rays the V_{max} and Pvar of the signals are distributed and shifted to higher values with SED fabricated with 1400 rpm rotation. The electron plays a major role in the case of bubble nucleation by gamma-rays. The electron with lower stopping power deposits maximum energy mainly at the end of its track over a larger

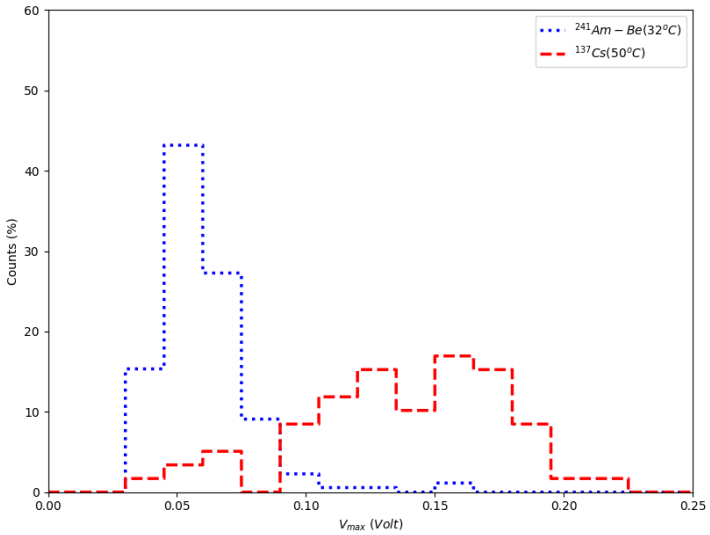

Figure 4.9: Distribution of the maximum voltage of neutron and gamma-ray induced nucleation signals with R-134a liquid SED and 1400 rpm rotation.

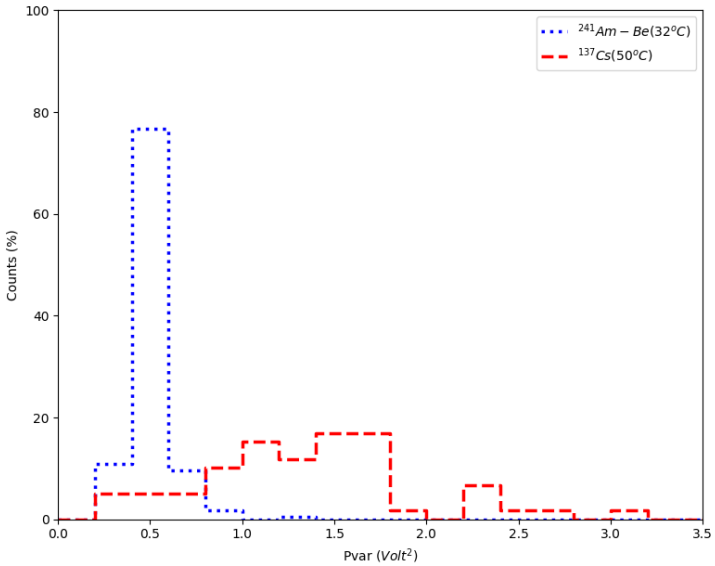

Figure 4.10: Distribution of the Pvar of neutron and gamma-ray-induced nucleation signals with R-134a liquid SED and 1400 rpm rotation.

range [78]. Along the track multiple bubbles grow and merge after nucleation as a result produces a signal having large V_{max} and Pvar using a SED with R-134a liquid and 1400 rpm speed. These variables from the signals of neutron and gamma-ray induced nucleations in the case of SED with R-134a liquid and 900 rpm are merged with each other. The size of the depletes depends on the rotational speed and size of droplets are different for two different rotational speeds. The average size of the droplets from 1400 rpm speed are smaller than the average size of the droplets from 900 rpm speed. The range of the recoil nucleus from neutrons is small and it remains constant despite the variation of the droplet size. As a result the V_{max} and Pvar of the neutron induced signals remain the same for two different rotational speeds of the detector. These variables shifted towards a lower value because the number of the droplets along the path of the electron is different for two different sizes of the droplets. In the case of 900 rpm rotation the number of droplets along the path of the electron is less than the number of droplets with 1400 rpm speed. The number of droplets is less along the path of the electron as a result it produces signals with low V_{max} and Pvar.

4.6.2 Time of maximum voltage of the signals

The bubble nucleated signal reaches to a maximum value at a certain time within the total duration of the signal. The time when the signal reaches the maximum voltage is collected from each signal from the experiments using the SED with R-134a liquid and 1400 rpm. The distribution of the time of the neutron and gamma-ray induced signals are presented in Figure 4.13. This information of the signal gives the dynamics of the

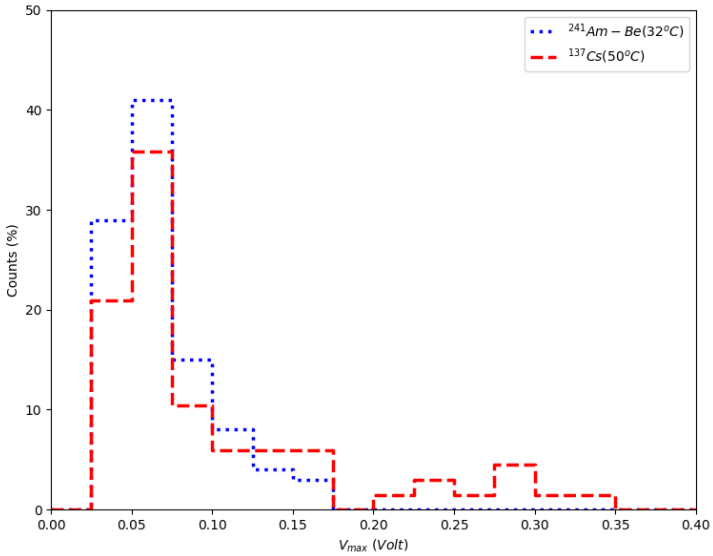

Figure 4.11: Distribution of the maximum voltage of neutron and gamma-ray-induced nucleation signals with R-134a liquid SED and 900 rpm rotation.

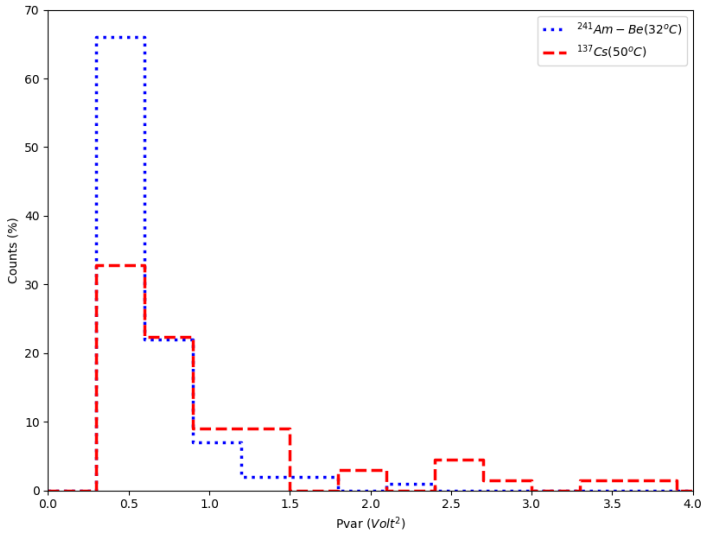

Figure 4.12: Distribution of the Pvar of neutron and gamma-ray-induced nucleation signals with R-134a liquid SED and 900 rpm rotation.

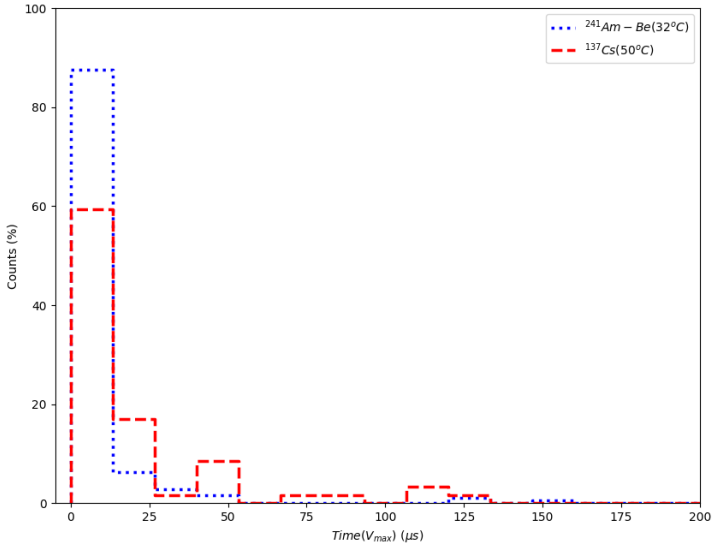

Figure 4.13: Distribution of the Time corresponding the maximum voltage of neutron and gamma-ray induced nucleation signals with R-134a liquid SED and 1400 rpm rotation.

signal which can indirectly reflect the dynamic of bubble nucleation. Here, only the discrimination was observed and the distribution shows that the time of occurrence of maxima is almost same for neutron and gamma-ray induced signals. The bubble growth dynamics and it's oscillations is independent of the types of particles that nucleate the bubble.

4.6.3 Duration and number of peaks of the signals

The signals from SEDs with R-134a liquid and 1400 rpm rotation speed are well studied here because theoretical work was done on this liquid for some future experiments. So, a few more parameters like duration of the signals and number of peaks of the

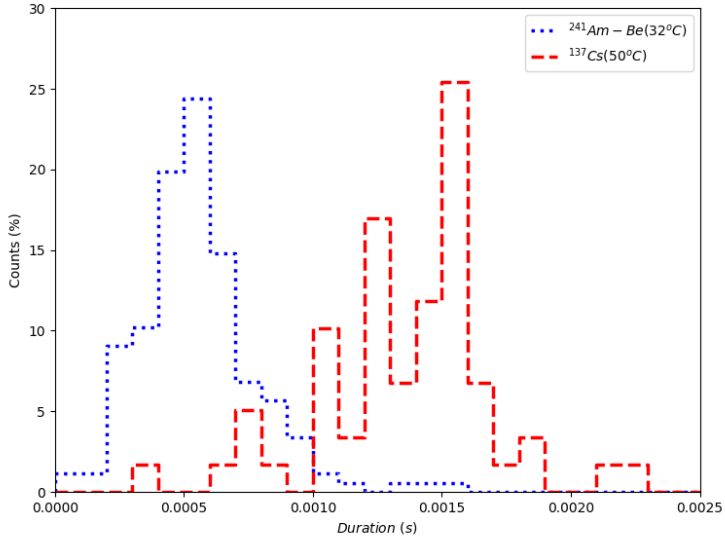

Figure 4.14: Distribution of the Duration of neutron and gamma-ray induced nucleation signals with R-134a liquid SED and 1400 rpm rotation.

signals have been calculated from each collected signal. The distribution of these parameters are displayed in Figures 4.14 and 4.15 respectively. The distributions show that the number of peaks and duration of gamma-ray induced signals are higher than those from neutrons. The reason is the same as explained before that the localized energy of the recoil nucleus produces a single nucleation. Electrons from gamma-rays in the liquid may contribute multiple vapour embryos in the extended track, which may merge into a larger single bubble and produce signals with high duration and number of peaks.

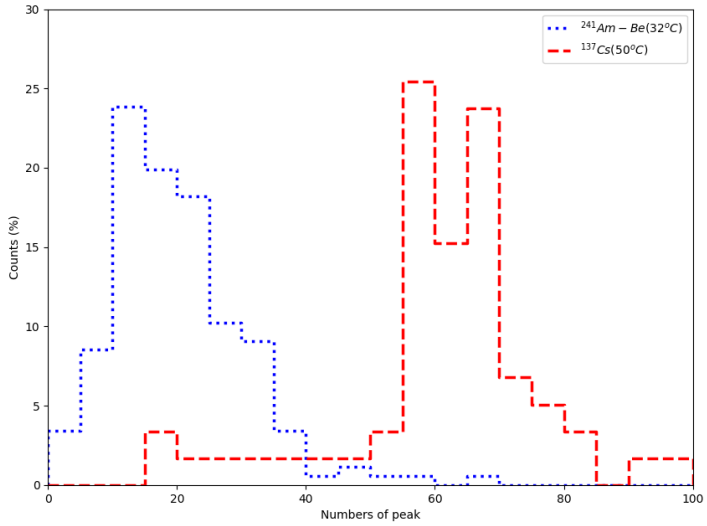

Figure 4.15: Distribution of the Numbers of Peaks of neutron and gamma-ray induced nucleation signals with R-134a liquid SED and 1400 rpm rotation.

4.6.4 Frequency spectrum of the signals

The FFT spectrum of the typical neutron and gamma-ray induced signals for R-134a liquid SED with 1400 rpm rotation are shown in Figures 4.7 and 4.8 respectively. The Figures show that the power spectrum is mostly limited within the frequency range of 15 kHz to 150 kHz. The distribution of frequencies in the FFT spectrum for the neutrons and gamma-rays induced signals are different. The FFT spectrum of a neutron induced signal shows that most of the peak frequencies are around 80 kHz. In the case of gamma ray induced signals there are several frequencies in the FFT spectrum with a broad distribution between 50 and 100 kHz and a narrow distribution within 15 kHz to 50 kHz. As discussed earlier in the chapter 2, the frequency is inversely proportional to the size of the bubble and the low frequency

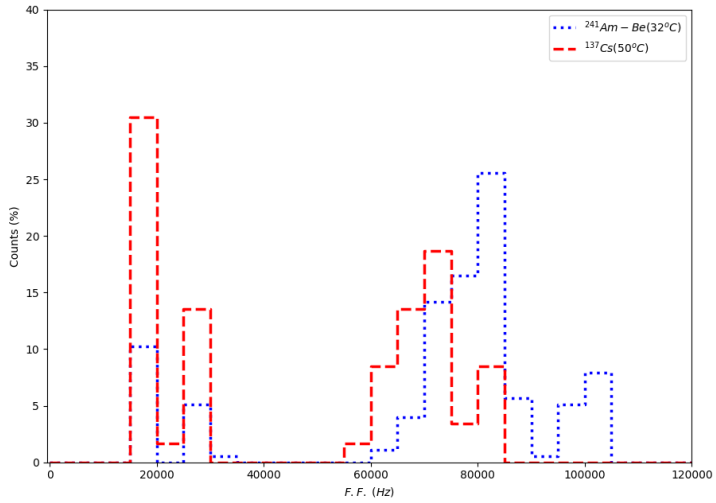

Figure 4.16: Distribution of the F.F. of neutron and gamma-ray induced nucleation signals with R-134a liquid SED and 1400 rpm rotation.

appears for the larger size of the bubble. The radius of the growing bubble is found to be 31.91 μm for a frequency of 80 kHz and 131.80 μm for a frequency of 20 kHz as calculated using Equation 2.11. These observed low frequencies in the gamma-ray induced bubble nucleated signals also show the merging of the multiple bubbles.

4.6.5 F.F. and the power of F.F. of the signals

The distribution of F.F. variable of neutrons and gamma-rays induced signals from the SED with R-134a liquid with 1400 rpm rotation speed is presented in Figure 4.16.The distribution shows that the F.F. of maximum neutron induced signals lies between 70 kHz to 100 kHz. The F.F. distribution of the gamma-ray induced signals shows F.F. lies in two frequency bands. The F.F. of about 50 % of gamma-ray induced

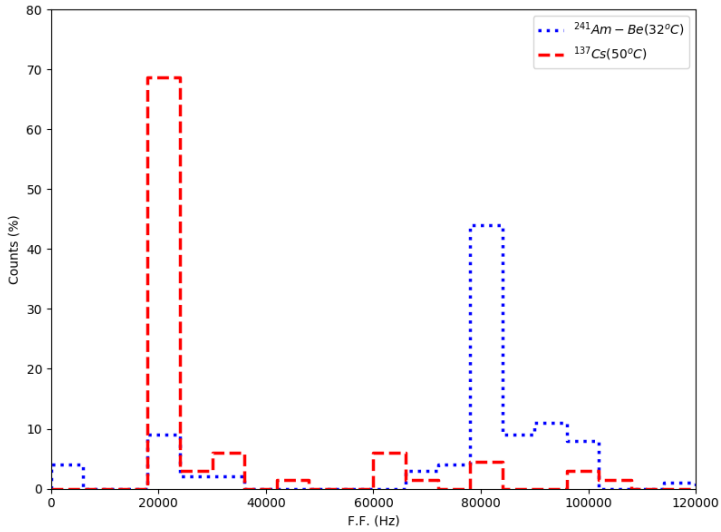

Figure 4.17: Distribution of the F.F. of neutron and gamma-ray induced nucleation signals with R-134a liquid SED and 900 rpm rotation.

signals lies between the 70 kHz to 90 kHz band and for the remaining signals the F.F. lies between 15 kHz to 35 kHz band. The presence of a low frequency band in the FFT spectrum for gamma-ray induced nucleation makes it different from the neutron induced nucleation. The distribution of F.F. variable corresponding to neutrons and gamma-rays induced signals from the SED with R-134a liquid with 900 rpm rotation speed are presented in Figure 4.17. The same distribution using SED with R-12 liquid with 1400 rpm rotation speed is presented in Figure 4.18. Both the distribution show that the F.F. of the signals from gamma-rays are lower than those of the neutrons and allows discrimination of neutrons from gamma-rays. F.F. variables are important for the discrimination using the SED with liquid R-134a with 900 rpm rotation and with R-12 liquid with 1400 rpm rotation. The F.F. is a weak parameter to discriminate neutron and gamma-ray induced signals using SED with R-134a liquid and 1400 rpm

rotation. The new parameter is the power which corresponds to the power of the fundamental frequency (F.F.) of each signal. This new parameter power has been collected from each signal of neuron and gamma-ray induced nucleations and the distribution is presented in Figure 4.19. The distribution reflects that the power of F.F. of the gamma-ray induced signals are larger than the power of F.F. of the neutron induced signals. The acoustical signal from the localised energy disposition of the recoil nucleus from neutrons would excite only high frequency components with lower power. On the other hand the extended path of the electrons and the merging of the bubbles of various sizes produce bubbles of different lower frequency with higher power values. The duration of the signals and growth rate of the bubbles are low and it produces several low frequencies in the FFT spectrum of gamma-ray induced signals.

4.7 Conclusion

In this chapter studies have been done on the voltage and frequency spectrum of the bubble nucleated signals from neutrons and gamma-rays using R-134a SED with 1400 rpm and 900 rpm rotational speed. R-134a is a environmentally friendly liquid and suitable for neutron and dark matter detection. Experiments using the detector with R-12 liquid and 1400 rpm rotation have been done in presence of neutron and gamma-rays source as a reference. The V_{max} and Pvar parameters of neutron induced signals are smaller than those of the gamma-ray induced signals for the SED with R-134a liquid and 1400 rpm rotation. The V_{max} and Pvar parameters of neutron

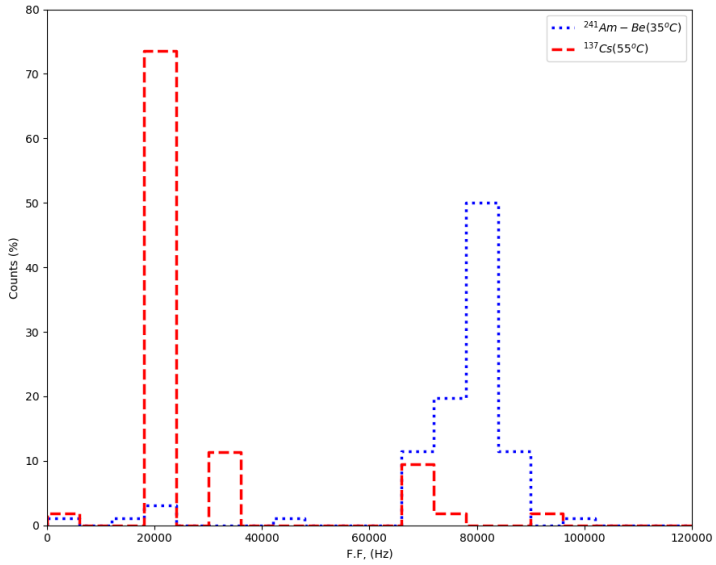

Figure 4.18: Distribution of the F.F. of neutron and gamma-ray-induced nucleation signals with R-12 liquid SED and 1400 rpm rotation.

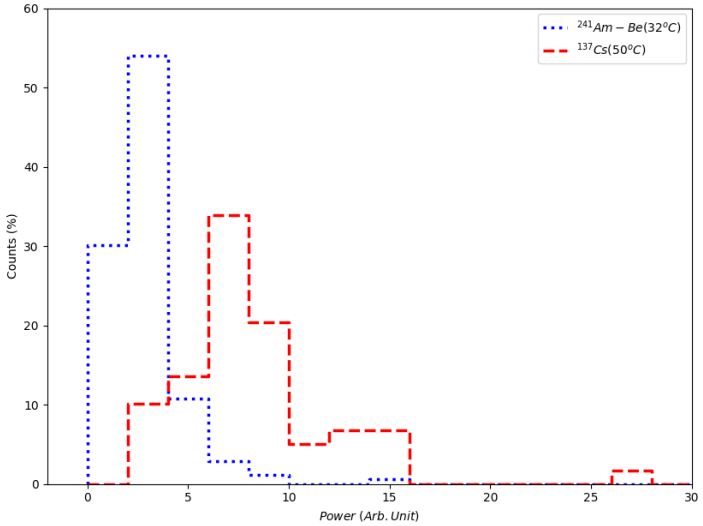

Figure 4.19: Distribution of the Power of the F.F. of neutron and gamma-ray induced nucleation signals with R-134a liquid SED and 1400 rpm rotation.

and gamma-ray induced signals are similar for the SED with R-134a and R-12 liquid with 900 rpm and 1400 rpm rotational speed respectively. The time of occurrence of maxima is almost same for neutron and gamma-ray induced signals which reflect that the dynamics of the bubble growth and oscillation of the bubble is independent of the types particle that nucleate the bubble. The FFT spectrum shows that the gamma-ray induced signals contain several low frequencies which are absent in neutron induced signals. The duration and number of peaks of the neutron induced signals are smaller than those of the gamma-ray induced signals for SED with R-134a liquid and 1400 rpm rotation. The F.F. parameter significantly discriminates the neutrons induced signals from the gamma-rays induced signals using the SED with R-134a and R-12 liquid with 900 rpm and 1400 rpm rotational speed respectively. The power of F.F. of the gamma-ray induced signals are larger than the power of F.F. of the neutron induced signals. The localised energy disposition of the recoil nucleus and extended path of the electron from gamma-rays are the origin of these differences between the neutron and gamma-ray induced signals.

Part - B: Advanced discrimination techniques of bubble nucleated signals by nonlinear analysis

A research paper based on the work presented in this chapter has been communicated in journal.

4.8 Introduction

SED is efficient in neutron detection both in dosimetry and in spectrometry [20]. The detector becomes sensitive to gamma-rays at low threshold energy of the detector. The discrimination of the neutron and gamma-ray induced events is necessary for SED in the detection of neutrons over a wide range of temperatures and pressure ranges. In part - A of the present chapter, the high frequency acoustic signals from the bubble nucleation of R-134a superheated liquid droplets while irradiated with neutrons and gamma-rays have been investigated. The high frequency acoustic signals have been measured from the bubble nucleation of R-134a superheated liquid droplets while irradiated with neutrons and gamma-rays and these signals have been analysed [198]. The spectral analysis using Fast Fourier Transformation (FFT) revealed the presence of frequency components during gamma-ray irradiation that were absent in the neutron induced signals. The parameters like Pvar, duration and number of peaks of the neutron induced signals are smaller than those of the gamma-ray induced signals as observed in the previous studies. The nonlinear analysis of the bubble nucleated acoustical signals from neutron and gamma-rays show that the homogeneous nucleation exhibits chaotic behaviour and it has been verified by the positive value of the

Lyapunov exponent [199]. The R/S analysis of the signals shows a difference in persistency between the neutron and gamma-ray induced signals. The nonlinear analysis reflects differences in the 3D attractor reconstruction, FFT, and R/S plots between the neutron and gamma-ray induced signals and also shows the chaotic nature of the signals. Any chaotic signals are characterized by high fluctuations, non-stationary, intermittency with a broadband nature and may consist of a superposition of localized structures in time. The Empirical Mode Decomposition (EMD) is commonly used for processing nonlinear signals [200–203] as introduced by Huang et al. [203]. The EMD does not require predefined basis functions, unlike wavelet analysis [204]. The EMD is a data-driven expansion, similar to wavelet analysis that helps to extract the natural oscillation frequencies present in a signal. The coherent structures one of the important features of the signal are typically identified as the modes with the highest energy concentration, although more than one coherent structure can exist [204, 205]. Given that EMD has proven to be an effective data-driven, wavelet-like tool, it is suitable for detecting coherent structures. The present work is done by the EMD on the nonlinear and chaotic signals of bubble nucleation in R-134a SED. The new parameters using EMD from the nucleation of superheated liquid droplets in a higher frequency range have been defined to observe the discrimination between neutron and gamma-ray induced signals. The aim of this work is to detect the coherent modes in bubble nucleated chaotic signals using EMD and to explore the coherent mode in differentiating the neutron and gamma-ray induced signals.

4.9 Analysis

The bubble nucleated signal has been resolved into its inherent modes called intrinsic mode functions (IMFs) using the EMD approach in Matlab. The approach is based on detecting local maxima and minima of the signals. Local maxima and minima have been collected and connected to form an envelope. Average of maxima and minima have been computed and the residue has been calculated by subtracting the average from original signals. The steps are repeated until the stopping condition is satisfied for the calculation of the IMF. The correlation coefficient (CC) of an IMF gives an idea about its contribution to the original signal and is estimated using the relation (Equation 4.1) [202] where X(n) is a signal and IMF(n) is one of the resolved intrinsic modes of the signal.

$$CC = \frac{\sum_{n=1}^{N} IMF(n)X(n)}{\sqrt{\sum_{n=1}^{N} IMF(n)IMF(n)}\sqrt{\sum_{n=1}^{N} X(n)X(n)}} \tag{4.1}$$

The value of correlation coefficient is normalized with the maximum value of correlation coefficient and it lies between 0 and 1. The energy based empirical variance of an IMF is expressed by the relation as given in Eq. 4.2, where k represents the mode index or IMF number and N denotes the data length of the IMF.

$$V(k) = \frac{1}{N}\sqrt{\sum_{n=1}^{N} IMF_k^2(n)} \tag{4.2}$$

The log variance plot represents a peak for a specific mode and it indicates the maximum energy concentration at that IMF. The IMF with maximum variance signifies

the coherent mode of the signal. In this study, the effort has been made to detect the coherent mode of the neuron and gamma-ray induced bubble nucleated signals. The bubble after nucleation can be treated as an oscillatory body and various parameters are necessary to determine the model equation. Details of nonlinear nature of bubble oscillation, different non-linear models and resonance frequency of bubble oscillation are discussed in chapter 2.

4.10 Result and discussions

The intrinsic mode functions (IMFs) of the acoustical signals from neutron and gamma-ray induced bubble nucleation have been constructed. A total of eight IMFs have been constructed from the signals. The Figure 4.20 and Figure 4.21 represents the different IMFs of a typical neutron and gamma-ray induced signal respectively. The correlation coefficient and variance of each IMF of the signal have been estimated. The values of correlation coefficient of all the IMFs from the neutron and gamma-ray induced nucleated signals are presented in Figure 4.22. The figure shows that the correlation coefficient of the second IMF is maximum for both neutron and gamma-ray induced signals. The maximum correlation coefficient indicates that the second IMF contributes most to the original signal for both neutron and gamma-ray induced signals. The variance of all the IMFs from the neutron and gamma-ray induced nucleated signals are presented in Figure 4.23. The variance of the neutron induced signal is maximum for the second IMF and indicates that the energy concentration of the second IMF is maximum. Therefore the second IMF can be considered

as the coherent mode of the neutron induced nucleated signal. Two different types of gamma-ray induced signals are obtained, one which is similar to neutron induced signal with maximum variance at the second IMF. In other types of signals, two peaks with variances have been observed, one at the second IMF and another at the fourth IMF as shown in Figure 4.23. The magnitudes of the variances are high compared to neutron induced signals. Between the two peaks in the gamma-ray induced signals, the fourth IMF has the maximum value as shown in Figure 4.23. Large numbers of gamma-ray induced signals have been observed and it shows that the maximum variance altered between the second and the fourth IMF. The IMF with maximum variance is the coherent mode of the signal which also alters between the second and the fourth IMF for the gamma-ray induced signals. The earlier result [198] shows the differences in the power spectrum the whole neutron and gamma-ray induced signals. In the present work, an effort has been made to study the frequency spectrum of each IMF extracted from the original signal. The frequency with maximum power in the frequency spectrum is known as the fundamental frequency (F.F.) of the signals. The F.F. distributions of the neutron and gamma-ray induced nucleation are presented in Figure 4.24. The distribution shows that the F.F. of the maximum numbers of neutron induced signals lies between 70 kHz to 100 kHz. The F.F. distribution of the gamma-ray induced signals shows that FF distribution lies in two frequency bands. The F.F. of about 50 % of gamma-ray induced signals lies between 70 kHz to 90 kHz band and for the remaining signals, the F.F. lies between 15 kHz to 35 kHz band. The presence of low frequency band in the frequency spectrum for gamma-ray induced nucleation makes it different from the neutron induced nucleation [198]. To get more information about the frequencies of the signals, the power spectrum has

been constructed from each IMF of the neutron and gamma-ray induced nucleated signals. The power spectrum of the first four IMFs of a typical neutron induced nucleated signal is shown in Figure 4.25. The figure shows that the F.F. and the frequency range between 70 kHz to 100 kHz are present in the power spectrum of the second IMF. The variance of the second IMF is the maximum for these signals. The F.F. and frequency band in the range between 15 kHz to 35 kHz is observed in the power spectrum of the fourth IMF. The variance of this fourth IMF becomes maximum for these gamma-ray induced signals. This result indicates that the variance is maximum for those IMFs that contain the F.F. of the whole signal. The first possible reason for the shifting of the coherent mode and frequency of the gamma-ray induced signals may be the effect of the operating temperature of the detector. The experiment in the presence of gamma-rays has been done at 50 ^oC. The theoretical resonance frequency of the bubble after nucleation has been determined by the Equation 2.12 and compared to the present experimental results. The Figure 4.26 shows the calculated resonance frequency of the bubble for a given radius and the operating temperature of the detector. Figure 4.26 shows that the frequency shifts towards higher value with increasing temperature. In the present experiment, the low frequency band appears at a higher operating temperature at 50 ^oC when exposed to gamma-ray source. Theoretically the effect of temperature shows the opposite behaviour as observed in the experiment. Therefore the high operating temperature of the detector is not the origin of this low frequency band in gamma-ray induced signals. The second possible reason is the nucleation mechanism and energy deposition of the electrons and recoil nuclei from the gamma-ray and neutron respectively. The stopping power of the electrons and the linear energy transfer of the recoil nuclei are different. Using Equation 2.12,

the diameter of the bubbles oscillating with a frequency of 80 kHz at a temperature of 32 ^oC has been calculated and the value is 170 μm. The diameter of the bubble at 50 ^oC temperature, which oscillates with a frequency of 80 kHz or 20 kHz is 230 μm or 900 μm respectively. Figure 4.26 also shows that a bubble of larger size can oscillate with a low resonance frequency and produce low frequency signals. The gamma-ray induced bubbles should be larger which produces these low frequencies in the range between 15 kHz to 35 kHz. The range of the electrons from gamma-rays is substantially greater than the range of recoil nuclei from the neutrons. The range of the electron is 2.5 mm and the number of droplets along the track is found to be about eight. The calculated range of the recoil nuclei, ^{12}C and ^{19}F are 3.81 μm and 2.62 μm respectively in R-134a and ^{1}H is not sensitive at this experimental temperature. The electron nucleates multiple bubbles along the track, these bubbles start growing and may merge to produce the bubbles of larger sizes. The number of droplets and their merging was also discussed by Sahoo et. al. [194] in order to explain the power value in R-134a SED. The merged bubble generates low frequency signals and as a result the variance is shifted to the fourth IMF for the gamma-ray induced signals. The features like low frequency band in the frequency spectrum, low F.F. and maximum variance at the fourth IMF of the gamma-ray induced signals make it different from the neutron induced signals.

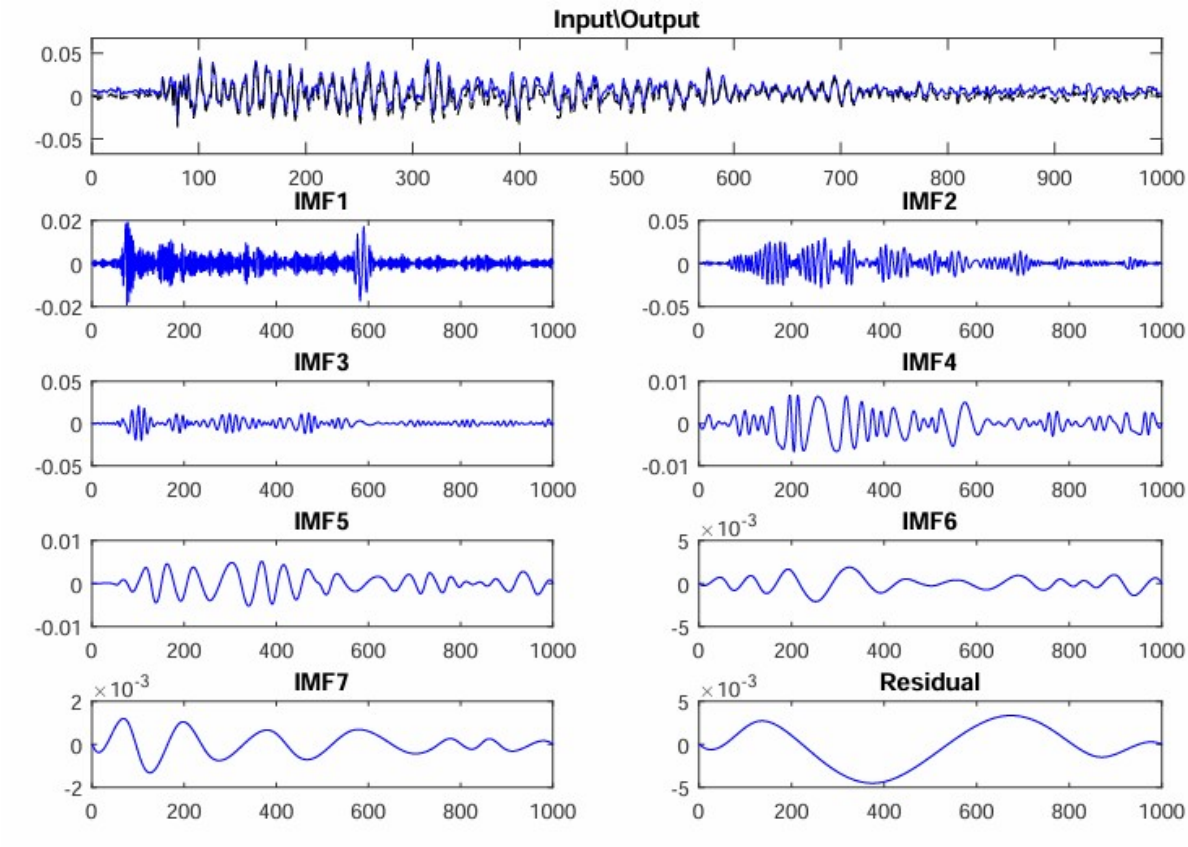

Figure 4.20: Different Empirical Mode Function (IMF) of a typical neutron induced signal.

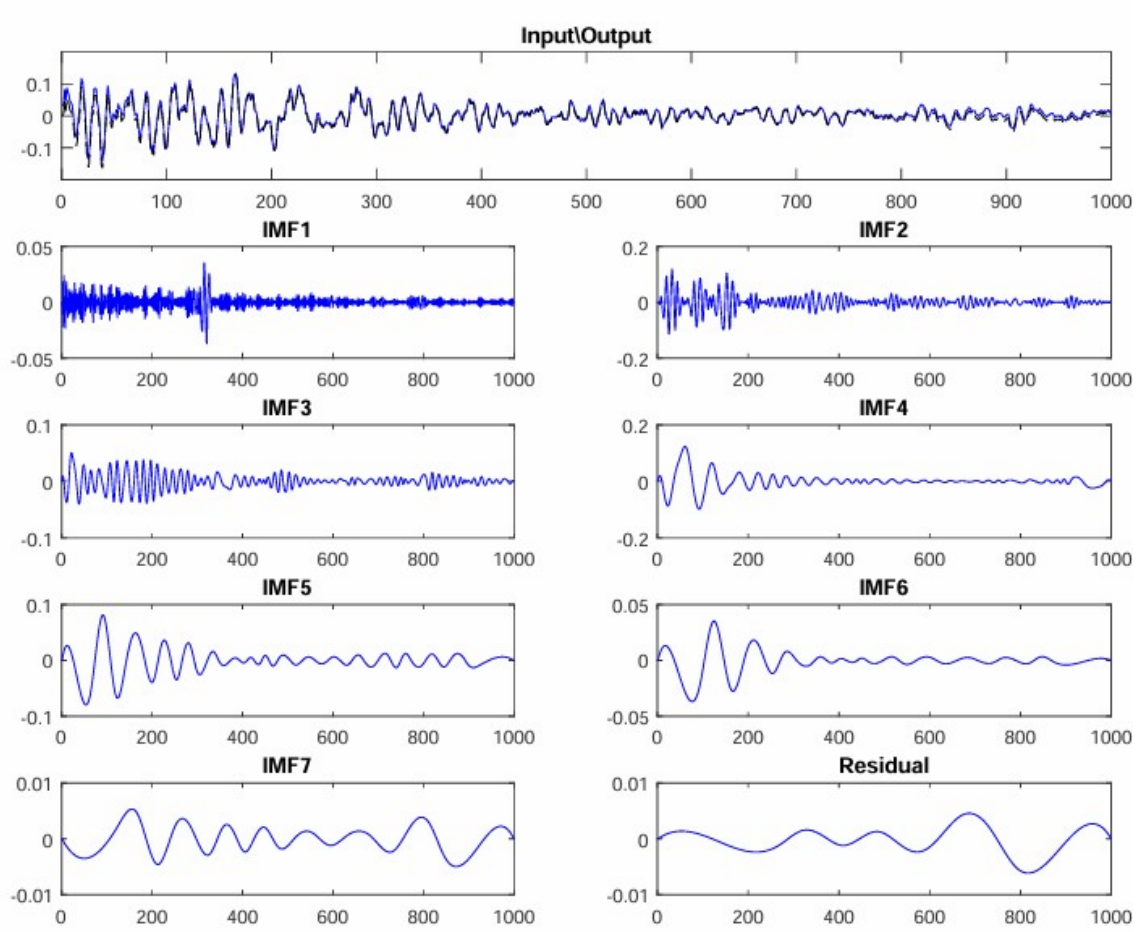

Figure 4.21: Different Empirical Mode Function (IMF) of a typical gamma-ray induced signal.

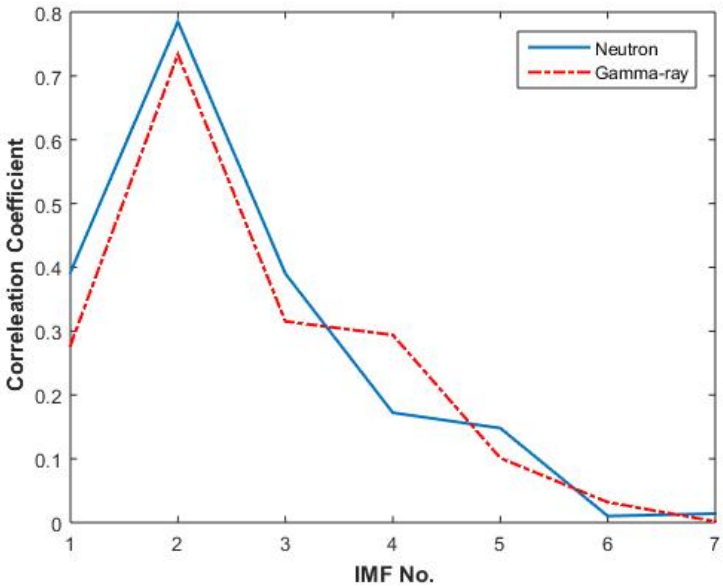

Figure 4.22: Correlation coefficient of different IMF of a neutron and gamma-ray induced signal.

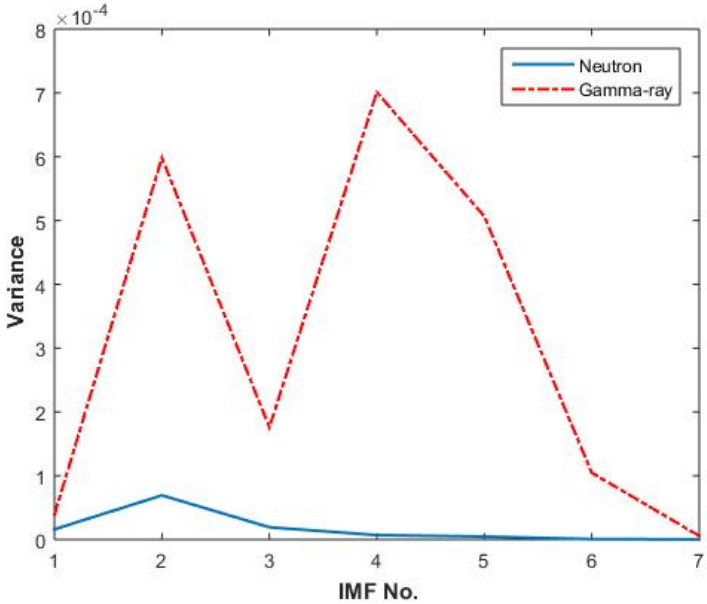

Figure 4.23: Variance of different IMF of a neutron and gamma-ray induced signal.

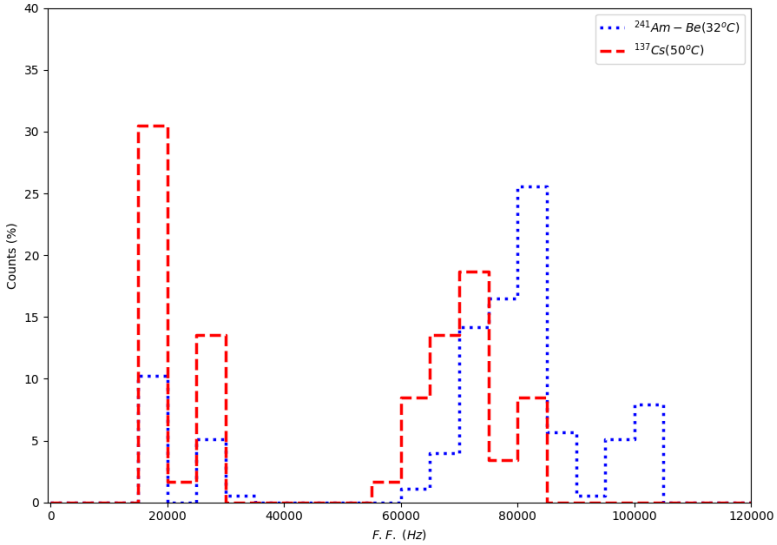

Figure 4.24: Fundamental frequency (F.F.) distribution of neutron and gamma-ray induced signals.

4.11 Conclusion

In the present work, the extraction of the IMFs by the empirical mode decomposition (EMD) of the bubble nucleated signals from SED have been discussed. The correlation coefficient and variance of each IMF from the neutron and gamma-ray induced nucleated signals have been estimated. The importance of correlation coefficient and variance has been observed in the detection of coherent mode. The IMF that contributes to the coherent structures is fixed for neutron induced signals but it varies for the gamma-ray induced signals which helps in identifying the neutron and gamma-ray induced signals. The low frequency band, low F.F. and maximum variance at the fourth IMF present in the gamma-ray induced nucleation is the effect

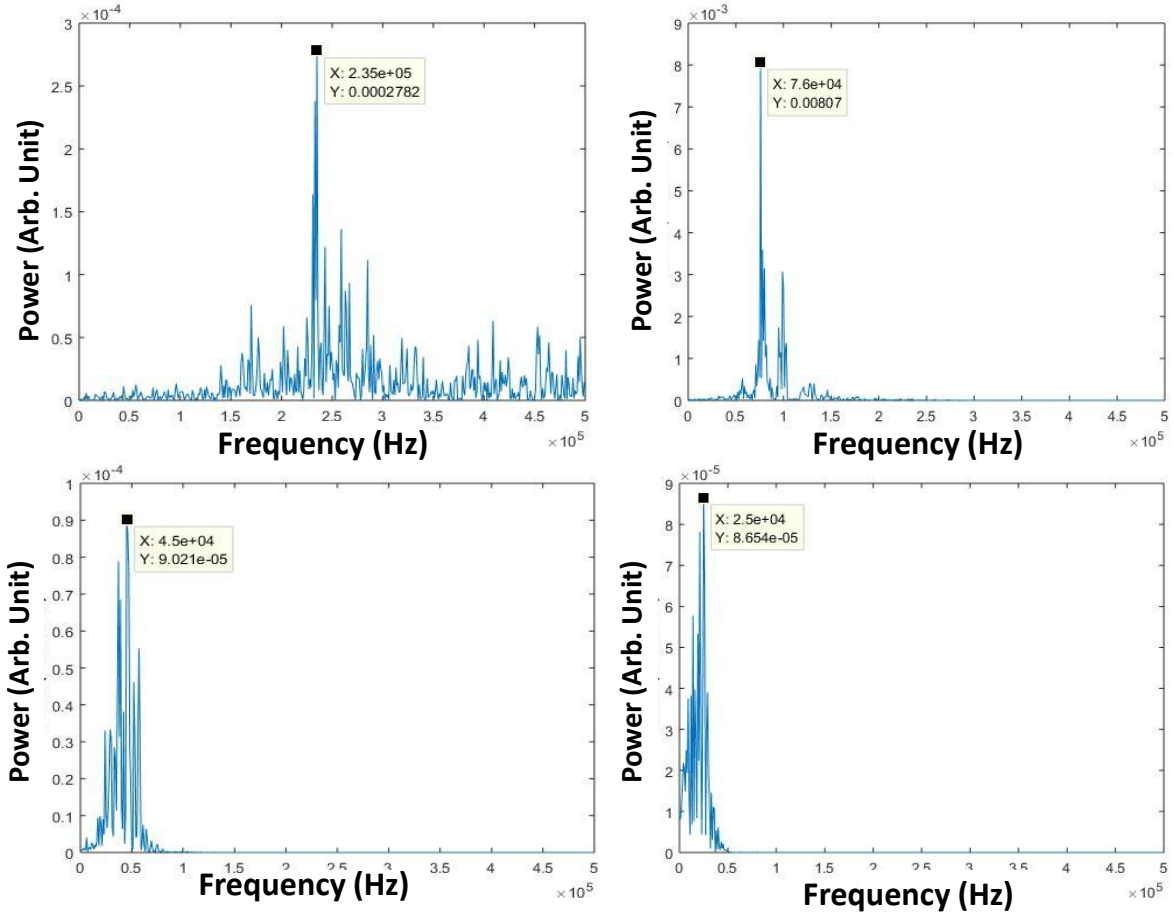

Figure 4.25: Power spectrum of first four IMFs of neutron induced signal.

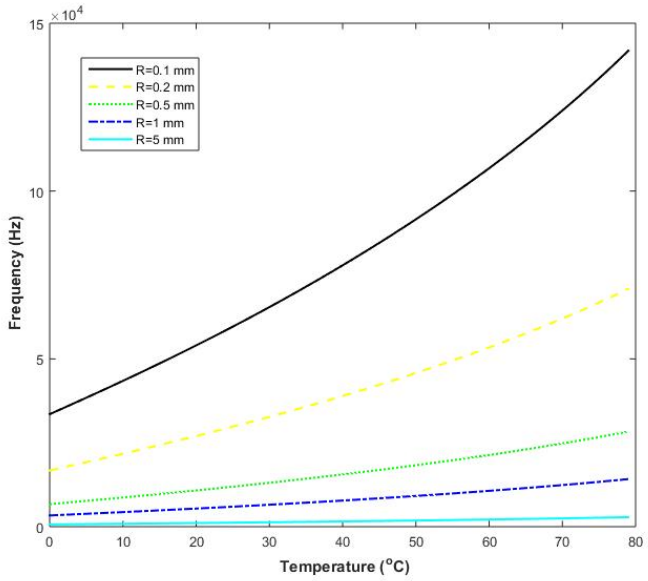

Figure 4.26: Variation of frequency of bubble with temperature for bubble of different radius.

of the extended path of the electron and temperature has no role in it. The droplets along the track of electrons from gamma-ray may produce the bubbles of larger size. This large bubble emits a low frequency signal relative to neutron induced signal and shifts the maximum variance at the fourth IMF. This study improves the identification process of the neutron and gamma-ray induced nucleated signal while operating SED in a region of neutron and gamma-rays.

Chapter 5

Spectroscopic characterization of the gel matrix for the fabrication of a stable SED

5.1 Introduction

Any molecules in an external electromagnetic radiation can absorb quanta of energy. This energy is equal to the gap between the discrete energy levels. The molecules can be excited in this process as it goes to the higher energy single states from the ground state. These molecules in the higher energy state are not stable. It can return into the ground state through various radiative and non-radiative processes [206]. The common types of radiative processes are fluorescence and phosphorescence [206]. There are many other non-radiative processes like resonance energy transfer by short range dipole-dipole coupling, collision loss, vibration loss. The electrically excited molecules can also take such a process. The fluorescence process is associated with the release of a photon due to an electron transition between the same states of spin multiplicity [207,208]. On the other hand, the phosphorescence is the process in which the photon is emitted. In this process the photon is emitted from the transition of the electron between different spin multiplicity states. The wavelength of the light from the phosphorescence is more than the fluorescence and generally take higher decay time. The fluorescence is associated with the intrinsic lifetime of the excited singlet states. The absorption property of the sample is also important information. This is one of the important pieces of information to understand the various ground state

molecular mechanisms. These states are sensitive to the electronic distribution of the molecules in the compound. The atom or molecule absorbs the photon of suitable wavelength that falls on it. Then the atom goes to a higher energy state. After absorbing energy from the photon the electron goes to the anti bonding molecules from the bonding or non bonding orbital. The energy of the transition lies in the ultraviolet to visible region of light. The vibrational and the rotational transition lie in the energy range of infra-red and microwave radiation. The electron in the higher energy state may retain in that state. The state should be a singlet or any other state with higher multiplicity. The transition probability is more in the lower multiplicity than in the states with higher multiplicity. The whole process of excitation and de-excitation of the electron is instantaneous. The electron returns to the ground state through various radiative and non-radiative pathways. The molecule in a solution frequently leads to the formation of molecular aggregates. Through the strong intermolecular Vander Waals like force or enhanced intermolecular vibrational coupling. These molecules under Vander Walls like force are responsible for the formation of the aggregates. The shifting of the electronic absorption and emission peak reflect the formation of aggregates. The formation of new bands in the absorption and emission spectra can also reflect the formation of aggregates. Kasha proposes the molecular excitation theory. Which successfully explained the aggregates formation in different organic molecules [209]. The aggregates formation associated with the ground and excited states of the molecule also explained by Kasha and co-worker. The theory explains that the shift in the UV-Vis absorption band is due to the strong electronic transition in some composite molecular systems [210]. This strong electronic excitation interacts with the transition dipole moment of the molecule. As a

result it affects the geometrical arrangement of the molecule. In the present study the Ultraviolet-Visible (UV-Vis) absorption spectroscopy and Fluorescence spectroscopy of the gel matrix of the SED has been done. The SED detector is fabricated using a superheated liquid droplet dispersed in a gel matrix. The SEDs comprise two essential components one of them is a metastable liquid as the active component. The liquid is maintained at specific temperature and pressure conditions. The other component is a three-dimensional gel matrix serving as the support matrix. The detectors have been made using $R-134a$ and $R-12$ refrigerant liquid. To ensure minimal contamination, fabrication of the detector components take place in a clean-room environment. The purification of all the components of the detector are also necessary. The first stage involves purifying all chemical ingredients, including water, used gel in preparation. The proprieties of the gel matrix should match to the few properties of the droplets and ensure stable detector and uniform dispersion of the droplets. This gel matrix is prepared by the mixture of glycerine and aquasonic gel and it is degassed under vacuum. After that the superheated liquid has been poured into the autoclave container at high pressure and cooled. This high pressure and cooling step ensures that the active component which is superheated liquid remains in its liquid state. The stability of the SED detector depends on the quality of the gel matrix. The present studies have been done to check the quality of the gel matrix and quantify the proper physical condition of the gel matrix for a stable detector.

5.2 Characterization technique

Ultraviolet-Visible absorption spectroscopy

Light of an appropriate wavelength interacts with matter, such as solutions or bulk crystalline forms. If the energy matches the gap between discrete electronic energy levels of the molecules, the matter absorbs some of the energy of the light. This absorption induces changes in the vibrational and rotational energy levels of the electrons of atoms. The incident light also initiates electronic transitions between different vibrational and rotational energy levels. These levels are associated with the ground and excited states of the molecules. Ultraviolet and visible light excite molecules by the electronic transitions between different molecular orbitals. The most probable transitions occur between two states; they are the highest occupied molecular orbital (HOMO) and the lowest unoccupied molecular orbital (LUMO). Experimental UV-Vis absorption spectra of most molecular species display broadened absorption bands rather than sharp peaks. This broadening results from the simultaneous transitions between various vibrational and rotational levels. Also these transitions happen as well as between ground and excited singlet states. UV-Vis spectroscopy typically employs light in the wavelength from 190 nm to 900 nm. The absorption intensity band depends on the population of molecules. The populations lie in lower energy states within a specific environment. A higher number of absorbing molecules leads to more intense absorption peaks. The intensity of the absorption band generally increases with the concentration of the sample in the medium. The solutions and suspensions are analysed in quartz cuvettes with a specific path length. In this study,

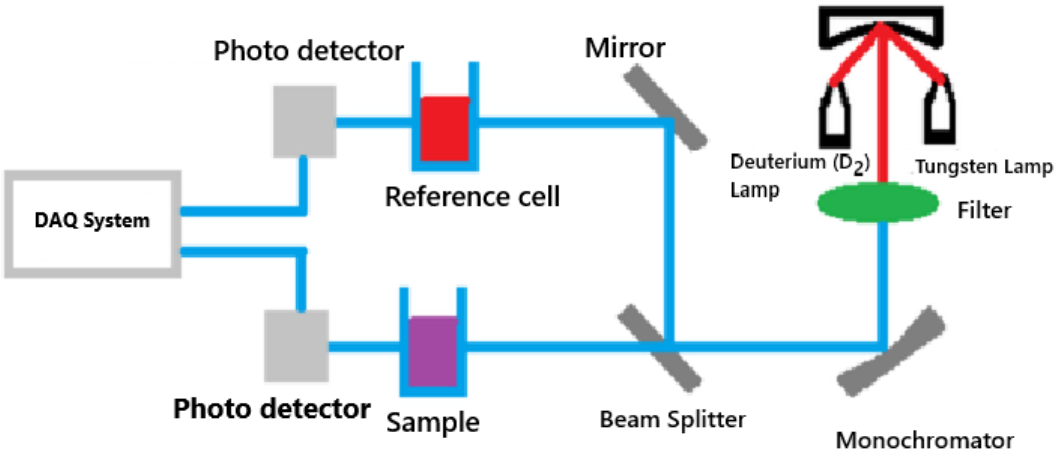

Figure 5.1: Schematic representation of the working principle of a double beam UV-vis absorption spectrophotometer.

the UV-Vis absorption spectra of the gel were measured using a UV-Vis absorption spectrophotometer (Model: UV-1800, Shimadzu Corp., Japan). The operational schematic diagram of the spectrophotometer is illustrated in Figure 5.1. The image of the actual experimental setup is provided in Figure 5.2.

Fluorescence spectroscopy

Fluorescence is a radiative process in which electronically excited molecules take a transition from excited singlet states to the ground state. The radiative pathways involved in fluorescence emission are discussed in the introduction. The fluorescence emission involves electronic transitions between states of the same multiplicity. The analysis of fluorescence emission is a powerful approach in molecular spectroscopy for studying molecular properties. Such properties are associations, dynamics, energy

Figure 5.2: UV-Vis absorption spectrophotometer (UV 1800, Shimadzu Corporation, Japan).

transfer, or complex photochemical reactions. Fluorescence emission results from electronic transitions involving various vibrational states between the ground and excited electronic states. Many non-radiative losses can be caused by vibrational relaxation [207]. This fluorescence spectrum is transferred to higher wavelengths relative to the absorption spectrum. This phenomenon is known as the Stokes shift. This shift provides critical insights into the behaviour of molecules. The commercially available fluorescence spectrophotometer (Model: Fluoromax-4, Horiba Scientific, USA) has been used in the experiment. Fluorescence measurements were conducted using fluorescence-grade quartz cells having 1 cm path length. The excitation monochromator wavelength was set based on the absorption profile of the sample and the fluorescence spectrum has been recorded. A schematic diagram of the steady-state fluorescence spectrophotometer operation is provided in Figure 5.3. The image of the experimental setup in the laboratory is shown in Figure 5.4.

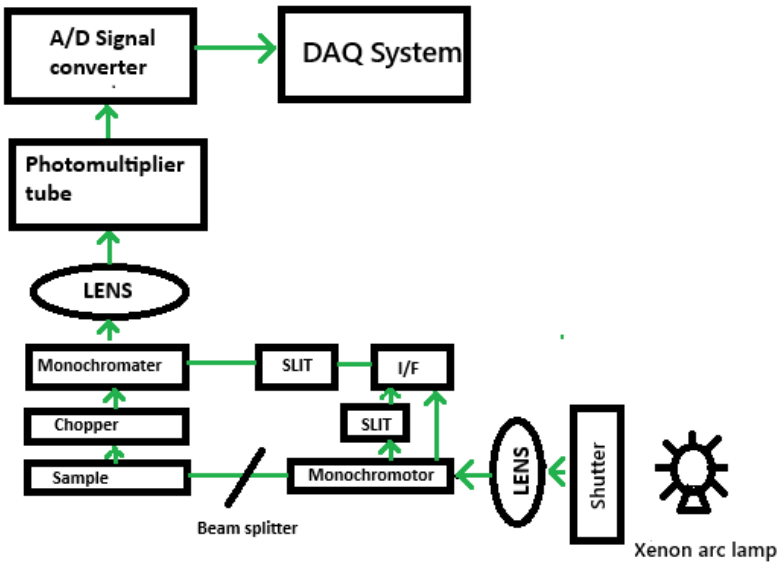

Figure 5.3: Schematic diagram of a steady sate fluorescence spectrophotometer.

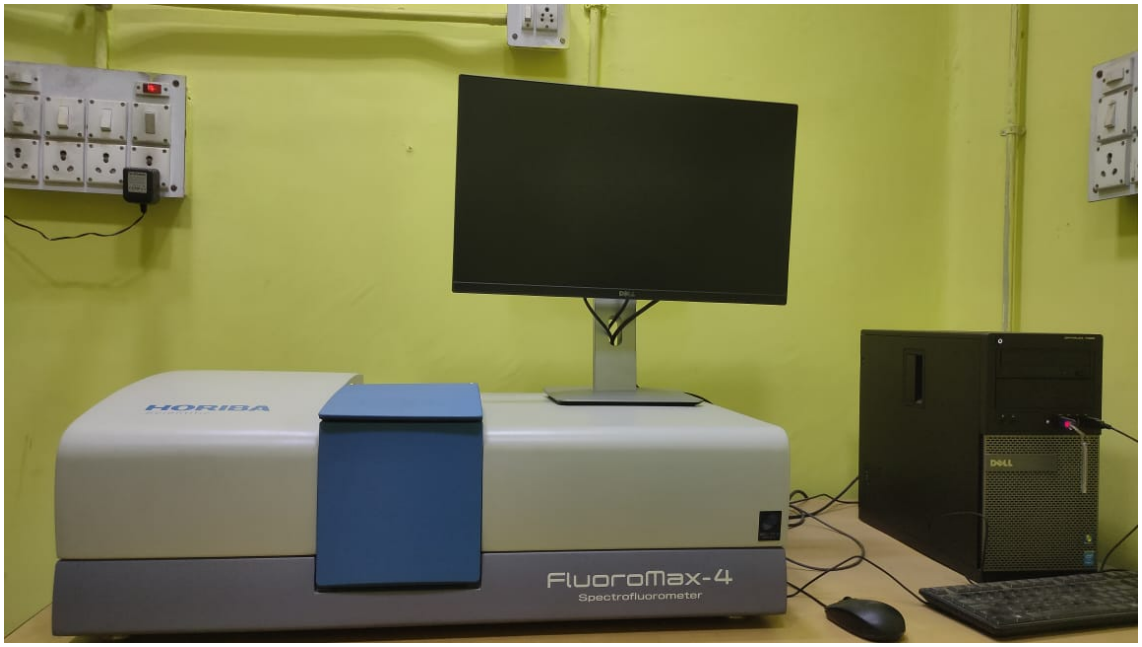

Figure 5.4: Fluorescence spectrophotometer (Model: Fluoromax 4C, Horiba Scientific incorporated, USA.

5.3 Experiment

The preparation of the gel matrix is the first step of the experiment and small droplets of superheated liquid are suspended inside this gel matrix. The gel matrix has been prepared by the combination of glycerol and ultrasound gel. 40 ml of glycerol and 10 g of ultrasound gel were mixed in a clean conical flask and the conical flask was placed on a magnetic stirrer for 30 minutes to mix well the glycerol and ultrasound gel. Many air pockets were trapped in the gel matrix during the mixing and made it very unsuitable for detectors. These air pockets have been removed from the gel matrix using vacuum pumps which extract the trapped air pockets. This process is known as degassing of the gel matrix, this process was continued for three days to a smooth and air pockets free gel matrix. Similar processes have been done to prepare the gel matrix with 5 g, 7.5 g, and 12.5 g of ultrasound gel with 40 ml of glycerol. To understand the detailed photo physical behaviour of the gel matrix with different concentration in the glycerine UV-Vis absorption spectroscopy has been done. Also steady state fluorescence emission spectrophotometer has been used in ambient conditions to understand the emission properties of the gel matrix.

5.4 Result and discussions

UV-Vis absorption spectroscopic study gives the information about the molecular organization as well as molecular mechanism. All this information is related to the ground electronic states of the sample. In this work we have used ultrasound gel

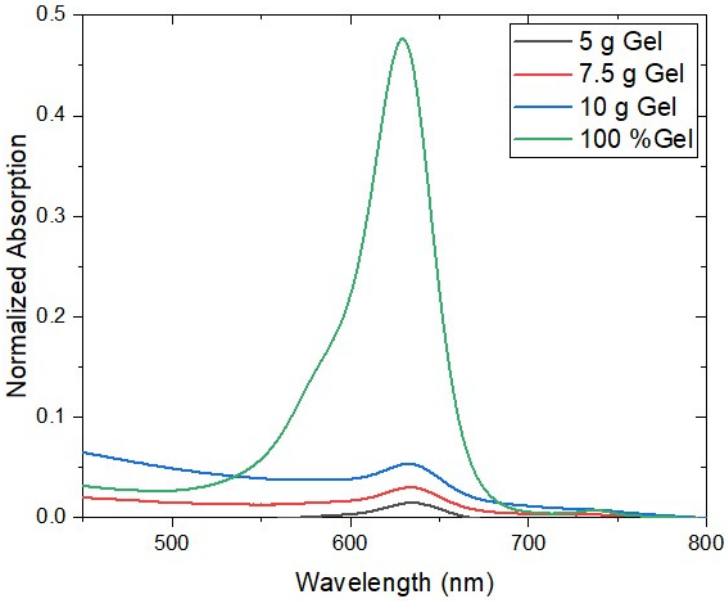

Figure 5.5: Ultraviolet-Visible (UV-Vis) absorption spectroscopy of gel matrix of different concentration.

which is the organic mix compound which mainly composed of water, propylene glycol, carbopol 980 NF polymer, etc. The UV-Vis absorption spectrum of pure ultrasound gel exhibits a absorption band with peak centred at around 629.5 nm with maximum absorption intensity shown in Figure 5.5. This intense peak indicates a high concentration of molecular species capable of absorbing of light at the ground electronic state. In the mixture with glycerine and the ultrasound gel the spectrum shifts to a peak at 634 nm and the intensity of absorption also decreases in these mixtures. The decrease in intensity as well as peak shift may attributed to the change in the molecular environment and closer association of ultrasound gel molecule in the glycerine medium.

To get more knowledge of the molecular arrangement and electronic states, steady

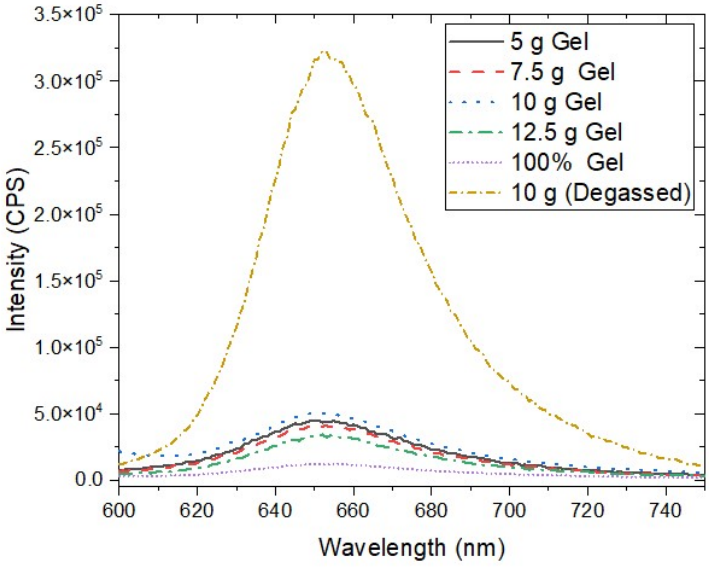

Figure 5.6: Fluorescence emission spectrum of gel matrix of different amount of gel in glycerine medium.

state fluorescence emission spectroscopic study has been performed on the ultrasound gel with different amount in glycerine medium. The excitation wavelength for all these samples were considered at 575 nm and the slit width remained fixed during the experiment. Figure 5.6 shows the steady state fluorescence emission spectra of the samples. The various amount (5 g, 7.5 g, 10 g and 12.5 g) of ultrasound gel in glycerine show almost similar band patterns but only with slide change in fluorescence intensity distribution. It is known that pure gel does not show any significant and appreciable fluorescence. however their mixture with glycerine with different amount of ultrasound gel show fluorescence emission band centred at around 652 nm when excited at 575 nm. Interestingly a mixture of 10 g ultrasound gel with 40 ml glycerine shows maximum fluorescence emission intensity compared to that for other mixtures. In this work we have also removed trapped air from the mixture (10 g ultrasound gel with 40 ml glycerine) for three days and subsequently recorded

the emission spectrum. It is observed that, the fluorescence intensity significantly become high as shown in Figure 5.6. The mechanism responsible for this observation is not yet readily understood. It must be noted in this context that pure glycerine does not show any fluorescence emission [211]. It may be assumed that the non-radiative decay channels of the excited molecules might be less for the mixture with 10 g ultrasound gel due to restriction imposed in molecular vibration. On the other hand for higher concentrations of gel, the relative distance between the molecules should be less causing greater intermolecular interactions in the glycerine medium. As a result, the fluorescence intensity is quenched. Also at higher concentration the collisions between the molecules and the radiation increases, which may increase the number of non-radiative pathways in the mixture after photo-excitation. At the time of detector fabrication the superheated droplets are most stable at a mixture of 10 g ultrasound gel with 40 ml glycerine. This means that the stability of the superheated droplets may be correlated with the inter-molecular distances of the molecule of the ultrasound gel in the glycerine.

5.5 Conclusion

The UV-Vis absorption spectrum of pure ultrasound gel exhibits a absorption band with peak centred at around 629.5 nm and in the mixture of glycerine with the ultrasound gel the spectrum shifts to a peak at 634 nm. This intense peak indicates a high concentration of molecular species capable of absorbing light at the electronic ground state. The peak shifted to 634 nm because the molecules in the mixture may

alter their electronic excitation energy levels. The fluorescence emission intensity is maximum for a mixture of 10 g ultrasound gel with 40 ml glycerine compared to other amount of ultrasound gel in the mixtures. Non-radioactive channels in the mixture after photo-excitation may be minimum in the mixture of 10 g gel and 40 ml glycerine. So this ratio of the gel and glycerine is possibly suitable for achieving stable SED.

Chapter 6

Application of SED and few R & D

6.1 Introduction

SEDs are well known for its ability to detect energetic radiation or particle. The physics of nucleation caused by the energetic particle like neutron interactions in superheated emulsions and its potential applications in various fields was discussed in the chapter 1. The use of superheated emulsions as neutron dosimeters is already well established. In the studies the different superheated liquid with different boiling point were used. In an experiment neutrons produced with a 45 MeV electron linear accelerator (linac) at Hokkaido University was used to study the response of a self-fabricated superheated emulsion. This study provides an approach to applying superheated emulsions in neutron detection within a mix radiation environments, as both neutron and gamma-ray radiation simultaneously exists in accelerators sites. In previous chapter 4, well established parameters and new parameters have been studied to identify the neutron and gamma-ray events using SED. In the present chapter few applications of these parameters have been discussed. First an experiment was done on 26 December 2019 which was an annular solar eclipse day, to understand the variation of radiation during solar eclipse. Previously, it was observed that the gamma-ray flux decreases about 4% during the solar eclipse [212]. Antonova et. al. were investigated the neutron flux variations during the solar eclipse and reported that the dynamics of the neutron intensity variation is due to geophysical sources of

disturbances [213]. Volodichev et. al. has estimated the share of the neutrons from the terrestrial crust into the general background flux of neutrons as about 10% during the complete solar eclipse [213, 214]. In the present measurement, the variation of background neutron induced events on a normal day and on a solar eclipse day has been studied using R-134a superheated emulsion detector which is described in section 6.2. A pressurization system has been modified to reuse the detector after the experiment and this pressurization system converts the bubble into liquid state. All initial experiments were conducted using a 100 ml SED fabricated at the laboratory of SINP. The primary requirement for the detection of DM is larger and sensitive SED. A large 1 litre Bell-Jar type SED has been fabricated to meet the requirements of DM detection. The test experiment has done using the 1 litre Bell-Jar type SED. The construction and the results of the experiments have been discussed in the following sections.

6.2 Measurement of neutron during solar eclipse

An experiment has been carried out at the laboratory of SINP (Kolkata, India) on 26 December 2019 which was an annular solar eclipse day that starts at 8:06 am. The eclipse ends at 11:10 am. The measurement has also been done at normal day on 31 January 2020 at the same place for the same period of time. R-134a superheated emulsion was used with the high frequency sensor using the experimental setup as described before in chapter 4. The operating temperature of the SED is 40 ^oC. The measurements on the solar eclipse day and the normal day were carried out for 3 hours

5 minutes. The experimentally observed variation of the number of bubble nucleated by backgrounds has been shown in Figure 6.1 for the solar eclipse day and for the normal day. This Figure 6.1 shows that the initial count rate of bubble nucleation is large on the day of solar eclipse compared to the normal day. The expected count rate by background neutrons has been calculated as described in this section. The neutron passes through the emulsion and it produces hydrogen, carbon and fluorine recoil nuclei which is produced by the collision of neutrons with the active liquid. The maximum energy transfer to the nucleus by the elastic head on collision by the incident particle. The count rate of bubble nucleation due to a mono-energetic neutron with energy E_n is given by the Equation 6.1.

$$R(E_n, T) = \phi(E_n) V_l \Sigma \epsilon^i(E_n, T) N^i \sigma_n^i(E_n) \tag{6.1}$$

In the above expression $R(E_n, T)$, $\phi(E_n)$, V_l, $\epsilon^i(E_n, T)$, N^i and $\sigma_n^i(E_n)$ are rate of nucleation, flux of neutrons, volume of the active liquid, efficiency of the detector, atomic number density and elastic scattering cross section of neutron with atomic nucleus. Substituting all the values [22, 78, 215] in Equation 6.1, the expected count rate of bubble nucleation have been estimated as 3.39x10^{-6}, 4.03x10^{-6}, 1.67x10^{-6} and 1.38x10^{-6} per second for 1 keV, 10 keV, 1 MeV and 10 MeV neutrons respectively. It is to be noted that the energy of the background neutrons has a distribution but for simplicity the expected rate has been calculated for the interaction cross section of some specific energies of neutrons [215]. The experimental count rate on the day of solar eclipse is 7.75x10^{-3} $\pm$ 0.84x10^{-3} per second and on the normal day is 2.16x10^{-3} $\pm$ 0.44x10^{-3} per second. The experimentally observed variation of Pvar and F.F. of

the signals obtained in solar eclipse day, normal day with neutron and gamma-ray sources are displayed in Figure 6.2. The Figure 6.2 is divided into five regions, like A, B, C, D and E. It shows that most of the neutron induced signals fall in the regions A and D. The gamma-rays induced signals are mostly in B and C regions. Most of the background signals both on solar eclipse day and normal day are in A and D regions. The above results show that the higher counts of bubble nucleation on solar eclipse day is mainly due to neutrons that signifies the enhancement of neutron flux during the solar eclipse. The effect of the small variation of gamma-ray flux during the solar eclipse as reported earlier [212] is not visible in this measurement. The reason of increasing the neutron flux during solar eclipse is expected to be due to the increase of radon emission from the crust of earth due to the disturbances from the geophysical sources [213, 214]. The radon decays via alpha emission and thereby producing the neutrons by (α, n) reactions that causes the increase of the neutron flux [214].

6.2.1 Conclusion

The Pvar and F.F. of these events it lies in the regions A and D in the Figure 6.2 which is dominated by the neutron induced signals. This analysis from the experiments show that most of the bubble nucleation counts from the background both on solar eclipse day and normal day are from neutrons. The experimentally observed count shows that the initial count rate is higher on the day of the solar eclipse compared to the normal day. The experimental and the expected count rate of bubble nucleation have been evaluated. The measurement with the present setup and calculated count rate shows an enhancement of the neutron induced counts on a solar eclipse day as

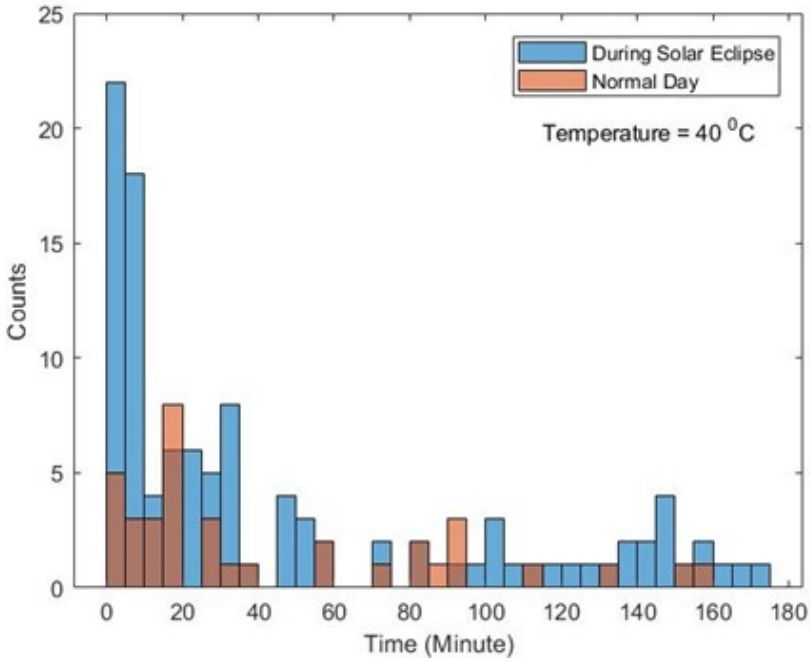

Figure 6.1: Number of nucleated signals from backgrounds on solar eclipse day and a normal day.

compared to the normal day.

6.3 Pressurization of SED

The droplets of the detector is converted into vapour bubble after completing the experiment with the SED. The SED can go through a pressurization process to converts the nucleated bubbles into liquid droplets. The process of pressurization the detectors can be helpful to reuse the SED in the subsequent experiments. Previously a pressurization system has been designed and few experiments were done. The picture of this pressurization system is shown in Figure 6.3. The important part of the pressur-

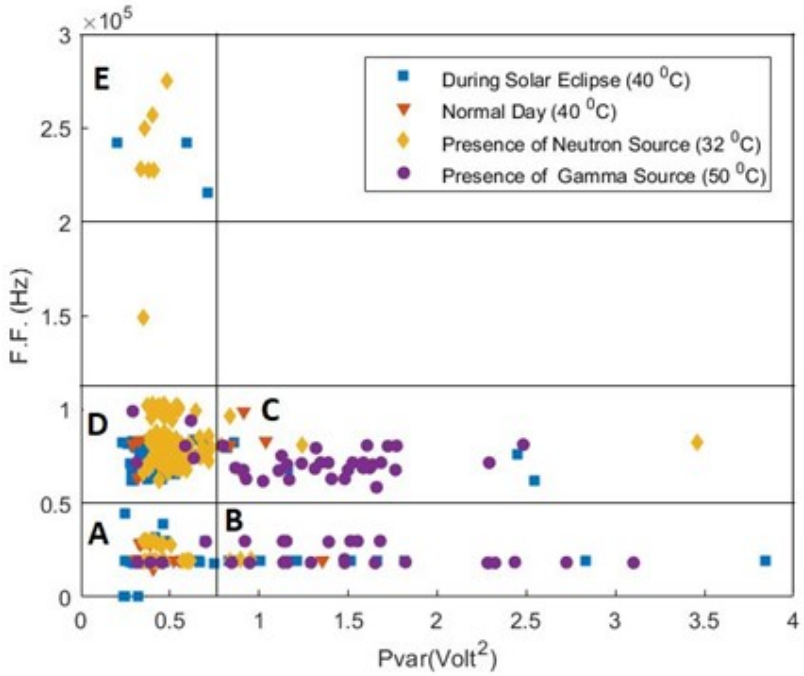

Figure 6.2: The distribution of Pvar and F.F. variables of the bubble nucleated signals.

ization system is a hydraulic manifold, a mineral oil tank and a nitrogen gas cylinder. The nitrogen gas cylinder is connected to the hydraulic manifold. The nitrogen gas was used to fill the mineral oil into the SED using a hydraulic diaphragm. The hydraulic diaphragm is connected between the container of the cylinder of mineral oil and nitrogen gas. The hydraulic diaphragm separates the mineral oil and nitrogen gas. The previous experiments concluded that there was some technical limitations to the pressure regulator. The maximum limit of the pressure regulator was 6.0 bar. The pressure can not be increased beyond 6.0 bar during testing. High pressure is necessary to convert the bubbles into droplets because the vapour pressure of $C_2H_2F_4$ liquid at 30.0 ^oC is 7.70 bar. In the present modification the maximum limit of the pressure regulator is 25.0 bar. The experiments with this modified system shown in

Figure 6.3, the experiment with modified setup shows that the bubbles were converted into the liquid droplets but after the pressurization the detector become completely filled with the mineral oil. It is difficult to separate the mineral oil from the SED. The pressurization system has been further modified by introducing a stainless steel collecting chamber between the mineral oil tank and the SED shown in Figure 6.4. This collecting chamber works well and the mineral oil remain stored in the chamber. After the pressurization, the SED will remain free from the contamination of the mineral oil. During the pressurization the SED was placed inside a low temperature box (Figure 6.5) for the safety reasons. It also provide the low temperature environments, helps the process of pressurization because the vapour pressure of the liquid decreases at low temperature. The experiments has been done with the modified arrangements and the result has been discussed in the next section.

6.3.1 Experiments and observations

The temperature of SED has been maintained at -31.6 ^oC during pressurization inside a low temperature chamber. The pressure of the nitrogen gas and mineral oil during the process was 6.0 bar. The pressurization was done over a period of 5 hours. Vapour bubbles inside the SED disappeared after the pressurization. Count rate were measured using ^{137}Cs (5 mCi) gamma-rays source with the same SED before and after the pressurization. The count rate of the SED before pressurization is 3.09 counts/sec but after the pressurization the number of counts is zero. Visually we can expect that the pressurization system effectively compresses the vapour bubble of SED into liquid droplets. The visual inspection shows the effectiveness of the

modified pressurisation system.

6.4 Construction of Bell-Jar type SED (BJ-SED)

The WIMPs, one of the candidates DM is present throughout the Universe. The density of the WIMPs is very low so the possibility of detecting the particle by scattering with normal matter is also very low. The occurrence of the scattering are extremely rare so a highly sensitive detectors is necessary for the detection. The backgrounds particle of environment of the detector should be low. The background rejection capabilities of the detector should be high. To increase the sensitivity of the detector, the size of the detector should be increased. In the case of SED, the sensitivity can be increased by increasing the detector mass and reducing the threshold. At low threshold the discrimination capability of the detector should be high and many parameters have been discussed in previous chapter 4 for the discrimination. In this section the fabrication of a large size detector to change the sensitivity of the SED for the detection of WIMPs is described. At first the size of the SED is increased to 1 litre and a Bell-Jar (BJ) has been chosen for the fabrication. All the mechanical arrangements of the Bell-Jar type SED (BJ-SED) have been carried out by the help of mechanical workshop of SINP. The test experiment has been done and the bubble nucleated signals are collected by using the acoustic sensors. For this large size detector the number of sensors have been increased. Total four acoustic sensors planned are to be used surroundings the detector. Three sensor is placed symmetrical at the outer side of the detector at an angle of 120 ^{o} and one sensor is placed at the bottom

Figure 6.3: The modified pressurization system.

Figure 6.4: The detector and the collecting chamber used in the experiment.

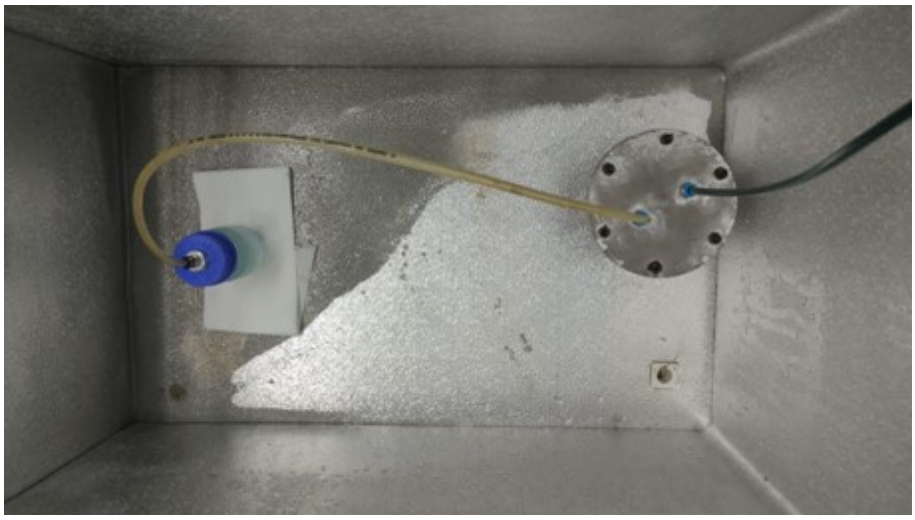

Figure 6.5: The detector and the collecting chamber inside the cold temperature bath.

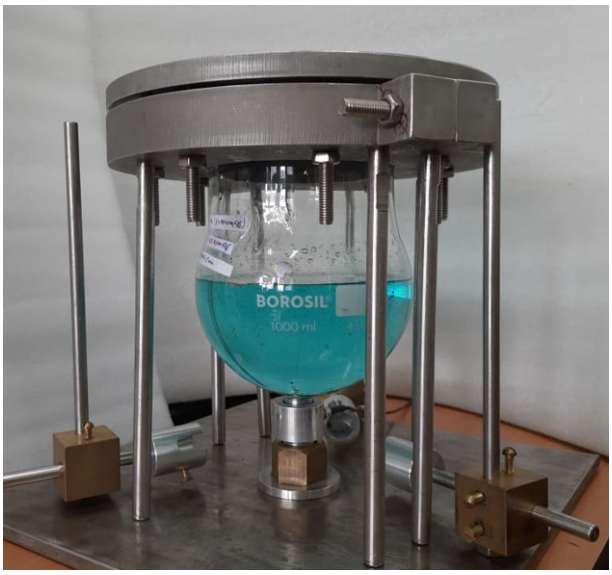

Figure 6.6: Diagram of Bell-Jar type SED.

of the detector. The setup of the detector is shown in Figure 6.6. In the present setup all the sensors are connected externally in contact with the outer wall of the detector.

6.4.1 Testing the BJ-SED

All the previous experiments have been done by using a detector of size 100 ml and only one acoustic sensor was mounted on upper part of the detector. This acoustic sensor in 100 ml SED was placed in contact with the detector material. The present experiments have been done using a 1 litre BJ-SED and the detector of has been fabricated in the laboratory of SINP. During the experiments only one acoustic sensor has been placed below the detector because of the lack of the number of sensors. A background run experiment was done at 32 ^oC at the laboratory of SINP for 2 hours.

Figure 6.7: SED after the experiment.

The experimental arrangement is similar to the arrangement as discussed in chapter 3 and the numbers of events have been stored in the LabView files. The picture of the detector after the experiment is presented in Figure 6.7. The collected signals have been analysed but none of the signals looking like actual bubble nucleated signals and hence actual bubble nucleated events was zero. The BJ-SED in Figure 6.7 shows large number of vapour bubble appears after the experiment. One of the reason for this zero recorded events may lies in the arrangement of the acoustic sensor with the BJ-SED. All the previous experiments with 100 ml SED, the sensor is in internally contact with the detector. The present experiment, the sensor is externally connected with the detector and there is few mm thick glass between the sensor and the detector. The present results shows that the sensors are only able to detect the bubble nucleated acoustical signals when it is placed in contact with the gel matrix.

Chapter 7

Conclusion and future plan

"Robert Apfel" 1979 developed a Superheated Droplet Detector (SDD) by modifying the concept of bubble chamber [1] and SDD is useful in different research fields like radiation physics [36, 37], high energy physics [38], health physics [39], space physics [40], nuclear astrophysics [41], etc. The details about the Superheated Liquid, Superheated Liquid Detector, the nucleation mechanism of superheated liquid drops, different efficiency and the present use of SEDs are presented in the Chapter 1. The growth of homogeneous nucleation of superheated liquid droplets, its oscillation and dynamics of the bubble are described in chapter 2. The homogeneous nucleation is nonlinear in nature and it shows chaos. The experimental studies and models on nonlinear bubble oscillation are also discussed in chapter 2.

The process of bubble nucleations can be studied by the bubble nucleated signals. In the chapter 3, the detailed experimental investigation of the nonlinearly of acoustical signals from neutron and gamma-ray induced bubble nucleation were analysed. The analysis shows the chaotic behaviour in homogeneous bubble nucleation. The behaviour of the gamma-ray induced signals are different from neutron induced signals. The parameters which shows the differences between neutron and gamma-ray induced signals were identified through the nonlinear analysis. These parameters are the complex 3D attractor reconstruction, broadband FFT spectrum and R/S plot. This study contributes to the understanding of chaos in homogeneous nucleation and

it also identifies the neutron and gamma-ray induced signals.

The discrimination of the bubble nucleated signals is important in detection and identification of individual particles in a mix radiation fields. The voltage and frequency spectrum of the bubble nucleated signals from neutrons and gamma-rays using R-134a SED with 1400 rpm and 900 rpm rotational speed have been studied in chapter 4.A for the identification of neutron and gamma-ray induced events. The experiments using the detector with R-12 liquid, fabricated with 1400 rpm rotation, have been done in presence of neutrons and gamma-rays source as a reference. The V_{max} and Pvar parameters of neutron induced signals are smaller than those of the gamma-ray induced signals for the SED with R-134a liquid and 1400 rpm rotation. The V_{max} and Pvar parameters of neutron and gamma-ray induced signals are similar for the SED with R-134a and R-12 liquid with 900 rpm and 1400 rpm rotational speed respectively. The FFT spectrum shows that the gamma-ray induced signals contain several low frequencies which are absent in the neutron induced signals. The duration and number of peaks of the neutron induced signals are smaller than those of the gamma-ray induced signals for SED with R-134a liquid and 1400 rpm rotation. The F.F. parameter significantly discriminates the neutron induced signals from the gamma-rays induced signals using the SED with R-134a and R-12 liquid with 900 rpm and 1400 rpm rotational speed respectively. These differences between the neutron and gamma-ray induced signals are useful in future experiments with SED.

The discrimination of the signals further extended in the chapter 4.B by the ex-

traction of the IMFs using the empirical mode decomposition (EMD) of the bubble nucleated signals from SED in presence of neutrons and gamma-ray sources. The correlation coefficient and variance of each IMF from the neutron and gamma-ray induced nucleated signals have been estimated. The IMF that contributes to the coherent structures is fixed for neutron induced signals but it varies for the gamma-ray induced signals can identify the neutron and gamma-ray induced signals. The low frequency band, low F.F. and maximum variance at the fourth IMF are present in the gamma-ray induced nucleation. This study improves the identification process of the neutron and gamma-ray induced nucleated signal while operating SED in a region of mix field of neutrons and gamma-rays.

The fabrication of a stable SED is the primary requirement before all the measurements using these SED. The stability of the SED depends on the few properties of the gel matrix. These properties are related to the density of the droplets of the liquid. Here efforts have been made to understand the detailed photo physical behaviour of the gel matrix with different concentration of the glycerine. UV-Vis absorption spectroscopy and fluorescence emission spectrophotometer has been used in ambient conditions to understand the emission properties of the gel matrix. The UV-Vis absorption spectrum and Fluorescence of pure ultrasound gel studies have been done and described in chapter 5. The studied shows that it exhibit a absorption band with a peak centred at around 629.5 nm. The peak of the spectrum shifts to a peak at 634 nm in the mixture of glycerine and the ultrasound gel. The Fluorescence emission intensity is maximum for a mixture of 10 g ultrasound gel with 40 ml glycerine

compared to other ratios of the mixtures as studied in the work. Non-radioactive channels in the mixture after photo-excitation is minimum in the 10 g gel and 40 ml glycerine mixture. These studies show that this combination is highly suitable for achieving the stable SED.

The developed discrimination techniques have been used in many experiments done at SINP laboratory. The first experiment was carried out at the laboratory of SINP (Kolkata,India) on 26 December 2019 which was an annular solar eclipse day and discussed in chapter 6. The same measurement has also been done on a normal day on 31 January 2020 at the same place for the same period of time. The analysis from the experiments shows that the most the of the bubble nucleation counts due to the background, both on solar eclipse day and normal day are from neutrons. The present measurement and calculated count rate from the experimental data shows an enhancement of the neutron induced counts on a solar eclipse day as compared to the normal day. After the experiments the droplets of the detector are converted into vapour bubbles by nucleation. A pressurization system has been modified and the testing have been done with the modified arrangements. The visual inspection of the measurement by the pressurization system signifies the effectiveness of the modified pressurization system. To increase the sensitivity of the detector, the size of the detector should be increased. A large size SED of volume one litre using a Bell-Jar (BJ) has been fabricated with a modified sensor arrangement. These sensors are placed outside the Bell-Jar without any contact with the gel matrix of the detector. The test results using the BJ-SED shows that the sensors are only able to detect the bubble

nucleated acoustical signals when it is placed in contact with the gel matrix. These results from the present studies will be useful in the detection of neutrons in mix radiation field and in the detection of WIMPs.

The nonlinear analysis is the potential tool to understand the each steps of bubble nucleation and model the bubble nucleation. In future more nonlinear analysis will be done on the bubble nucleated signals to develop a model of the homogeneous bubble nucleation. The new variables presented in the thesis are effective in the discrimination of the neutrons and gamma-rays induced signals, I will extend my research to improve the discrimination by identifying more new variable from the bubble nucleated signals. Emphasis will also be given to develop a more sensitive SED and improve the pressurization technique to reuse the detector.

Bibliography

[1] Glaser, D. Some effects of ionizing radiation on the formation of bubbles in liquids. *Physical Review*. **87**, 665 (1952)

[2] Roy, S. Superheated liquid and its place in radiation physics. *Radiation Physics And Chemistry*. **61**, 271-281 (2001)

[3] D'Errico, F. Radiation dosimetry and spectrometry with superheated emulsions. *Nuclear Instruments And Methods In Physics Research Section B: Beam Interactions With Materials And Atoms*. **184**, 229-254 (2001)

[4] Apfel, R. The superheated drop detector. *Nuclear Instruments And Methods*. **162**, 603-608 (1979)

[5] Das, M., Chatterjee, B., Roy, B. & Roy, S. How high can the temperature of a liquid be raised without boiling?. *Physical Review E*. **62**, 5843 (2000)

[6] Callen, H. Thermodynamics and an Introduction to Thermostatistics. (John wiley & sons,1991)

[7] Maris, H. & Balibar, S. Negative pressures and cavitation in liquid helium. *Physics Today*. **53**, 29-34 (2000)

[8] Gibbs, J. On the equilibrium of heterogeneous substances. *American Journal Of Science*. **3**, 441-458 (1878)

[9] Ing, H. & Birnboim, H. A bubble-damage polymer detector for neutrons. *Nuclear Tracks And Radiation Measurements (1982)*. **8**, 285-288 (1984)

[10] Guo, S., Li, L., Guo, H., Tu, C., Wang, Y., Doke, T., Kato, T., Ozaki, K., Kyan, A., Piao, Y. & Others High energy heavy ion tracks in bubble detectors. *Radiation Measurements*. **31**, 167-172 (1999)

[11] Das, M., Yasuda, N., Homma, A. & Sawamura, T. Threshold temperatures of heavy ion-induced nucleation in superheated emulsions. *Nuclear Instruments And Methods In Physics Research Section A: Accelerators, Spectrometers, Detectors And Associated Equipment*. **543**, 570-576 (2005)

[12] Guo, S., Li, L., Doke, T., Kikuchi, J., Kyan, A., Yoshihira, E., Kato, T. & Murakami, T. Characteristics of heavy ion tracks in bubble detectors. *Radiation Measurements*. **34**, 269-272 (2001)

[13] Guo, S., Li, L., Chen, B., Doke, T., Kikuchi, J., Terasawa, K., Komiyama, M., Hara, K., Fuse, T. & Murakami, T. Status of bubble detectors for high-energy heavy ions. *Radiation Measurements*. **36**, 183-187 (2003)

[14] Lo, Y. & Apfel, R. Prediction and experimental confirmation of the response function for neutron detection using superheated drops. *Physical Review A*. **38**, 5260 (1988)

[15] Mondal, P., Sarkar, R. & Chatterjee, B. Characterization of R-134a superheated droplet detector for neutron detection. *Applied Radiation And Isotopes*. **90** pp. 1-7 (2014)

[16] Roy, B., Das, M., Roy, S. & Chatterjee, B. Photon sensitivity of superheated drop at room temperature. *Nuclear Instruments And Methods In Physics Research Section A: Accelerators, Spectrometers, Detectors And Associated Equipment*. **455**, 782-783 (2000)

[17] Roy, B., Das, M., Roy, S. & Chatterjee, B. Threshold temperature for g-ray detection in superheated drop detector. *Radiation Physics And Chemistry*. **61**, 509-510 (2001)

[18] Sahoo, S., Seth, S. & Das, M. The threshold of gamma-ray induced bubble nucleation in superheated emulsion. *Nuclear Instruments And Methods In Physics Research Section A: Accelerators, Spectrometers, Detectors And Associated Equipment*. **931** pp. 44-51 (2019)

[19] Ing, H. The status of the bubble-damage polymer detector. *International Journal Of Radiation Applications And Instrumentation. Part D. Nuclear Tracks And Radiation Measurements*. **12**, 49-54 (1986)

[20] Apfel, R. & Lo, Y. Practical neutron dosimetry with superheated drops. *Health Physics*. **56**, 79-83 (1989)

[21] D'Errico, F., Alberts, W., Dietz, E., Gualdrini, G., Kurkdjian, J., Noccioni, P. & Siebert, B. Neutron ambient dosimetry with superheated drop (bubble) detectors. *Radiation Protection Dosimetry*. **65**, 397-400 (1996)

[22] Das, M., Chatterjee, B., Roy, B. & Roy, S. Superheated drop as a neutron spectrometer. *Nuclear Instruments And Methods In Physics Research Section A: Accelerators, Spectrometers, Detectors And Associated Equipment*. **452**, 273-279 (2000)

[23] Das, M., Roy, B., Chatterjee, B. & Roy, S. A sensitive neutron dosimeter using superheated liquid. *Applied Radiation And Isotopes*. **53**, 759-763 (2000)

[24] Apfel, R. & D'Errico, F. A neutron spectrometer based on temperature variations in superheated drop compositions. *Nuclear Instruments And Methods In Physics Research Section A: Accelerators, Spectrometers, Detectors And Associated Equipment*. **476**, 298-303 (2002)

[25] Bonin, H., Desnoyers, G. & Cousins, T. Fast neutron dosimetry and spectroscopy using bubble detectors. *Radiation Protection Dosimetry*. **46**, 265-271 (1993)

[26] Roy, S., Apfel, R. & Lo, Y. Superheated drop detector: a potential tool in neutron research. *Nuclear Instruments And Methods In Physics Research Section A: Accelerators, Spectrometers, Detectors And Associated Equipment*. **255**, 199-206 (1987)

[27] D'Errico, F., Agosteo, S., V. Sannikov, A. & Silari, M. High-energy neutron dosimetry with superheated drop detectors. *Radiation Protection Dosimetry*. **100**, 529-532 (2002)

[28] Roy, S. & Roy, B. Use of superheated liquid in neutron detection. *Current Science*. pp. 516-528 (2003)

[29] Evans, T. & Wang, C. Measurement of distributions of small-scale energy depositions from low-linear energy transfer particles using the superheated drop detector. *Radiation Research*. **151**, 19-30 (1999)

[30] Guo, S., Li, L., Chen, B., Doke, T., Kikuchi, J., Terasawa, K., Komiyama, M., Hara, K. & Fuse, T. Proton tracks in bubble detector. *Nuclear Instruments And Methods In Physics Research Section B: Beam Interactions With Materials And Atoms*. **198**, 135-141 (2002)

[31] Ponraju, D., Jayashree, C., Krishnan, H., Viswanathan, S. & Indira, R. Development of superheated emulsion technique for alpha activity measurements. *Nuclear Instruments And Methods In Physics Research Section A: Accelerators, Spectrometers, Detectors And Associated Equipment*. **580**, 388-390 (2007)

[32] Apfel, R. & Roy, S. Investigations on the applicability of superheated drop detectors in neutron dosimetry. *Nuclear Instruments And Methods In Physics Research*. **219**, 582-587 (1984)

[33] Nath, R., Meigooni, A., King, C., Smolen, S. & D'Errico, F. Superheated drop detector for determination of neutron dose equivalent to patients undergoing high-energy x-ray and electron radiotherapy. *Medical Physics*. **20**, 781-787 (1993)

[34] Lamba, M., Holland, S., Elson, H., D'Errico, F. & Nath, R. Magnetic resonance imaging of microbubbles in a superheated emulsion chamber for brachytherapy dosimetry. *Medical Physics*. **25**, 2316-2325 (1998)

[35] D'Errico, F., Nath, R., Lamba, M. & Holland, S. A position-sensitive superheated emulsion chamber for three-dimensional photon dosimetry. *Physics In Medicine & Biology*. **43**, 1147 (1998)

[36] Sarkar, R., Chatterjee, B., Roy, B. & Roy, S. Radiation detection by using superheated droplets. *Radiation Physics And Chemistry*. **75**, 2186-2194 (2006)

[37] Apfel, R. & Roy, S. Superheated drop detector: A possible alternative for neutron dosimetry. *Radiation Protection Dosimetry*. **10**, 327-330 (1985)

[38] Benck, S., D'Errico, F., Denis, J., Meulders, J., Nath, R. & Pitcher, E. In-phantom spectra and dose distributions from a high-energy neutron therapy beam. *Nuclear Instruments And Methods In Physics Research Section A: Accelerators, Spectrometers, Detectors And Associated Equipment*. **476**, 127-131 (2002)

[39] D'Errico, F., Nath, R., Silvano, G. & Tana, L. In vivo neutron dosimetry during high-energy bremsstrahlung radiotherapy. *International Journal Of Radiation Oncology* Biology* Physics*. **41**, 1185-1192 (1998)

[40] Ing, H. & Mortimer, A. Space radiation dosimetry using bubble detectors. *Advances In Space Research*. **14**, 73-76 (1994)

[41] DiGiovine, B., Henderson, D., Holt, R., Raut, R., Rehm, K., Robinson, A., Sonnenschein, A., Rusev, G., Tonchev, A. & Ugalde, C. Bubble chambers for experiments in nuclear astrophysics. *Nuclear Instruments And Methods In Physics Research Section A: Accelerators, Spectrometers, Detectors And Associated Equipment*. **781** pp. 96-104 (2015)

[42] Mondal, P., Sarkar, R. & Chatterjee, B. A new method for measurement of droplet size distribution in superheated emulsions. *Measurement Science And Technology*. **21**, 045104 (2010)

[43] D'Errico, F., Di Fulvio, A., Maryañski, M., Selici, S. & Torrigiani, M. Optical readout of superheated emulsions. *Radiation Measurements*. **43**, 432-436 (2008)

[44] Das, M., Arya, A., Marick, C., Kanjilal, D. & Saha, S. An active drop counting device using condenser microphone for superheated emulsion detector. *Review Of Scientific Instruments*. **79** (2008)

[45] Apfel, R. Sonic effervescence: A tutorial on acoustic cavitation. *The Journal Of The Acoustical Society Of America*. **101**, 1227-1237 (1997)

[46] Ardid, M., Baschirotto, A., Burgio, N., Corcione, M., Cretara, L., De Matteis, M., Felis, I., Frullini, M., Manara, L., Quintino, A. & Others Effects of the thermodynamic conditions on the acoustic signature of bubble nucleation in superheated liquids used in dark matter search experiments. *The European Physical Journal C*. **79**, 1-9 (2019)

[47] Robinson, A. & Judd, R. The dynamics of spherical bubble growth. *International Journal Of Heat And Mass Transfer*. **47**, 5101-5113 (2004)

[48] Stawczyk, J. Experimental evaluation of LPG tank explosion hazards. *Journal Of Hazardous Materials*. **96**, 189-200 (2003)

[49] Simoes-Moreira, J. & Shepherd, J. Evaporation waves in superheated dodecane. *Journal Of Fluid Mechanics*. **382** pp. 63-86 (1999)

[50] Pinhasi, G., Ullmann, A. & Dayan, A. 1D plane numerical model for boiling liquid expanding vapor explosion (BLEVE). *International Journal Of Heat And Mass Transfer*. **50**, 4780-4795 (2007)

[51] Di Fulvio, A., Huang, J., Staib, L. & D'Errico, F. LET dependence of bubbles evaporation pulses in superheated emulsion detectors. *Nuclear Instruments And Methods In Physics Research Section A: Accelerators, Spectrometers, Detectors And Associated Equipment*. **784** pp. 156-161 (2015)

[52] Das, M., Seth, S., Saha, S., Bhattacharya, S. & Bhattacharjee, P. Neutron-gamma discrimination by pulse analysis with superheated drop detector. *Nuclear Instruments And Methods In Physics Research Section A: Accelerators, Spectrometers, Detectors And Associated Equipment*. **622**, 196-199 (2010)

[53] Mondal, P., Seth, S., Das, M. & Bhattacharjee, P. Study of low frequency acoustic signals from superheated droplet detector. *Nuclear Instruments And Methods In Physics Research Section A: Accelerators, Spectrometers, Detectors And Associated Equipment*. **729** pp. 182-187 (2013)

[54] Archambault, S., Aubin, F., Auger, M., Beleshi, M., Behnke, E., Behnke, J., Beltran, B., Clark, K., Dai, X., Das, M. & Others New insights into particle detection with superheated liquids. *New Journal Of Physics*. **13**, 043006 (2011)

[55] Aubin, F., Auger, M., Genest, M., Giroux, G., Gornea, R., Faust, R., Leroy, C., Lessard, L., Martin, J., Morlat, T. & Others Discrimination of nuclear recoils

from alpha particles with superheated liquids. *New Journal Of Physics*. **10**, 103017 (2008)

[56] Felizardo, M., Morlat, T., Girard, T., Kling, A., Fernandes, A., Marques, J., Carvalho, F., Ramos, A., Collaboration, S. & Others Neutron–Alpha irradiation response of superheated emulsion detectors. *Nuclear Instruments And Methods In Physics Research Section A: Accelerators, Spectrometers, Detectors And Associated Equipment*. **863** pp. 62-73 (2017)

[57] Seth, S. & Das, M. Radiation linear energy transfer and drop size dependence of the low frequency signal from tiny superheated droplets. *Nuclear Instruments And Methods In Physics Research Section A: Accelerators, Spectrometers, Detectors And Associated Equipment*. **837** pp. 92-98 (2016)

[58] Behnke, E., Besnier, M., Bhattacharjee, P., Dai, X., Das, M., Davour, A., Debris, F., Dhungana, N., Farine, J., Fines-Neuschild, M. & Others Final results of the PICASSO dark matter search experiment. *Astroparticle Physics*. **90** pp. 85-92 (2017)

[59] Antonicci, A., Ardid, M., Bertoni, R., Bruno, G., Burgio, N., Caruso, G., Cattaneo, D., Chignoli, F., Clemenza, M., Corcione, M. & Others MOSCAB: a geyser-concept bubble chamber to be used in a dark matter search. *The European Physical Journal C*. **77**, 1-7 (2017)

[60] D'Errico, F. & Alberts, W. Superheated-drop (bubble) neutron detectors and their compliance with ICRP-60. *Radiation Protection Dosimetry*. **54**, 357-360 (1994)

[61] D'Errico, F., Nath, R., Holland, S., Lamba, M., Patz, S. & Rivard, M. A position-sensitive neutron spectrometer/dosimeter based on pressurized superheated drop (bubble) detectors. *Nuclear Instruments And Methods In Physics Research Section A: Accelerators, Spectrometers, Detectors And Associated Equipment*. **476**, 113-118 (2002)

[62] D'Errico, F., Matzke, M. & Siebert, B. Energy-and angle-differential neutron fluence measurements with superheated drop (bubble) detectors. *Nuclear Instruments And Methods In Physics Research Section A: Accelerators, Spectrometers, Detectors And Associated Equipment*. **476**, 277-290 (2002)

[63] Sawamura, T., Kaneko, J., Abe, M., Tamura, M., Murai, I., Homma, A., Fujita, F. & Tsuda, S. Effect of lead converter on superheated drop detector response to high-energy neutrons. *Nuclear Instruments And Methods In Physics Research*

Section A: Accelerators, Spectrometers, Detectors And Associated Equipment. **505**, 29-32 (2003)

[64] Pless, I. & Plano, R. Negative pressure isopentane bubble chamber. *Review Of Scientific Instruments*. **27**, 935-937 (1956)

[65] Norman, A. & Spiegler, P. Radiation nucleation of bubbles in water. *Nuclear Science And Engineering*. **16**, 213-217 (1963)

[66] Bruno, G., Burgio, N., Corcione, M., Cretara, L., Frullini, M., Fulgione, W., Manara, L., Quintino, A., Santagata, A. & Zanotti, L. On the critical energy required for homogeneous nucleation in bubble chambers employed in dark matter searches. *The European Physical Journal C*. **79**, 183 (2019)

[67] Tenner, A. Nucleation in bubble chambers. *Nuclear Instruments And Methods*. **22** pp. 1-42 (1963)

[68] Bell, C., Oberle, N., Rohsenow, W., Todreas, N. & Tso, C. Radiation-induced boiling in superheated water and organic liquids. *Nuclear Science And Engineering*. **53**, 458-465 (1974)

[69] Seitz, F. On the theory of the bubble chamber. *The Physics Of Fluids*. **1**, 2-13 (1958)

[70] Bugg, D. Progress in Nuclear Physics. (Butterworth-Springer, London,1959)

[71] Sun, Y., Chu, B. & Apfel, R. Radiation-induced cavitation process in a metastable superheated liquid I. Initial and pre-bubble formation stages. *Journal Of Computational Physics*. **103**, 116-125 (1992)

[72] El-Nagdy, M. & Harris, M. EXPERIMENTAL STUDY OF RADIATION-INDUCED BOILING IN SUPERHEATED LIQUIDS.. (Babcock,1971)

[73] Deitrich, L. & Connolly, T. A study of fission-fragment-induced nucleation of bubbles in superheated water. *Nuclear Science And Engineering*. **50**, 273-282 (1973)

[74] Das, M. & Sawamura, T. Estimation of nucleation parameter for neutron-induced nucleation in superheated emulsion. *Nuclear Instruments And Methods In Physics Research Section A: Accelerators, Spectrometers, Detectors And Associated Equipment*. **531**, 577-584 (2004)

[75] Ziegler, J. SRIM (Stopping and Range of Ions in Matter) computer code. *Http://www. Srim. Org*.

[76] Apfel, R., Roy, S. & Lo, Y. Prediction of the minimum neutron energy to nucleate vapor bubbles in superheated liquids. *Physical Review A*. **31**, 3194 (1985)

[77] Apfel, R. Photon-insensitive, thermal to fast neutron detector. *Nuclear Instruments And Methods*. **179**, 615-616 (1981)

[78] Das, M., Sarkar, R., Mondal, P., Saha, S., Chatterjee, B. & Roy, S. Nucleation efficiency of R134a as a sensitive liquid for superheated drop emulsion detector. *Pramana*. **75** pp. 675-682 (2010)

[79] Das, M., Roy, B., Chatterjee, B. & Roy, S. Efficiency of neutron detection of superheated drops of Freon-22. *Radiation Measurements*. **30**, 35-39 (1999)

[80] Barnabé-Heider, M., Di Marco, M., Doane, P., Genest, M., Gornea, R., Guénette, R., Leroy, C., Lessard, L., Martin, J., Wichoski, U. & Others Response of superheated droplet detectors of the PICASSO dark matter search experiment. *Nuclear Instruments And Methods In Physics Research Section A: Accelerators, Spectrometers, Detectors And Associated Equipment*. **555**, 184-204 (2005)

[81] D'Errico, F., Alberts, W., Curzio, G., Guldbakke, S., Kluge, H. & Matzke, M. Active neutron spectrometry with superheated drop (bubble) detectors. *Radiation Protection Dosimetry*. **61**, 159-162 (1995)

[82] Bertone, G. & Hooper, D. History of dark matter. *Reviews Of Modern Physics*. **90**, 045002 (2018)

[83] Clowe, D., Bradač, M., Gonzalez, A., Markevitch, M., Randall, S., Jones, C. & Zaritsky, D. A direct empirical proof of the existence of dark matter. *The Astrophysical Journal*. **648**, L109 (2006)

[84] Jungman, G., Kamionkowski, M. & Griest, K. Supersymmetric dark matter. *Physics Reports*. **267**, 195-373 (1996)

[85] Bertone, G., Hooper, D. & Silk, J. Particle dark matter: Evidence, candidates and constraints. *Physics Reports*. **405**, 279-390 (2005)

[86] Archambault, S., Aubin, F., Auger, M., Behnke, E., Beltran, B., Clark, K., Dai, X., Davour, A., Farine, J., Faust, R. & Others Dark matter spin-dependent limits for WIMP interactions on 19F by PICASSO. *Physics Letters B*. **682**, 185-192 (2009)

[87] Behnke, E., Behnke, J., Brice, S., Broemmelsiek, D., Collar, J., Conner, A., Cooper, P., Crisler, M., Dahl, C., Fustin, D. & Others First dark matter search results from a 4-kg CF 3 I bubble chamber<? format?> operated in a deep underground site. *Physical Review D—Particles, Fields, Gravitation, And Cosmology*. **86**, 052001 (2012)

[88] Behnke, E., Benjamin, T., Brice, S., Broemmelsiek, D., Collar, J., Cooper, P., Crisler, M., Dahl, C., Fustin, D., Hall, J. & Others Direct measurement of the bubble-nucleation energy threshold in a CF 3 I bubble chamber. *Physical Review D—Particles, Fields, Gravitation, And Cosmology*. **88**, 021101 (2013)

[89] Amole, C. & Others Dark Matter Search Results from the PICO-2L CF Bubble Chamber. *Phys. Rev. Lett.*. **114**, 231302 (2015)

[90] Ardid, M., Bou-Cabo, M., Felis, I., Martınez-Mora, J., Collaboration, M. & Others MOSCAB: direct dark matter search using the geyser technique. *Nuclear And Particle Physics Proceedings*. **273** pp. 2354-2356 (2016)

[91] Martynyuk, Y., Smirnova, N. & Wood, J. Sound generation in superheated liquids by heavy charged particles. *Soviet Physics. Acoustics*. **37**, 376-378 (1991)

[92] Rayleigh, L. VIII. On the pressure developed in a liquid during the collapse of a spherical cavity. *The London, Edinburgh, And Dublin Philosophical Magazine And Journal Of Science*. **34**, 94-98 (1917)

[93] Plesset, M. & Zwick, S. The growth of vapor bubbles in superheated liquids. *Journal Of Applied Physics*. **25**, 493-500 (1954)

[94] Shepherd, J. Dynamics of vapor explosions: rapid evaporation and instability of butane droplets exploding at the superheat limit. (California Institute of Technology,1981)

[95] Minnaert, M. XVI. On musical air-bubbles and the sounds of running water. *The London, Edinburgh, And Dublin Philosophical Magazine And Journal Of Science*. **16**, 235-248 (1933)

[96] Strasberg, M. Onset of ultrasonic cavitation in tap water. *The Journal Of The Acoustical Society Of America*. **31**, 163-176 (1959)

[97] Crum, L. Measurements of the growth of air bubbles by rectified diffusion. *The Journal Of The Acoustical Society Of America*. **68**, 203-211 (1980)

[98] Gaitan, D., Crum, L., Church, C. & Roy, R. Sonoluminescence and bubble dynamics for a single, stable, cavitation bubble. *The Journal Of The Acoustical Society Of America*. **91**, 3166-3183 (1992)

[99] Lauterborn, W. Kavitation durch laserlicht. *Acustica.*. **31** pp. 51-78 (1974)

[100] Fong, S., Adhikari, D., Klaseboer, E. & Khoo, B. Interactions of multiple spark-generated bubbles with phase differences. *Experiments In Fluids*. **46** pp. 705-724 (2009)

[101] Unger, B. & Marston, P. Optical levitation of bubbles in water by the radiation pressure of a laser beam: an acoustically quiet levitator. *The Journal Of The Acoustical Society Of America*. **83**, 970-975 (1988)

[102] Prentice, P., Cuschieri, A., Dholakia, K., Prausnitz, M. & Campbell, P. Membrane disruption by optically controlled microbubble cavitation. *Nature Physics*. **1**, 107-110 (2005)

[103] Jones, P., Stride, E. & Saffari, N. Trapping and manipulation of microscopic bubbles with a scanning optical tweezer. *Applied Physics Letters*. **89** (2006)

[104] Garbin, V., Cojoc, D., Ferrari, E., Di Fabrizio, E., Overvelde, M., Van Der Meer, S., De Jong, N., Lohse, D. & Versluis, M. Changes in microbubble dynamics near a boundary revealed by combined optical micromanipulation and high-speed imaging. *Applied Physics Letters*. **90** (2007)

[105] Yang, K., Zhou, Y., Ren, Q., Ye, J. & Deng, C. Dynamics of microbubble generation and trapping by self-focused femtosecond laser pulses. *Applied Physics Letters*. **95** (2009)

[106] Holt, R. & Crum, L. Acoustically forced oscillations of air bubbles in water: Experimental results. *The Journal Of The Acoustical Society Of America*. **91**, 1924-1932 (1992)

[107] Tian, Y., Ketterling, J. & Apfel, R. Direct observation of microbubble oscillations. *The Journal Of The Acoustical Society Of America*. **100**, 3976-3978 (1996)

[108] Barber, B. & Putterman, S. Observation of synchronous picosecond sonoluminescence. *Nature*. **352**, 318-320 (1991)

[109] Barber, B. Synchronous picosecond sonoluminescence. (University of California, Los Angeles,1992)

[110] Matula, T. Inertial cavitation and single–bubble sonoluminescence. *Philosophical Transactions Of The Royal Society Of London. Series A: Mathematical, Physical And Engineering Sciences*. **357**, 225-249 (1999)

[111] Lauterborn, W. & Hentschel, W. Cavitation bubble dynamics studied by high speed photography and holography: part two. *Ultrasonics*. **24**, 59-65 (1986)

[112] Lauterborn, W. & Hentschel, W. Cavitation bubble dynamics studied by high speed photography and holography: part one. *Ultrasonics*. **23**, 260-268 (1985)

[113] Tomita, Y. & Shima, A. High-speed photographic observations of laser-induced cavitation bubbles in water. *Acta Acustica United With Acustica*. **71**, 161-171 (1990)

[114] Lauterborn, W. & Ohl, C. The peculiar dynamics of cavitation bubbles. *In Fascination Of Fluid Dynamics: A Symposium In Honour Of Leen Van Wijngaarden*. pp. 63-76 (1998)

[115] Greenspan, M. Radiation-induced acoustic cavitation; apparatus and some results. *J. Res. Nat. Bur. Stand., C*. **71** pp. 299-312 (1967)

[116] Trilling, L. The collapse and rebound of a gas bubble. *Journal Of Applied Physics*. **23**, 14-17 (1952)

[117] Jarman, P. Sonoluminescence: a discussion. *The Journal Of The Acoustical Society Of America*. **32**, 1459-1462 (1960)

[118] Wu, C. & Roberts, P. Shock-wave propagation in a sonoluminescing gas bubble. *Physical Review Letters*. **70**, 3424 (1993)

[119] Moss, W., Clarke, D., White, J. & Young, D. Hydrodynamic simulations of bubble collapse and picosecond sonoluminescence. *Physics Of Fluids*. **6**, 2979-2985 (1994)

[120] Metten, B. & Lauterborn, W. Molecular dynamics approach to single-bubble sonoluminescence. *Nonlinear Acoustics At The Turn Of The Millennium: ISNA 15, 15th International Symposium*. **524** pp. 429-432 (2000)

[121] Vuong, V. & Szeri, A. Sonoluminescence and diffusive transport. *Physics Of Fluids*. **8**, 2354-2364 (1996)

[122] Vuong, V., Szeri, A. & Young, D. Shock formation within sonoluminescence bubbles. *Physics Of Fluids*. **11**, 10-17 (1999)

[123] Nagrath, S., Jansen, K., Lahey Jr, R. & Akhatov, I. Hydrodynamic simulation of air bubble implosion using a level set approach. *Journal Of Computational Physics*. **215**, 98-132 (2006)s

[124] Lauterborn, W., Kurz, T., Mettin, R. & Ohl, C. Experimental and theoretical bubble dynamics. *Advances In Chemical Physics*. **110** pp. 295-380 (1999)

[125] Lauterborn, W., Kurz, T., Geisler, R., Kröninger, D. & Schanz, D. The single bubble–a hot microlaboratory. *Oscillations, Waves, And Interactions*. pp. 139-70 (2007)

[126] Vladimiroff, T., Carignan, Y., Macpherson, A. & Macpherson, P. The dynamics of hard spheres in a collapsing spherical container. *Molecular Physics*. **71**, 441-451 (1990)

[127] Matsumoto, M., Miyamoto, K., Ohguchi, K. & Kinjo, T. Molecular dynamics simulation of a collapsing bubble. *Progress Of Theoretical Physics Supplement*. **138** pp. 728-729 (2000)

[128] Yasui, K. Alternative model of single-bubble sonoluminescence. *Physical Review E*. **56**, 6750 (1997)

[129] Blake, J. & Gibson, D. Cavitation bubbles near boundaries. *Annual Review Of Fluid Mechanics*. **19**, 99-123 (1987)

[130] Isselin, J., Alloncle, A. & Autric, M. On laser induced single bubble near a solid boundary: contribution to the understanding of erosion phenomena. *Journal Of Applied Physics*. **84**, 5766-5771 (1998)

[131] Benjamin, T. & Ellis, A. The collapse of cavitation bubbles and the pressures thereby produced against solid boundaries. *Philosophical Transactions For The Royal Society Of London. Series A, Mathematical And Physical Sciences*. pp. 221-240 (1966)

[132] Chahine, G. & Bovis, A. Oscillation and collapse of a cavitation bubble in the vicinity of a two-liquid interface. *Cavitation And Inhomogeneities In Underwater Acoustics: Proceedings Of The First International Conference, Göttingen, Fed. Rep. Of Germany, July 9–11, 1979*. pp. 23-29 (1980)

[133] Blake, J. & Gibson, D. Growth and collapse of a vapour cavity near a free surface. *Journal Of Fluid Mechanics*. **111** pp. 123-140 (1981)

[134] Gregorčič, P., Petkovšek, R. & Možina, J. Investigation of a cavitation bubble between a rigid boundary and a free surface. *Journal Of Applied Physics*. **102** (2007)

[135] Hund, M. artin]: Untersuchungen zur Einzelblasenkavitation bei 10 Hz in einer wassergefüllten Druckkammer. *Acustica*. **21**, 269-282 (1969)

[136] Tomita, Y., Robinson, P., Tong, R. & Blake, J. Growth and collapse of cavitation bubbles near a curved rigid boundary. *Journal Of Fluid Mechanics*. **466** pp. 259-283 (2002)

[137] Brujan, E., Nahen, K., Schmidt, P. & Vogel, A. Dynamics of laser-induced cavitation bubbles near an elastic boundary. *Journal Of Fluid Mechanics*. **433** pp. 251-281 (2001)

[138] Brujan, E., Nahen, K., Schmidt, P. & Vogel, A. Dynamics of laser-induced cavitation bubbles near elastic boundaries: influence of the elastic modulus. *Journal Of Fluid Mechanics*. **433** pp. 283-314 (2001)

[139] Shaw, S., Jin, Y., Gentry, T. & Emmony, D. Experimental observations of the interaction of a laser generated cavitation bubble with a flexible membrane. *Physics Of Fluids*. **11**, 2437-2439 (1999)

[140] Turangan, C., Ong, G., Klaseboer, E. & Khoo, B. Experimental and numerical study of transient bubble-elastic membrane interaction. *Journal Of Applied Physics*. **100** (2006)

[141] Testud-Giovanneschi, P., Alloncle, A. & Dufresne, D. Collective effects of cavitation: Experimental study of bubble-bubble and bubble-shock wave interactions. *Journal Of Applied Physics*. **67**, 3560-3564 (1990)

[142] Vogel, A. & Lauterborn, W. Acoustic transient generation by laser-produced cavitation bubbles near solid boundaries. *The Journal Of The Acoustical Society Of America*. **84**, 719-731 (1988)

[143] Vogel, A., Lauterborn, W. & Timm, R. Optical and acoustic investigations of the dynamics of laser-produced cavitation bubbles near a solid boundary. *Journal Of Fluid Mechanics*. **206** pp. 299-338 (1989)

[144] Strasberg, M. The pulsation frequency of nonspherical gas bubbles in liquids. *The Journal Of The Acoustical Society Of America*. **25**, 536-537 (1953)

[145] Sato, K., Tomita, Y. & Shima, A. Numerical analysis of a gas bubble near a rigid boundary in an oscillatory pressure field. *The Journal Of The Acoustical Society Of America*. **95**, 2416-2424 (1994)

[146] Johnsen, E. & Colonius, T. Numerical simulations of non-spherical bubble collapse. *Journal Of Fluid Mechanics*. **629** pp. 231-262 (2009)

[147] Vogel, A., Engelhardt, R., Behnle, U. & Parlitz, U. Minimization of cavitation effects in pulsed laser ablation illustrated on laser angioplasty. *Applied Physics B*. **62** pp. 173-182 (1996)

[148] Devin Jr, C. Survey of thermal, radiation, and viscous damping of pulsating air bubbles in water. *The Journal Of The Acoustical Society Of America*. **31**, 1654-1667 (1959)

[149] Plesset, M. & Hsieh, D. Theory of gas bubble dynamics in oscillating pressure fields. *The Physics Of Fluids*. **3**, 882-892 (1960)

[150] Chapman, R. & Plesset, M. Thermal effects in the free oscillation of gas bubbles. (1971)

[151] Lauterborn, W. Numerical investigation of nonlinear oscillations of gas bubbles in liquids. *The Journal Of The Acoustical Society Of America*. **59**, 283-293 (1976)

[152] Guckenheimer, J. & Holmes, P. Nonlinear oscillations, dynamical systems, and bifurcations of vector fields. (Springer Science Business Media,2013)

[153] Prosperetti, A. Nonlinear oscillations of gas bubbles in liquids: steady-state solutions. *The Journal Of The Acoustical Society Of America*. **56**, 878-885 (1974)

[154] Prosperetti, A. Nonlinear oscillations of gas bubbles in liquids. Transient solutions and the connection between subharmonic signal and cavitation. *The Journal Of The Acoustical Society Of America*. **57**, 810-821 (1975)

[155] Prosperetti, A. Thermal effects and damping mechanisms in the forced radial oscillations of gas bubbles in liquids. *The Journal Of The Acoustical Society Of America*. **61**, 17-27 (1977)

[156] Fanelli, M., Prosperetti, A. & Reali, M. Radial oscillations of gas-vapour bubbles in liquids part ii: Numerical examples. *Acta Acustica United With Acustica*. **49**, 98-109 (1981)

[157] Crum, L. & Prosperetti, A. Nonlinear oscillations of gas bubbles in liquids: an interpretation of some experimental results. *The Journal Of The Acoustical Society Of America*. **73**, 121-127 (1983)

[158] Prosperetti, A., Crum, L. & Commander, K. Nonlinear bubble dynamics. *The Journal Of The Acoustical Society Of America*. **83**, 502-514 (1988)

[159] Prosperetti, A. The thermal behaviour of oscillating gas bubbles. *Journal Of Fluid Mechanics*. **222** pp. 587-616 (1991)

[160] Parlitz, U., Englisch, V., Scheffczyk, C. & Lauterborn, W. Bifurcation structure of bubble oscillators. *The Journal Of The Acoustical Society Of America*. **88**, 1061-1077 (1990)

[161] Cramer, E. The dynamics and acoustic emission of bubbles driven by a sound field. *Cavitation And Inhomogeneities In Underwater Acoustics: Proceedings Of The First International Conference, Göttingen, Fed. Rep. Of Germany, July 9–11, 1979*. pp. 54-63 (1980)

[162] Lauterborn, W. & Mettin, R. Nonlinear bubble dynamics: response curves and more. *Sonochemistry And Sonoluminescence*. pp. 63-72 (1999)

[163] Geist, K., Parlitz, U. & Lauterborn, W. Comparison of different methods for computing Lyapunov exponents. *Progress Of Theoretical Physics*. **83**, 875-893 (1990)

[164] Keller, J. & Miksis, M. Bubble oscillations of large amplitude. *The Journal Of The Acoustical Society Of America*. **68**, 628-633 (1980)

[165] Lauterborn, W. & Parlitz, U. Methods of chaos physics and their application to acoustics. *The Journal Of The Acoustical Society Of America*. **84**, 1975-1993 (1988)

[166] Lauterborn, W., Schmitz, E. & Judt, A. Experimental approach to a complex acoustic system. *International Journal Of Bifurcation And Chaos*. **3**, 635-642 (1993)

[167] Behnia, S., Sojahrood, A., Soltanpoor, W. & Sarkhosh, L. Towards classification of the bifurcation structure of a spherical cavitation bubble. *Ultrasonics*. **49**, 605-610 (2009)

[168] Fujiwara, T. & Shima, A. Nonlinear oscillations of bubbles in compressible hydraulic oils. *The Journal Of The Acoustical Society Of America*. **68**, 1502-1508 (1980)

[169] Shima, A., Rajvanshi, S. & Tsujino, T. Study of nonlinear oscillations of bubbles in Powell–Eyring fluids. *The Journal Of The Acoustical Society Of America*. **77**, 1702-1709 (1985)

[170] Tsujino, T., Shima, A. & Oikawa, Y. Effect of polymer additives on the generation of subharmonic and harmonic bubble oscillations in an ultrasonically irradiated liquid. *Journal Of Sound And Vibration*. **123**, 171-184 (1988)

[171] Brujan, E. The effect of polymer concentration on the non-linear oscillation of a bubble in a sound-irradiated liquid. *Journal Of Sound And Vibration*. **173**, 329-342 (1994)

[172] Moon, F. Chaotic Dynamics and Fractals: An Introduction for Applied Scientists and Engineers. (John Wiley Sons,1992)

[173] Shoji, M. Chaos in boiling on a small-size heater. *Proc. Fourth ASME-JSME Thermal Joint Conference, Maui, 1995*. **2** pp. 225-232 (1995)

[174] Grassberger, P. & Procaccia, I. Characterization of strange attractors. *Physical Review Letters*. **50**, 346 (1983)

[175] Kenning, D. & Yan, Y. Pool boiling heat transfer on a thin plate: features revealed by liquid crystal thermography. *International Journal Of Heat And Mass Transfer*. **39**, 3117-3137 (1996)

[176] Shoji, M., Negishi, N., Hatae, H. & Haramura, Y. Nonlinear chaotic characteristics of saturated pool boiling of water on a horizontal copper surface. *National Heat Transfer Symposium Of Japan*. **33** pp. 253-254 (1996)

[177] Wolf, A., Swift, J., Swinney, H. & Vastano, J. Determining Lyapunov exponents from a time series. *Physica D: Nonlinear Phenomena*. **16**, 285-317 (1985)

[178] Shoji, M. & Takagi, Y. Bubbling features from a single artificial cavity. *International Journal Of Heat And Mass Transfer*. **44**, 2763-2776 (2001)

[179] Zhang, L. & Shoji, M. Nucleation site interaction in pool boiling on the artificial surface. *International Journal Of Heat And Mass Transfer*. **46**, 513-522 (2003)

[180] Yanagita, T. Coupled map lattice model for boiling. *International Symposium On Imaging In Transport Processes.*. (1992)

[181] Yanagita, T. Phenomenology of boiling: A coupled map lattice model. *Chaos: An Interdisciplinary Journal Of Nonlinear Science*. **2**, 343-350 (1992)

[182] Ellepola, J. Nucleation site interactions in pool boiling. *Proceedings Of The 2nd European Thermal Sciences 14th UIT National Heat Transfer Conference, Rome, 29-31 May 1996*. (1996)

[183] Son, G. & Dhir, V. Numerical simulation of a single bubble during partial nucleate boiling on a horizontal surface. *Heat Transfer Conference*. **2** pp. 533-538 (1998)

[184] Baker, G. & Gollub, J. Chaotic dynamics: an introduction. (Cambridge university press,1996)

[185] Takens, F. Detecting strange attractors in turbulence. *Dynamical Systems And Turbulence, Warwick 1980: Proceedings Of A Symposium Held At The University Of Warwick 1979/80*. pp. 366-381 (2006)

[186] Hegger, R., Kantz, H. & Schreiber, T. Practical implementation of nonlinear time series methods: The TISEAN package. *Chaos: An Interdisciplinary Journal Of Nonlinear Science*. **9**, 413-435 (1999)

[187] Fraser, A. & Swinney, H. Independent coordinates for strange attractors from mutual information. *Physical Review A*. **33**, 1134 (1986)

[188] Froyland, J. Introduction to chaos and coherence. (Routledge,2022)

[189] Chen, Y., Ding, M. & Kelso, J. Long memory processes (1/f type) in human coordination. *Physical Review Letters*. **79**, 4501 (1997)

[190] Auracher, H. Transition boiling. *International Heat Transfer Conference Digital Library*. (1990)

[191] Mosdorf, R. & Shoji, M. Chaos in nucleate boiling—-nonlinear analysis and modelling. *International Journal Of Heat And Mass Transfer*. **47**, 1515-1524 (2004)

[192] Ziegler, J. & Biersack, J. The stopping and range of ions in matter. *Treatise On Heavy-ion Science: Volume 6: Astrophysics, Chemistry, And Condensed Matter*. pp. 93-129 (1985)

[193] Turner, J. Atoms, radiation, and radiation protection. (John Wiley Sons,2008)

[194] Sahoo, S. & Das, M. The adequacy of energy deposition over thermodynamic behaviour in explaining the acoustic energy in bubble nucleation of superheated droplets. *Radiation Physics And Chemistry*. **187** pp. 109578 (2021)

[195] Goodman, M. & Witten, E. Detectability of certain dark-matter candidates. *Physical Review D.* **31**, 3059 (1985)

[196] Amole, C., Ardid, M., Arnquist, I., Asner, D., Baxter, D., Behnke, E., Bressler, M., Broerman, B., Cao, G., Chen, C. & Others Dark matter search results from the complete exposure of the PICO-60 C 3 F 8 bubble chamber. *Physical Review D.* **100**, 022001 (2019)

[197] Felizardo, M., Girard, T., Morlat, T., Fernandes, A., Ramos, A., Marques, J., Kling, A., Puibasset, J., Auguste, M., Boyer, D. & Others The SIMPLE phase II dark matter search. *Physical Review D.* **89**, 072013 (2014)

[198] Ali, S. & Das, M. Discrimination of neutron and gamma ray induced nucleation events at high frequency in R134a superheated emulsion. *Nuclear Instruments And Methods In Physics Research Section A: Accelerators, Spectrometers, Detectors And Associated Equipment.* **1025** pp. 166186 (2022)

[199] Ali, S., Das, M., Iyengar, A. & Paul, P. Characterization of homogeneous nucleation of superheated liquid droplets by nonlinear analysis. *Nuclear Instruments And Methods In Physics Research Section A: Accelerators, Spectrometers, Detectors And Associated Equipment.* **1057** pp. 168777 (2023)

[200] Flandrin, P. & Goncalves, P. Empirical mode decompositions as data-driven wavelet-like expansions. *International Journal Of Wavelets, Multiresolution And Information Processing.* **2**, 477-496 (2004)

[201] Rilling, G., Flandrin, P., Goncalves, P. & Others On empirical mode decomposition and its algorithms. *IEEE-EURASIP Workshop On Nonlinear Signal And Image Processing.* **3**, 8-11 (2003)

[202] Jha, R., Raju, D. & Sen, A. Analysis of tokamak data using a novel Hilbert transform based technique. *Physics Of Plasmas.* **13** (2006)

[203] Huang, N., Shen, Z., Long, S., Wu, M., Shih, H., Zheng, Q., Yen, N., Tung, C. & Liu, H. The empirical mode decomposition and the Hilbert spectrum for nonlinear and non-stationary time series analysis. *Proceedings Of The Royal Society Of London. Series A: Mathematical, Physical And Engineering Sciences.* **454**, 903-995 (1998)

[204] Staszewski, W. & Worden, K. Wavelet analysis of time-series: coherent structures, chaos and noise. *International Journal Of Bifurcation And Chaos.* **9**, 455-471 (1999)

[205] Murguia, J. & Campos-Cantón, E. Wavelet analysis of chaotic time series. *Revista Mexicana De Fısica*. **52**, 155-162 (2006)

[206] Rohatgi-Mukherjee, K. Fundamentals of photochemistry. (New Age International,1978)

[207] Sauer, M., Hofkens, J. & Enderlein, J. Handbook of fluorescence spectroscopy and imaging: from ensemble to single molecules. (John Wiley Sons,2010)

[208] Lakowicz, J. Principles of fluorescence spectroscopy. (Springer,2006)

[209] Debnath, P., Chakraborty, S., Deb, S., Nath, J., Bhattacharjee, D. & Hussain, S. Reversible transition between excimer and J-aggregate of indocarbocyanine dye in Langmuir–Blodgett (LB) films. *The Journal Of Physical Chemistry C*. **119**, 9429-9441 (2015)

[210] Nilapwar, S., Nardelli, M., Westerhoff, H. & Verma, M. Absorption spectroscopy. *Methods In Enzymology*. **500** pp. 59-75 (2011)

[211] Feldman, H., Iron, M., Fixler, D., Moshkov, S., Zurgil, N., Afrimzon, E. & Deutsch, M. Fluorophore spectroscopy in aqueous glycerol solution: the interactions of glycerol with the fluorophore. *Photochemical Photobiological Sciences*. **20** pp. 1397-1418 (2021)

[212] Nayak, P., Gupta, S., Jain, A., Mazumdar, I., Raha, S., Saha, S., Bobrov, A., Osipov, A. & Shwartz, B. A study of the -ray flux during the total solar eclipse of 1 August 2008 at Novosibirsk, Russia. *Astroparticle Physics*. **32**, 286-293 (2010)

[213] Antonova, V., Volodichev, N., Kryukov, S., Chubenko, A. & Shchepetov, A. Effect of solar eclipses on neutron flux variations at the earth's surface. *Bulletin Of The Russian Academy Of Sciences: Physics*. **71** pp. 1054-1057 (2007)

[214] Volodichev, N., Zakharov, V., Kuzhevskij, B., Nechaev, O., Podorolski, A., Chubenko, A., Shepetov, A. & Antonova, V. The Flows of Neutrons of Spase Radiation and from Terrestrial Crust. *Proceedings Of The 27th International Cosmic Ray Conference. 07-15 August, 2001. Hamburg, Germany. Under The Auspices Of The International Union Of Pure And Applied Physics (IUPAP)., P. 4204*. **10** pp. 4204 (2001)

[215] Sato, T. Analytical model for estimating terrestrial cosmic ray fluxes nearly anytime and anywhere in the world: Extension of PARMA/EXPACS. *PloS One*. **10**, e0144679 (2015)

REPRINTS

Nuclear Instruments and Methods in Physics Research A 1057 (2023) 168777

Contents lists available at ScienceDirect

Nuclear Inst. and Methods in Physics Research, A

journal homepage: www.elsevier.com/locate/nima

Full Length Article

Characterization of homogeneous nucleation of superheated liquid droplets by nonlinear analysis

Suraj Ali [a,b,c], Mala Das [a,*], A. N. Sekar Iyengar [a], Pabitra Kumar Paul [b]

[a] Saha Institute of Nuclear Physics, 1/AF, Bidhannagar, Kolkata, 700064, India
[b] Jadavpur University, Department of Physics, 188 Raja S.C. Mallick Road, Kolkata, 700032, India
[c] Muralidhar Girls' College, Department of Physics, P411/14 Gariahat Road, Kolkata, 700029, India

ARTICLE INFO

Keywords:
Superheated liquid droplet
Nucleation
Nonlinearity
Neutron
Gamma-rays
Discrimination

ABSTRACT

The homogeneous bubble nucleation in superheated liquid droplets can be initiated by energetic particles or radiation. The nonlinearity in the heat transfer introduces chaos in the temperature time series of a boiling system. In the present study, the acoustical pulses from the homogeneous nucleation of superheated liquid droplets by neutrons and gamma-rays have been collected. Nonlinear time series analysis methods like 3D attractor reconstruction and Fast Fourier transformation (FFT) have been performed on the collected pulses. The analysis predicts the possibility of the existence of chaos, and the positive value of the largest Lyapunov exponent confirms it. The nonlinearity in the energy deposition by both the recoil nuclei and electrons from the neutrons and gamma-rays respectively, introduce chaos. A qualitative difference has been observed in the 3D attractor and Rescaled Range (R/S) plots between the neutron and gamma-ray-induced pulses, and the present differences are useful for the identification of these pulses.

1. Introduction

The boiling of liquid is a common phenomenon that was studied a few thousand years ago, but the underlying mechanism of boiling is still not fully understood because of the complexity of the process. The boiling process consists of many sub-processes and their mutual interaction, where the most important sub-process is the nucleation site problem [1]. In this case, mutual interaction between bubbles and the heating surface and interaction with neighbouring nuclear sites play important roles. The complexity level is high because the interacting bubble creates a complex dynamical system that includes many processes like heat transfer, phase change, coalescence, and their combined effects. Nonlinear dynamical systems under selected conditions are able to show chaos. A system is said to be chaotic where the output is not proportional to the input, and under some conditions, such systems exhibit unpredictable long-term behaviour. Irregularity of motion and sensitivity to the initial conditions are the key signatures of the chaotic system. A computer simulation with appropriate mathematical tools can confirm the experimentally observed chaotic behaviour of a system. However, the chaotic behaviour of an experiment can be directly identified from experimental data using nonlinear time series analysis. The effect of the conjugate sub-process of boiling was explained by analysing the wall temperature fluctuation [2]. Shoji et al. described the nonlinear behaviour of the heterogeneous nucleation of water using the power spectrum (Fourier spectrum) and the attractor reconstructed from the temperature time series using the embedding method [3]. Ellepola et al. carried out a nonlinear analysis of the temporal temperature distribution of a boiling system on a thin stainless steel plate and concluded that the boiling system is a chaotic system [4]. Macdonald et al. numerically observed that the radial oscillation of gas bubbles and encapsulated microbubbles can be periodic as well as chaotic [5]. In this paper, nonlinear time series analysis methods have been used to identify the chaotic behaviour of the homogeneous nucleation of superheated liquid droplets from the produced acoustical pulse during nucleation. The normal boiling that we experience every day is referred to as heterogeneous nucleation. This type of nucleation occurs in the presence of a discontinuity like any impurity, air bubbles, gas pockets, or at the interface of two mediums such as solid–liquid, liquid–liquid, and liquid–vapour. The term nucleation means the formation of the nuclei of a new phase. In homogeneous nucleation, the phase transition occurs inside the bulk liquid. This type of nucleation also occurs in liquid, maintained in a superheated state. A liquid kept at temperature and pressure values within vapour region is called a superheated liquid. This is a metastable state of a liquid that is fragile and short-lived. The liquid can be maintained in the superheated state by fractionating it into droplets and dispersing them into a visco-elastic gel [6] or soft polymer [7] matrix

* Corresponding author.
E-mail address: mala.das@saha.ac.in (M. Das).

https://doi.org/10.1016/j.nima.2023.168777
Received 1 June 2023; Received in revised form 28 September 2023; Accepted 9 October 2023
Available online 12 October 2023

by the emulsification process. The host liquid or emulsifier material must be clean and de-gassed to avoid heterogeneous nucleation. This emulsification procedure is used to fabricate a superheated emulsion detector (SED), consisting of droplets of superheated halocarbon and hydrocarbon inside an aqueous-based gel matrix. SED is used as a neutron [8], gamma-ray [9,10], and charged particle [11,12] detector. This detector is suitable for detecting neutrons in the background of gamma-rays because the threshold energy of nucleation of this detector depends on the operating temperature, pressure, and type of active liquid used in the detector. SED is also used in search of WIMPs (Weakly Interacting Massive Particles) a cold dark matter candidate [13,14]. The superheated droplets inside SED, are homogeneously nucleated by the recoil nucleus. The complete process of bubble growth after nucleation is a complex phenomenon similar to normal boiling or heterogeneous nucleation of liquid, involving many nonlinear thermodynamic processes [15]. The nucleation process is associated with a high internal pressure of around 10 MPa and a high temperature of the order of kilokelvin, which leads to an observable phenomenon like an acoustic pulse formation. This pulse can be recorded in real-time by an acoustic sensor [16]. Conventionally, different parameters (e.g. Amplitude, Fundamental Frequency, Time constant, Decay time, Number of peaks, and Duration of signal) [17–19] were studied by analysing the time and frequency domains of the acoustical pulses. It has been shown that the nucleated bubble by an alpha particle in $R-3110$ (C_4F_{10}) and $R-115$ (C_2ClF_5) releases more energy than the neutron-induced bubble [20,21]. The gamma-ray-induced pulses for $R-218$ (C_3F_4) SED in the frequency range of 10 kHz to 1 MHz were found to have a higher power than the neutron-induced pulses [22]. The nucleated bubble with $R-114$ and $R-12$ SED in a low-frequency range (0–10 kHz) was observed to produce lower amplitude pulses from gamma-rays than neutrons [18,23]. Sahoo et al. (2020) observed adequacy over the thermodynamic behaviour in the energy released during the bubble growth from neutron and gamma-ray-induced pulses in the audible frequency range (20 Hz to 20 kHz) with the SED containing $R-134a$ ($C_2H_2F_4$) liquid [24]. Mostly the amplitude, energy, or power [18,20–24] of the nucleated pulse from SED are considered as important variables and these variables were studied with different active liquids. Aubin et al. [20], Felizardo et al. [25], Behnke et al. [13], Archambault et al. [26] have observed the acoustic signature of the bubble nucleated pulses in the dark matter search experiment using SED. There is not enough literature available on the nonlinear dynamical behaviour in the acoustic signature of the bubble-nucleated pulse and the nucleation process. In the present work, the nonlinear analysis has been carried out on acoustical pulses from the homogeneous nucleation of superheated droplets by neutrons and gamma-rays. The analysis shows the existence of chaos, and characteristic differences have been observed in the neutron and gamma-ray-induced pulses. An attempt has been made to explain these observations by the nonlinearity of the deposited energy by recoil nuclei and electrons.

2. Condition of homogeneous bubble nucleation

The superheated state is a metastable state of the liquid, and the liquid droplets in the superheated state nucleate and become an observable vapour bubble if the energy deposited by the particle or recoil nucleus is equal to or greater than the critical energy (E_c) over the path length of $L_c = bR_c$. Where b is the nucleation parameter and R_c [27] is the critical radius. The values of the critical energy and radius are different at different operating temperatures and pressures of the liquid. According to Seitz's model [27], due to the energy deposition by the energetic particles inside the superheated liquid, embryonic vapour bubbles are formed along its path. If the radius of the micro-bubble is greater than the critical radius (R_c) the micro-bubble grows and becomes an observable vapour bubble by vaporizing the surrounding liquid. The bubbles whose radius is smaller than the critical radius (R_c) collapse and return to the liquid state. The expressions of the critical radius (R_c) [27] and critical energy (E_c) [27,28] are given in Eq. (1) and (2) respectively,

$$R_c = \frac{2\sigma(T)}{(P_v - P_l)} \tag{1}$$

$$E_c = 4\pi R_c^2(\sigma - T(\frac{\partial\sigma}{\partial T})) + \frac{4\pi}{3}R_c^3\rho_v(h_v - h_l) - \frac{4\pi}{3}R_c^3(P_v - P_l) \tag{2}$$

where $\sigma(T)$ is the liquid–vapour interfacial tension at temperature T, P_v and P_l are the vapour and liquid pressure, ρ_v is the vapour density, and h_v and h_l are the specific enthalpies of the vapour bubble and liquid respectively.

The mechanism of nucleation by neutrons and gamma-rays are different. The neutron collides elastically with the target nucleus of the atom of the superheated liquid. After receiving energy by the elastic collision, the recoil nucleus loses energy along its track. The amount of energy received by the nucleus depends on the atomic weight of the nucleus and it deposits the whole energy until it comes to rest. The amount of deposited energy is determined by the linear energy transfer (LET) of the recoil nucleus. The bubble will nucleate when the deposited energy exceeds the minimum energy needed for nucleation over the path length of L_c, represented by the Eq. (3),

$$E_{dip}(T) = \int_0^{L_c} \left(\frac{dE}{dx}\right) dx \geq E_c \tag{3}$$

where dE/dx is the linear energy transfer (LET) of the incident particle. In the case of gamma-rays, while passing through the SED, it produces electrons and these electrons lose energy by electromagnetic interaction. Such deposited energy inside the SED nucleates bubble after satisfying the nucleation conditions.

3. Dynamics of bubble and acoustical pulse formation

The complete growth of the vapour bubble and its dynamics can be divided into three stages, which are (i) surface tension controlled stage (ii) inertia controlled stage and (iii) heat diffusion controlled stage [29,30]. After satisfying the nucleation conditions the bubble starts growing, and at the first stage of nucleation (surface tension controlled stage), the expansion of the bubble is driven by the energy stored in the bubble itself and its surroundings. In this stage, the radial velocity of the bubble experiences opposition by the surface tension of the liquid and it becomes less important at the larger radius of the bubble. The inertia-controlled stage is described by Rayleigh–Plesset equation [29] and the solution shows that the radius increases linearly with time. The last (heat diffusion controlled) stage the bubble growth is due to the continuous evaporation of the liquid layer located just behind its surface, as described by Plesset and Zwick equation [30] and the radius is proportional to the square root of time. The complete time evolution of the bubble through the three stages as described by Robinson and Judd [15] is represented by Eq. (4),

$$R(t) = R_c + \frac{2}{3}C_o((t+4C)^{\frac{2}{3}} - t^{\frac{2}{3}} - (4C)^{\frac{2}{3}}) \tag{4}$$

The expression of the constants C_o, C and J_a are

$$C_o = \sqrt{\frac{\pi}{27\alpha_l}}(\frac{P_v - P_l}{\rho_l J_l}) \tag{5}$$

$$C = \frac{9\rho_l\alpha_l J_a^2}{2\pi(P_v - P_l)} \tag{6}$$

$$J_a = \frac{\rho_l c_l(T - T_b)}{\rho_v L} \tag{7}$$

where α_l, ρ_l, ρ_v, L, C_l, T, and T_b are the thermal diffusivity, liquid, vapour phase density, latent heat of vaporization, specific heat of the superheated liquid at constant pressure, temperature and boiling point of the liquid respectively. The droplets become a freely oscillating vapour bubble after a complete phase transition and oscillate about their equilibrium radius. Minnaert [31] has calculated the resonance

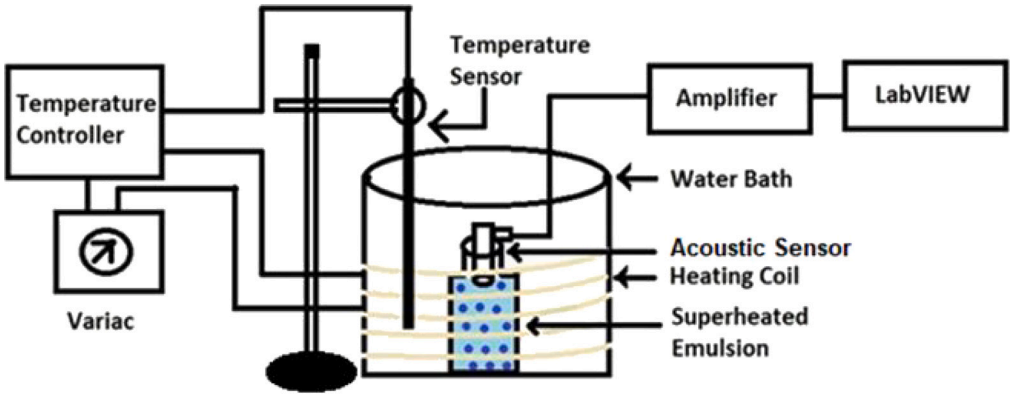

Fig. 1. Schematic diagram of the present experimental setup.

frequency of the harmonic bubble oscillator. The acoustical pulses emitted from the oscillating vapour bubble of radius R(t) are proportional to the acceleration of the volume of the bubble and these pulses can be detected by a piezoelectric transducer. In the present experiment acoustics sensor has been used to detect these pulses, the complete experimental detail is described in the next section.

4. Experimental details

In the present experiment, superheated liquid in the form of droplets, suspended in a visco-elastic gel matrix was fabricated. First, the supporting gel matrix was prepared by mixing the aquasonic gel with glycerol and the mixture was degassed for four days to remove the air pockets to avoid heterogeneous nucleation. The degassed gel and active liquid, $C_2H_2F_4$ ($R-134a$) were transferred inside an autoclave system. The pressure inside the autoclave is maintained at the vapour pressure of $R-134a$ liquid. The liquid and the gel were stirred to form micron-sized droplets of the superheated liquid. After that, the pressure of the autoclave was released very slowly to maintain the superheated state of the droplets. The superheated emulsion from the autoclave system was transferred into the glass vials when the pressure inside the system was reduced to atmospheric pressure. In the present experiment, these glass vials containing the dispersed droplets of superheated liquid in a gel matrix have been used as detectors (SEDs).

During the experiment, an acoustic sensor ($AE-WS\alpha$ by Physical Acoustics Corporation) in the frequency range of few kHz to 1 MHz was placed on top of the glass vial and in contact with the emulsion. The sensor converts the nucleated acoustical pulse into an electrical signal. The schematic diagram of the present experiment is shown in Fig. 1. The detector was placed inside a water bath wounded by the heating coil to maintain the temperature of the detector. The temperature was controlled by a temperature sensor and controller (METRAVI, DTC 200) with precision ±1 °C. The electrical signals from bubble nucleation were collected and stored in files using LabVIEW software and hardware. The bubble-nucleated acoustical pulses by neutrons were recorded in the presence of a ^{241}Am – Be (activity - 10 mCi) source and the temperature of the detector was maintained at 32 °C. 32 °C temperature was chosen as the SED is not sensitive to gamma-rays at this low temperature. The pulses from the gamma-ray-induced nucleation were collected using ^{137}Cs (activity – $5mCi$) at a temperature of 50 °C as $C_2H_2F_4$ SED becomes sensitive to gamma-ray at a temperature of 38.5 ± 1.4 °C [32].

5. Nonlinear analysis of the acoustical pulses

The classical nucleation theory estimates the energy barrier, critical bubble radius, and rate of nucleation. The general and exact solution is unattainable because of the complicated thermal and hydrodynamic interactions of the vapour and liquid at the bubble wall,

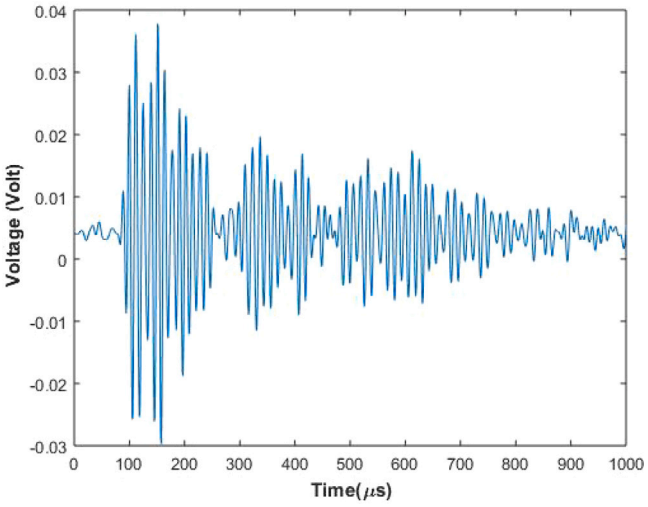

Fig. 2. Filtered bubble nucleated pulse by neutron-induced nucleation.

pressure-temperature dependence, and the coupling between the liquid momentum and energy equations through nonlinear convection term [15]. Martynyuk and Smirnova first described the particle-induced bubble nucleation [33], while later Rayleigh [29] and Plesset and Zwick [30] theoretically studied the nucleation based on the Navier–Stokes equation. In order to experimentally understand the nucleation phenomenon, nonlinear analysis was carried out on the acoustical pulses (see Figs. 2, and 3).

5.1. Attractor reconstruction

The reconstruction of the state space (known as the attractor) is an important part of nonlinear analysis, it represents the trajectory of the measured time series. Any prior information about the system is not required for the estimation of the attractor. The 3D attractor reconstruction of an experimental time series gives important information about the chaotic nature of the time series. The embedding theorem [34] is applied to construct the attractor, theorem by Hegger et al. [35] states that if X_i is the sequence of measurements of a state of a system, then $x_{i+\tau}$, $x_{i+2\tau}$, $x_{i+3\tau}$ are the embedding vectors. Where τ is the time delay of the reconstructed attractor. Present case, the 3D attractor reconstruction has been done by selecting the embedding space method and the variable sets are $x(t)$, $x(t+\tau)$, and $x(t+2\tau)$. τ has been chosen as the time of the first local minimum of mutual information of the time series [36]. Mutual information is a commonly used method for experimental time series to find the value of τ. First, the bubble-nucleated pulses were filtered using a 15 kHz to 100 kHz band-pass

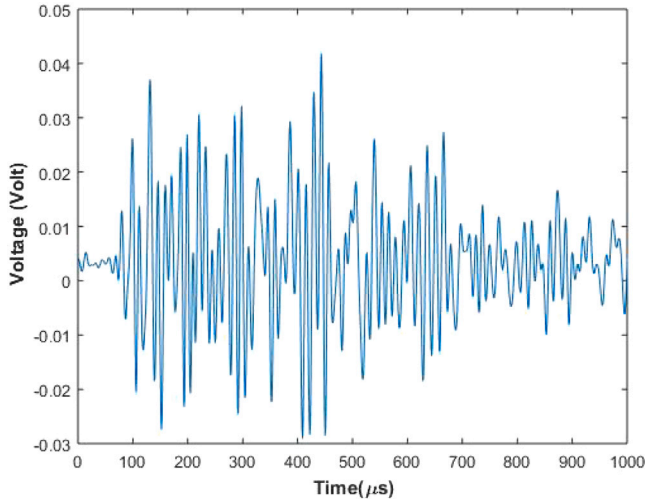

Fig. 3. Filtered bubble nucleated pulse by gamma-ray-induced nucleation.

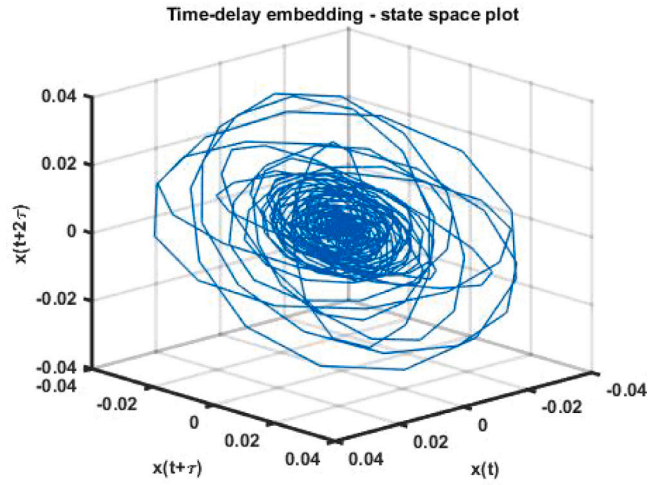

Fig. 4. The 3D attractor reconstruction of the bubble nucleated pulse by neutron-induced nucleation.

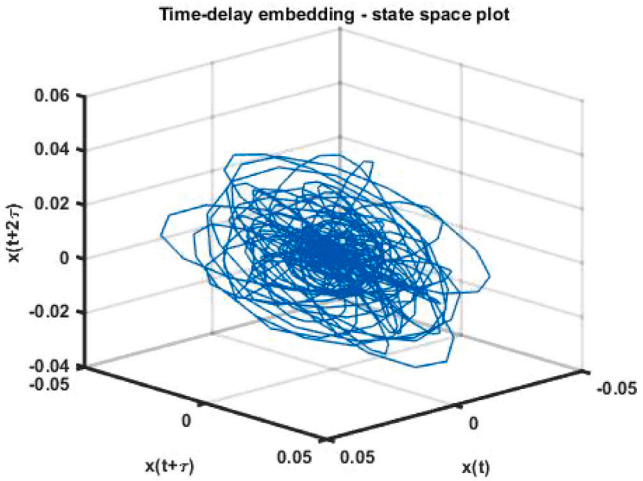

Fig. 5. The 3D attractor reconstruction of the bubble nucleated pulse by gamma-ray-induced nucleation.

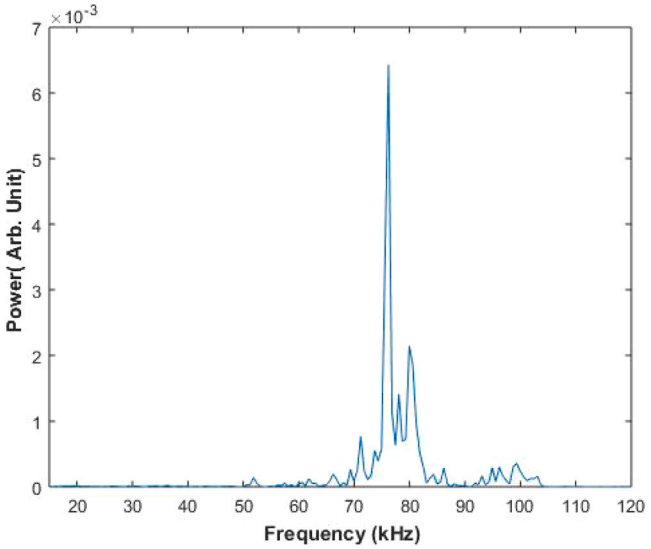

Fig. 6. Power spectrum of the bubble nucleated pulse by neutron-induced nucleation.

filter to reject very low and high-frequency noises. The values of τ for neutron and gamma-ray-induced pulses are 3 μs and 4 μs respectively. The attractor reconstruction of this filtrate acoustical pulses from the neutron and gamma-ray-induced events is shown in Figs. 4 and 5. The structure of the attractor suggests the bubble-nucleated pulses contain chaotic oscillation, which implies the existence of chaos in the homogeneous nucleation of superheated liquid droplets. Comparing the 3D attractor of both pulses, it is observed that there is a difference in the line density of the trajectories and the convergence nature of the curve. The trajectory by gamma-ray-induced pulse shows a rather complicated pattern than the neutron-induced pulse. The 3D attractor of the neutron-induced pulse systematically converges to the centre of the curve but the 3D attractor of the gamma-ray-induced pulse does not show such a converging trend. The converging nature of the 3D attractor concludes that the neutron-induced bubble is more stable than the gamma-ray-induced bubble.

5.2. Fast fourier transformation

The frequency spectrum of the bubble-nucleated pulses has been constructed by Fast Fourier Transformation (FFT), and the spectrum is presented in Figs. 6, and 7. The periodic oscillation can be indicated by a frequency spectrum containing sharp peaks at some specific frequency, whereas a continuous frequency spectrum indicates chaotic or quasi-periodic oscillation. Here the frequency spectrum of both the neuron and gamma-ray-induced pulses contain peaks with irregular frequency intervals, but the spectrum of the gamma-ray-induced pulse is distributed over a wide frequency band. Both the FFT spectrums suggest the existence of chaos in the system according to the analysis by Baker and Gollub [37], and further nonlinear analysis has been carried out to confirm the existence of chaos.

5.3. Lyapunov exponent

The Lyapunov exponent is a well-known parameter representing the nonlinear characteristics of attractors and is a useful diagnostic for chaotic systems. It quantitatively measures the sensitivity to change in the initial condition and also represents how the system diverges or converges from its infinitesimally close trajectories in phase space [38]. Any two points in phase space x and $x + \Delta x$ are functions of time, and the separation between them (Δx) will also be a function of time. The Lyapunov exponent is defined as the mean exponential rate of divergence of two initially close orbits characterized by Eq. (8). The

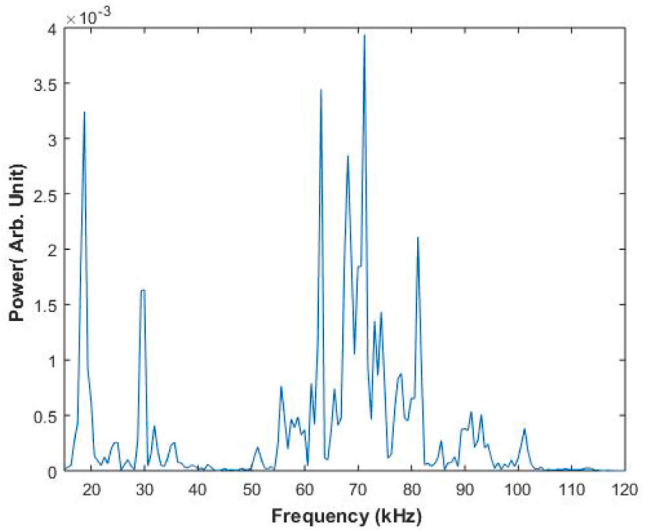

Fig. 7. Power spectrum of the bubble nucleated pulse by gamma-ray-induced nucleation.

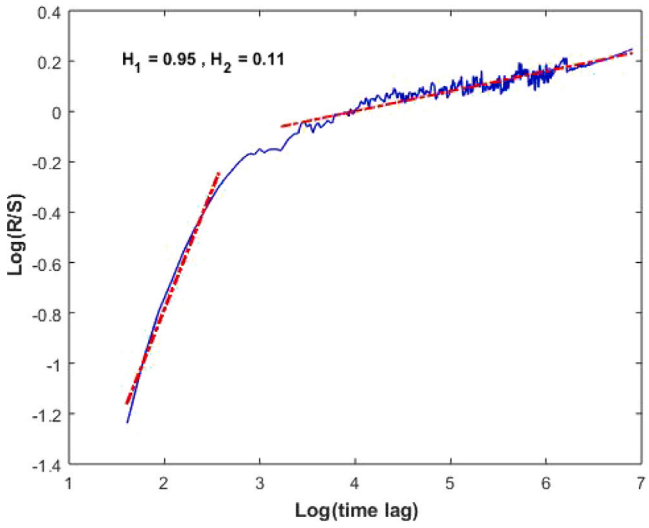

Fig. 8. The R/S analysis of the bubble nucleated pulse by neutron-induced nucleation.

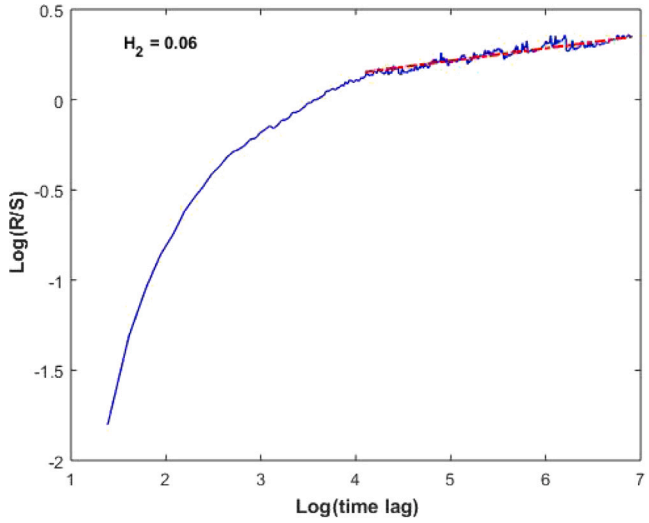

Fig. 9. The R/S analysis of the bubble nucleated pulse by gamma-ray-induced nucleation.

exponential divergence means the system behaves differently, whose initial differences are not able to resolve. There is a straight-forward technique for the estimation of the Lyapunov exponent for those systems having explicitly known equations of motion but this method is not valid for experimental data. The one-dimensional Lyapunov exponent can be calculated using Eq. (8), where λ is the order from largest to smallest. The sign of the Lyapunov exponent quantitatively indicates the dynamics of the system, a system with chaos should have one positive Lyapunov exponent. The largest Lyapunov exponent of the pulses are 13.60 (neutron-induced pulse) and 8.34 (gamma-ray-induced pulse) respectively, and the positive value of the largest Lyapunov exponent confirms the existence of chaos. It implies that periodicity is lost in the process of bubble nucleation or pulse generation, and the loss of periodicity leads to a chaotic appearance in the acoustical pulse.

$$\lambda = \lim_{t\to\infty}\left(\frac{1}{t}\right)\ln\frac{\Delta x(t)}{\Delta x(0)} \tag{8}$$

5.4. Rescaled range analysis

The Rescaled range known as R/S, is one of the cornerstones of fractal analysis and has been applied in many disciplines to analyse the signals, originating from different types of probes. For the signals having self-similar scaling properties, the ratio of R/S is a power law of window size (n) [39]. The persistent and anti-persistent behaviour of a time series can be quantified by Hurst exponent and it determines the random or long-term memory of a time series. The R/S (shown in Eq. (9)) algorithm estimates the value of the Hurst exponent, which scales like cn^H as $n \to \infty$, where c is constant, and H is the Hurst exponent of the time series [40,41].

$$\frac{R(n)}{S(n)} = \frac{max(0, W_1, W_2, \ldots, W_n) - min(0, W_1, W_2, \ldots, W_n)}{\sqrt{S^2(n)}} \tag{9}$$

$$W_k = x_1 + x_2 + x_3 + \cdots + x_k - k\overline{X(n)}, \tag{10}$$

where $\overline{X(n)}$, $S^2(n)$, and n are the mean, variance, and time lag of the signal respectively. The slope of the R/S plot of a completely random point is constant, and for a periodic system, it gets saturated and starts oscillating. The value where it starts oscillating gives the period of the oscillation, which gives information about the frequency of the signal. The Hurst exponent of a completely random and a purely periodic time series are 0.5 and 1 respectively. The Hurst exponent of a chaotic system should be different from 0.5 and 1 because it is temporally aperiodic in nature. The exponent of the bubble-nucleated signals from neutrons and gamma-rays has been calculated, which shows different features and the values of the slopes differ from 0.5 and 1. The R/S plot of the bubble nucleated pulse by neutrons (see Fig. 8) clearly shows two distinct regimes with slopes of 0.95 and 0.11. The first Hurst exponent (slope) reflects that the neutron-induced pulse is composed of oscillations that are strongly correlated with each other and have persistence (conservation of current trends). As time goes on, the slope becomes 0.11, which is interpreted as anti-persistence (fluctuation or frequency reversal of trends). The slopes of the R/S plot of the gamma-ray-induced pulse are different at every point, and the slope approaches zero as the time lag increases. The persistency or anti-persistency in the signal cannot be determined for a gamma-ray-induced pulse (see Fig. 9).

The nuclear boiling of a single vapour bubble depends on the surface temperature of the heating surface. Local fluctuations of heat flux from nuclear boiling of $R-114$ liquid and local temperature changes transform into chaotic behaviour with increasing the temperature [42]. R. Mosdorf [43] explained that the nonlinearity of heat transfer originates chaos in pool boiling. Here, in the case of homogeneous nucleation, the

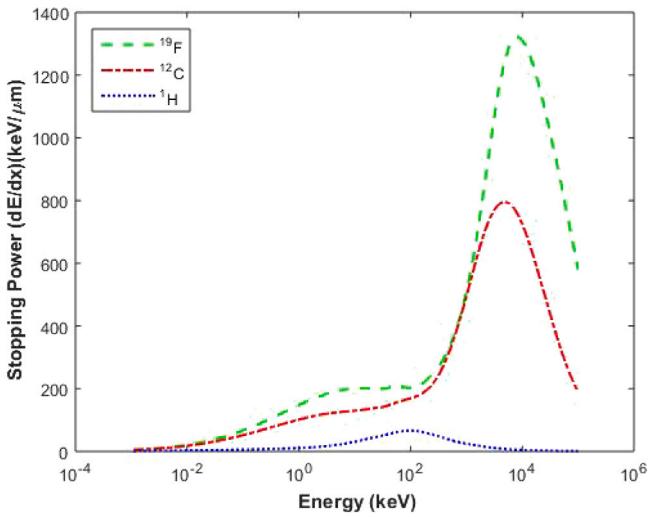

Fig. 10. Stopping power (dE/dx) of recoil nuclei in R-134a liquid.

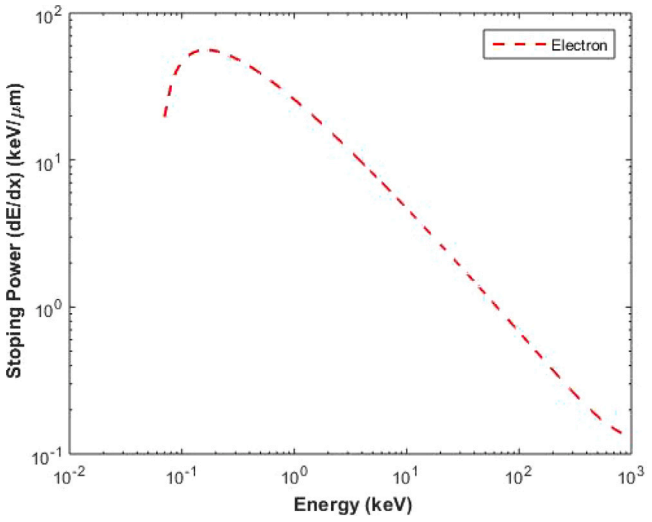

Fig. 11. Stopping power (dE/dx) of electron in R-134a liquid.

analysis confirms the presence of chaos in both the neutron and gamma-ray-induced pulses. The droplets of $R-134a$ liquid nucleate because of the energy deposited by the recoiling nuclei or electrons. The LET or stopping power (dE/dx), of the recoiling nucleus and of the electrons from the neutrons and gamma-rays in $R-134a$ liquid droplets are shown in Figs. 10, and 11. The LET of the recoil nucleus in $R-134a$ liquid has been calculated using SRIM 2008 code [44]. The stopping power of the electron has been calculated using Bethes equation [45,46]. The LET or dE/dx of the recoil nuclei and electrons shown in Figs. 10, and 11 are nonlinear. The nonlinear nature of the LET or dE/dx of recoil nuclei and electrons at the end of the track introduces chaos in the neutron and gamma-ray-induced nucleation. The present results confirm that chaos is present in homogeneous nucleation, like other types of boiling, and verify the model of R. Mosdorf [43] about the origin of chaos, which is the nonlinear nature of heat or energy transfer.

Difference has been observed in the neutron and gamma-ray-induced bubble nucleated pulses in the above three plots (3D attractor reconstruction, FFT, and R/S plot). It is due to the difference in the nucleation mechanisms of neutrons and gamma-rays. The recoiling nuclei from neutrons and electrons from gamma-rays deposit energy along their paths and, this deposited energy after satisfying nucleation conditions generates vapour bubbles along its track. The number of droplets along the path of the recoil nuclei (H, C, and F) and electrons are about 1 and 11 respectively [24]. The number is large for electrons because the range of the electron is larger than the recoil nuclei. The recoil nucleus mostly produces a bubble from a single droplet along its total track when it satisfies the bubble nucleation conditions. In the case of an electron from gamma-rays, the bubble will form if one of the bubbles along its track satisfies the bubble nucleation conditions and the growing bubbles merge with other bubbles along the track. The bubble-nucleated pulse from neutrons carries the information of the growing bubble that originated from a single droplet. The gamma-ray-induced nucleated pulse carries the information of the growing bubble, which merged with other bubbles. The merging is the origin of the crowded attractor, broadband frequency spectrum, and R/S plot without any persistency for the gamma-ray-induced pulse.

6. Conclusions

The nonlinear analysis of the acoustical pulses from neutron and gamma-ray-induced bubble nucleation shows that the homogeneous nucleation exhibits chaotic behaviour, and the positive Lyapunov exponent confirms it. The R/S analysis of the pulses shows that initially, the neutron-induced nucleated pulse has a long-range persistency that vanishes as time goes on. In the case of a gamma-ray-induced pulse, this type of behaviour is not observed. The present nonlinear analysis shows significant differences between the neutron and gamma-ray-induced pulses. Merging of the droplets along the track of the electrons is the reason for the complicated 3D attractor reconstruction, broadband FFT spectrum, and R/S plot without any persistency for the gamma-ray-nucleated pulses. This study will be useful in understanding the chaos in homogeneous nucleation and the identification of neutrons and gamma-ray-induced pulses.

Declaration of competing interest

The authors declare that they have no known competing financial interests or personal relationships that could have appeared to influence the work reported in this paper.

Data availability

Data will be made available on request.

Acknowledgements

The authors sincerely acknowledge the help and support of Mr. Nilanjan Biswas, India, and Mr. Sudipta Barman, SINP, India, during the experiment. The authors are thankful to the Health Physics Unit, VECC, Kolkata for the ^{241}Am – Be source.

References

[1] R. Judd, On nucleation site interaction, J. Heat Transfer 110 (1988) 475.
[2] M. Shoji, Chaos in boiling on a small-size heater, in: Proc. Fourth ASME-JSME Thermal Joint Conference, Maui, Vol. 2, 1995, pp. 225–232.
[3] M. Shoji, N. Negishi, H. Hatae, Y. Haramura, Nonlinear chaotic characteristics of saturated pool boiling of water on a horizontal copper surface, in: National Heat Transfer Symposium of Japan, Vol. 33, 1996, pp. 253–254.
[4] J. Ellepola, Nucleation site interactions in pool boiling, in: Proceedings of the 2nd European Thermal Sciences & 14th UIT National Heat Transfer Conference, Rome, 29-31 May, 1996.
[5] C. Macdonald, J. Gomatam, Chaotic dynamics of microbubbles in ultrasonic fields, Proc. Inst. Mech. Eng. C 220 (3) (2006) 333–343.
[6] R.E. Apfel, The superheated drop detector, Nucl. Instrum. Methods 162 (1979) 603.
[7] H. Ing, H. Birnboim, A bubble-damage polymer detector for neutrons, Nucl. Tracks Radiat. Meas. 8 (1984) 285.
[8] B. Mukherjee, D. Rybka, D. Makowski, T. Lipka, S. Simrock, Radiation measurement in the environment of FLASH using passive dosimeters, Meas. Sci. Technol. 18 (8) (2007) 2387.

[9] F. d'Errico, R. Nath, R. Nolte, A model for photon detection and dosimetry with superheated emulsions, Med. Phys. 27 (2) (2000) 401–409.
[10] B. Roy, M. Das, S. Roy, B. Chatterjee, Threshold temperature for γ-ray detection in superheated drop detector, Radiat. Phys. Chem. 61 (3–6) (2001) 509–510.
[11] S.-L. Guo, L. Li, H.-Y. Guo, C.-Q. Tu, Y.-L. Wang, T. Doke, T. Kato, K. Ozaki, A. Kyan, Y. Piao, et al., High energy heavy ion tracks in bubble detectors, Radiat. Meas. 31 (1–6) (1999) 167–172.
[12] S. Tsuda, T. Sawamura, A. Homma, M. Narita, Pressure dependence of neutron detection sensitivity in a superheated drop detector, Radiat. Prot. Dosim. 87 (2) (2000) 87–92.
[13] E. Behnke, J. Behnke, S. Brice, D. Broemmelsiek, J. Collar, P. Cooper, M. Crisler, C. Dahl, D. Fustin, J. Hall, et al., Improved limits on spin-dependent WIMP-proton interactions from a two liter CF 3 I bubble chamber, Phys. Rev. Lett. 106 (2) (2011) 021303.
[14] M. Felizardo, T. Morlat, A. Fernandes, T. Girard, J. Marques, A. Ramos, M. Auguste, D. Boyer, A. Cavaillou, C. Sudre, et al., First results of the phase II SIMPLE dark matter search, Phys. Rev. Lett. 105 (21) (2010) 211301.
[15] A. Robinson, R. Judd, The dynamics of spherical bubble growth, Int. J. Heat Mass Transfer 47 (23) (2004) 5101–5113.
[16] R.E. Apfel, Sonic effervescence: A tutorial on acoustic cavitation, J. Acoust. Soc. Am. 101 (3) (1997) 1227–1237.
[17] S. Seth, M. Das, Radiation linear energy transfer and drop size dependence of the low frequency signal from tiny superheated droplets, Nucl. Instrum. Methods Phys. Res. A 837 (2016) 92–98.
[18] P.K. Mondal, S. Seth, M. Das, P. Bhattacharjee, Study of low frequency acoustic signals from superheated droplet detector, Nucl. Instrum. Methods Phys. Res. A 729 (2013) 182–187.
[19] S. Ali, M. Das, Discrimination of neutron and gamma ray induced nucleation events at high frequency in R134a superheated emulsion, Nucl. Instrum. Methods Phys. Res. A 1025 (2022) 166186.
[20] F. Aubin, M. Auger, M. Genest, G. Giroux, R. Gornea, R. Faust, C. Leroy, L. Lessard, J. Martin, T. Morlat, et al., Discrimination of nuclear recoils from alpha particles with superheated liquids, New J. Phys. 10 (10) (2008) 103017.
[21] M. Felizardo, T. Morlat, T. Girard, A. Kling, A. Fernandes, J. Marques, F. Carvalho, A. Ramos, S. Collaboration, et al., Neutron–Alpha irradiation response of superheated emulsion detectors, Nucl. Instrum. Methods Phys. Res. A 863 (2017) 62–73.
[22] A. Di Fulvio, J. Huang, L. Staib, F. d'Errico, LET dependence of bubbles evaporation pulses in superheated emulsion detectors, Nucl. Instrum. Methods Phys. Res. A 784 (2015) 156–161.
[23] M. Das, S. Seth, S. Saha, S. Bhattacharya, P. Bhattacharjee, Neutron-gamma discrimination by pulse analysis with superheated drop detector, Nucl. Instrum. Methods Phys. Res. A 622 (1) (2010) 196–199.
[24] S. Sahoo, M. Das, The adequacy of energy deposition over thermodynamic behaviour in explaining the acoustic energy in bubble nucleation of superheated droplets, Radiat. Phys. Chem. 187 (2021) 109578.
[25] M. Felizardo, R. Martins, A. Ramos, T. Morlat, T. Girard, F. Giuliani, J. Marques, New acoustic instrumentation for the SIMPLE superheated droplet detector, Nucl. Instrum. Methods Phys. Res. A 589 (1) (2008) 72–84.
[26] S. Archambault, F. Aubin, M. Auger, M. Beleshi, E. Behnke, J. Behnke, B. Beltran, K. Clark, X. Dai, M. Das, et al., New insights into particle detection with superheated liquids, New J. Phys. 13 (4) (2011) 043006.
[27] F. Seitz, On the theory of the bubble chamber, Phys. Fluids 1 (1) (1958) 2–13.
[28] C. Amole, M. Ardid, D.M. Asner, D. Baxter, E. Behnke, P. Bhattacharjee, H. Borsodi, M. Bou-Cabo, S. Brice, D. Broemmelsiek, et al., Dark matter search results from the PICO-60 CF 3 I bubble chamber, Phys. Rev. D 93 (5) (2016) 052014.
[29] L. Rayleigh, VIII. On the pressure developed in a liquid during the collapse of a spherical cavity, Lond. Edinb. Dublin Philos. Mag. J. Sci. 34 (200) (1917) 94–98.
[30] M.S. Plesset, S.A. Zwick, The growth of vapor bubbles in superheated liquids, J. Appl. Phys. 25 (4) (1954) 493–500.
[31] M. Minnaert, XVI. On musical air-bubbles and the sounds of running water, Lond. Edinb. Dublin Philos. Mag. J. Sci. 16 (104) (1933) 235–248.
[32] S. Sahoo, S. Seth, M. Das, The threshold of gamma-ray induced bubble nucleation in superheated emulsion, Nucl. Instrum. Methods Phys. Res. A 931 (2019) 44–51.
[33] V. Rysakov, Acoustoelectronic instability in piezosemiconductors, Sov. Phys. Uspekhi 34 (12) (1991) 1027.
[34] F. Takens, Detecting strange attractors in turbulence, in: Dynamical Systems and Turbulence, Warwick 1980: Proceedings of a Symposium Held At the University of Warwick 1979/80, Springer, 2006, pp. 366–381.
[35] R. Hegger, H. Kantz, T. Schreiber, Practical implementation of nonlinear time series methods: The TISEAN package, Chaos 9 (2) (1999) 413–435.
[36] A.M. Fraser, H.L. Swinney, Independent coordinates for strange attractors from mutual information, Phys. Rev. A 33 (2) (1986) 1134.
[37] G.L. Baker, J.P. Gollub, Chaotic Dynamics: An Introduction, Cambridge University Press, 1996.
[38] J. Froyland, Fractals, in: Introduction to Chaos and Coherence, Institute of Physics Publishing, 1992, pp. 3–8.
[39] Y. Chen, M. Ding, J.S. Kelso, Long memory processes (1/f α type) in human coordination, Phys. Rev. Lett. 79 (22) (1997) 4501.
[40] B. Carreras, B.P. Van Milligen, M. Pedrosa, R. Balbın, C. Hidalgo, D. Newman, E. Sanchez, M. Frances, I. Garcıa-Cortés, J. Bleuel, et al., Self-similarity of the plasma edge fluctuations, Phys. Plasmas 5 (10) (1998) 3632–3643.
[41] N.C. Adhikary, A.R. Pal, H. Bailung, J. Chutia, Self-similarity of electrostatic fluctuations in a linear magnetised plasma system, Phys. Lett. A 350 (5–6) (2006) 380–385.
[42] H. Auracher, Transition boiling, in: Proceedings of the Ninth Irrtelnational Heat Transfer Conference, Jerusalem, Istael, Vol. 1, 1990, pp. 69–89.
[43] R. Mosdorf, M. Shoji, Chaos in nucleate boiling—nonlinear analysis and modelling, Int. J. Heat Mass Transfer 47 (6–7) (2004) 1515–1524.
[44] J.F. Ziegler, J.P. Biersack, U. Littmark, The stopping and range of ions in matter, 1995, SRIM: http://www.srim.org.
[45] F. d'Errico, Radiation dosimetry and spectrometry with superheated emulsions, Nucl. Instrum. Methods Phys. Res. B 184 (1–2) (2001) 229–254.
[46] J.E. Turner, Atoms, Radiation, and Radiation Protection, John Wiley & Sons, 2008.

Nuclear Inst. and Methods in Physics Research, A 1025 (2022) 166186

Contents lists available at ScienceDirect

Nuclear Inst. and Methods in Physics Research, A

journal homepage: www.elsevier.com/locate/nima

Discrimination of neutron and gamma ray induced nucleation events at high frequency in R134a superheated emulsion

Suraj Ali [a,b,1], Mala Das [a,*,2]

[a] Astroparticle Physics & Cosmology Division, Saha Institute of Nuclear Physics, 1/AF Bidhan nagar, Kolkata 700064, India
[b] Department of Physics, Jadavpur University, 188 Raja S.C. Mallick Rd, Kolkata 700032, India

ARTICLE INFO

Keywords:
Superheated emulsion
Discrimination
Neutron
Gamma rays
FFT

ABSTRACT

Nucleation of superheated droplet and subsequent vapour oscillation produces an acoustic pulse that contains important information about the bubble nucleation process. The high frequency acoustic pulses during the bubble nucleation of R-134a liquid droplets have been observed in the frequency range of few kHz to MHz by irradiating with neutrons and gamma rays. The spectral analysis of the gamma ray induced signals indicates the existence of several frequency components, which are not present for the neutron induced signals. Acoustic power, duration and number of peaks of the signals have also been studied which show a significant discrimination between the neutron and gamma ray induced events.

1. Introduction

Superheated emulsion contains the microscopic droplets of refrigerant liquid in superheated state distributed in a gel or polymer medium [1,2]. Superheated state is a metastable state where the liquid maintains its liquid state above its boiling point. Superheated droplets can be converted into vapour bubbles when particles or radiation pass through the droplets and the Seitz theory of bubble nucleation explains the phenomena of nucleation according to the 'thermal spike' model [3]. Sun et al. proposed the dynamical model of bubble nucleation by studying the cavitation phenomenon of superheated liquid by neutrons from microscopic point of view [4]. Superheated emulsion is a threshold detector and the threshold energy of bubble nucleation depends on the operating temperature and pressure of the detector. It is used in neutron spectrometry [5], neutron dosimetry [6] at certain operating pressure and temperature regions where it is insensitive to gamma rays. Recoil nucleus from neutrons due to its high linear energy transfer (LET) nucleate bubble at moderate superheat of the detector. There is an empirical formula which shows that the liquid becomes sensitive to gamma rays at a temperature above the midpoint of the boiling point and critical temperature of the liquid [7,8]. Several refrigerant liquids (e.g. R-12, R-21, R-22, R-114, R-115, R-134a, R-404 etc.) have been studied for the neutron detection [5,9]. In the present work, R-134a ($C_2H_2F_4$, b.p. = −26.3 °C, T_c = 101.2 °C) superheated droplets are investigated. It was reported that R-134a becomes sensitive to 662 keV gamma rays at 38.5° ± 1.4 °C that corresponds to 1.29 keV threshold [10]. Therefore to detect neutrons at lower threshold (or higher operating temperature), the study of the discrimination between the neutron and the gamma ray induced events is important. One of the useful applications of the superheated emulsion is for the search of WIMPs (Weakly Interacting Massive Particles), a favoured candidate of dark matter. The WIMPs can undergo elastic collision with the nuclei of detector material similar to neutron interaction and the recoil nucleus can initiate a bubble nucleation if it satisfies the bubble nucleation condition [11–14]. Low mass WIMPs (below 10 GeV) which is an interesting topic of current and future investigation can be explored by lowering the threshold energy of the detector. As mentioned above, at low threshold energy the detector becomes sensitive to gamma rays therefore the discrimination between nuclear recoils and gamma rays is important in identifying the WIMPs induced signals from the huge background of gamma rays. The bubble nucleation process is associated with the high internal pressure which leads to the production of shock waves. The acoustic detection of shock wave accompanying bubble expansion is a direct method for real-time counting of nucleated bubbles [15]. The discrimination between the neutron and gamma ray induced signals at low frequency (below 30 kHz) with condenser microphone was studied with R-114 and R-12 liquid and the gamma ray induced pulses were observed to be of smaller amplitude than the neutron induced pulses [16,17]. The spectral density distribution was also studied and reported that the frequency of the primary harmonic of gamma ray induced signals is smaller than the neutron induced signals in the audio frequency range [16].

It is reported in the frequency range of 10 kHz to 1 MHz that the gamma ray induced pulses have higher acoustic power than the neutron

* Correspondence to: Saha Institute of Nuclear Physics, Kolkata 700064, India.
E-mail addresses: suraj.ali@muralidhargirlscollege.ac.in (S. Ali), mala.das@saha.ac.in (M. Das).
[1] Present Address : Muralidhar Girls' College, P414/14 Gariahat Road, Kolkata 700029, India.
[2] Present Address : High Energy Nuclear & Particle Physics Division, Saha Institute of Nuclear Physics, Kolkata 700064, India.

https://doi.org/10.1016/j.nima.2021.166186
Received 18 August 2021; Received in revised form 15 November 2021; Accepted 6 December 2021
Available online 13 December 2021
0168-9002/

induced pulses with R-218 superheated liquid and the neutron induced pulses have a peculiar pattern in 200–400 kHz frequency range which is absent in the FFT spectrum of the gamma ray induced pulses [15]. A comparative study was made for R-12 and R-134a superheated emulsion in the audio frequency range using condenser microphone and the gamma ray induced events are observed to be of higher acoustic power in R-134a than that of the neutron induced events whereas the reverse effect is observed for the R-12 liquid which is explained by the thermodynamic consideration and by the energy deposition inside the liquids [17,18]. In the present work, the studies were carried out with R-134a superheated liquid in the higher frequency range above the audio frequency to observe the discrimination of neutron and gamma ray induced signals. The R-134a is an environment friendly liquid and is suitable for neutron detection [19,20]. It is also reported that R-134a is a potential target searching for the low mass dark matter at higher superheat values [21]. The following sections describe the frequency of emission and the radius of growing bubble during the bubble nucleation process, present experiment, results, discussion and conclusions of the present study.

2. The frequency emission and radius of growing bubble

The physics of bubble nucleation based on the 'thermal spike' model of Seitz [3] is described by various authors [22–25]. A bubble will nucleate if a minimum amount of energy (E_c) known as critical energy of bubble nucleation is deposited within a length of $L_{\text{eff}} = b\,R_c$, where the nucleation parameter b varies from 2 to 12.96 [26]. The value of b depends on the type of the liquid, particle and its energy. For a specific liquid, it depends on to the degree of superheat and LET of the particle [26]. The mathematical expression of critical energy (E_c) [3] is shown by the Eq. (1),

$$E_c = 4\pi R_c^2\left(\sigma - T\frac{\partial\sigma}{\partial T}\right) + \frac{4\pi}{3}R_c^3\rho_v\left(h_v - h_l\right) - \frac{4\pi}{3}R_c^3(P_v - P_l) \tag{1}$$

where R_c is the critical radius of the bubble, σ (T) is the liquid–vapour interfacial tension at temperature T, P_v and P_l are the vapour and liquid pressure, h_v and h_l are the specific enthalpies of the vapour bubble and liquid respectively and ρ_v is the vapour density. The radius of the bubble should be greater than R_c to overcome the surface tension of the liquid. If the radius is greater than R_c the bubble becomes unstable and the entire liquid drop vaporizes otherwise it collapses back to its liquid state. At any temperature and pressure the expression of the critical radius (R_c) is represented by Eq. (2).

$$R_c = 2\sigma(T)/(P_v - P_l) \tag{2}$$

The proto-bubble forms, if $E_{dip} \geq E_c$ where E_{dip} is the deposited energy by the radiation as given by the Eq. (3).

$$E_{dip}(T) = \int_0^{L_c}\frac{dE}{dx}dx \geq E_c(T) \tag{3}$$

where dE/dx is the LET of the incident particle and it should be sufficient to satisfy the bubble nucleation condition.

When the size of the droplet exceeds its critical value the droplet vaporizes suddenly and its expansion generates a shock wave. The time scale of the formation of the proto-bubble is of the order of sub-nanoseconds and completes droplet evaporation occurs in milliseconds, leaving aside the proto-bubble formation stage [27]. The evolution of the vapour bubble can be identified into three subsequent growth regimes known as surface tension controlled, inertia controlled and the heat diffusion controlled regime [28,29]. In the surface tension controlled regime the evolution is retarded by the surface tension of the liquid and hence the radius of the bubble increases by a small value. In inertia controlled regime the liquid drop pushes the surrounding liquid using the heat energy stored inside the liquid and the radius of the bubble is proportional to the time [28]. Rayleigh–Plesset solution shows that the rate is proportional to the square root of the superheat [28]. The bubble is continuously increasing its radius in the heat diffusion

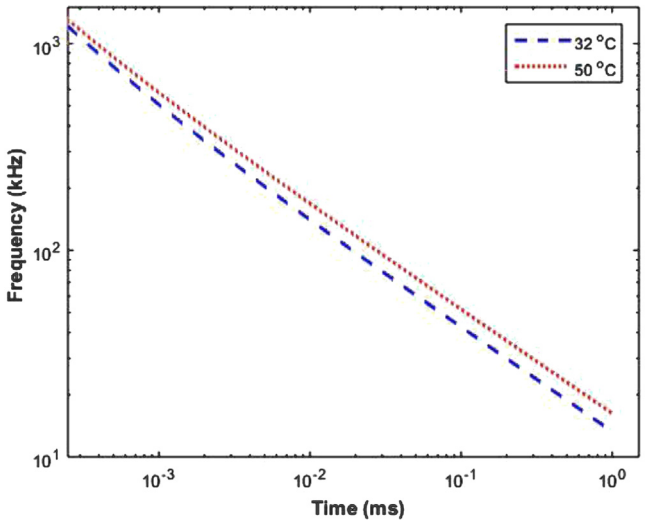

Fig. 1. The emitted frequency of the oscillating bubble with bubble growth time.

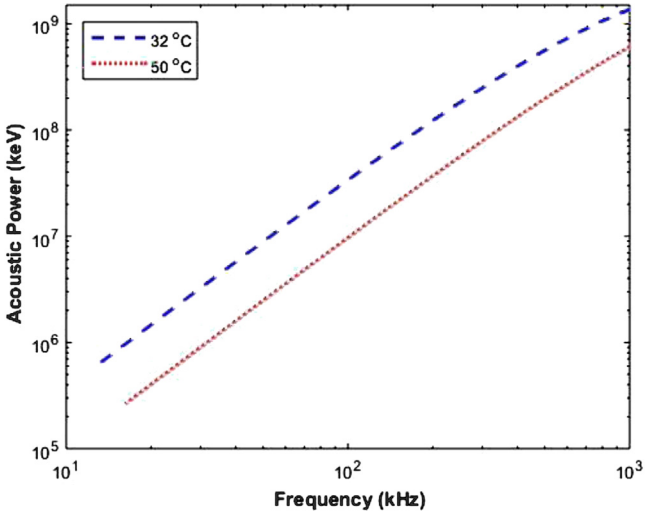

Fig. 2. Variation of the Acoustic Power of the oscillating bubble with the frequency of the oscillation.

controlled regime by the evaporation of the surrounding liquid and the necessary heat is supplied from the outer layer of the liquid. In this regime the radius is proportional to the square root of time [29]. After complete evaporation of the liquid it becomes an oscillating vapour bubble of frequency $\upsilon(R)$ [30] which is represented by the Eq. (4).

$$\upsilon(R) = \frac{1}{2\pi R}\sqrt{\frac{3kP_o}{\rho_l}} \tag{4}$$

where R is the equilibrium radius of the vapour bubble, ρ_l is the density of the surrounding liquid, k is the polytropic coefficient of the gas and P_o is the ambient equilibrium pressure. The Eq. (4) reflects that the frequency of the oscillating bubble at any instant of time is inversely proportional to its instantaneous radius. Robinson and Judd derived the relation of the radius $R(t)$ at any instant of time which includes all the three evolution states of the bubble [31] as

$$R(t) = R_c + \frac{2}{3}C_0\left((t+4C)^{\frac{3}{2}} - t^{\frac{3}{2}} - (4C)^{\frac{3}{2}}\right) \tag{5}$$

with,

$$C_0 = \sqrt{\frac{\pi}{27\alpha_l}}\left(\frac{\Delta P}{\rho_l J_a}\right)$$

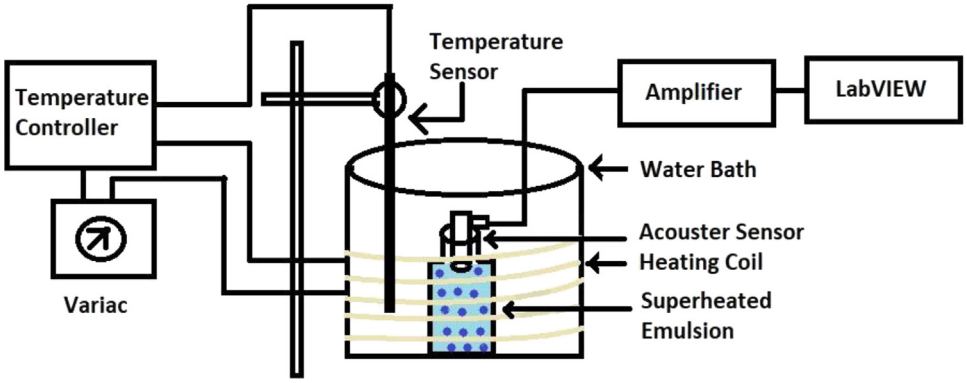

Fig. 3. Schematic diagram of the experimental setup.

$$C = \frac{9\rho_l \alpha_l J_a^2}{2\pi \Delta P}$$

$$J_a = \frac{\rho_l c_l \Delta T}{\rho_v L}$$

Here α_l, ρ_l and ρ_v are the thermal diffusivity, the liquid and vapour phase density of the superheated liquid respectively. C_l is specific heat at constant pressure and J_a is the Jakob number. The emitted frequency from the bubble at different instant of time is shown in Fig. 1. The Fig. 1 shows that initially the bubble oscillates with high frequencies but with time the bubble size increases and the bubble starts oscillating with low frequency and at the end of the process it emits audio frequency components. Fig. 1 shows that the frequency of R-134a liquid is larger at higher temperature as the critical radius of the bubble is smaller. The emitted acoustic power of the nucleated bubble as calculated from thermodynamic consideration varies with the frequency of the oscillating bubble, as shown in Fig. 2.

3. The experiment

The superheated emulsion was fabricated by suspending the superheated droplets of R-134a in aquasonic gel matrix and the detail of the detector fabrication process is given elsewhere [18,32]. The Fig. 3 is the schematic diagram of the experimental setup. The detector and a temperature sensor were kept inside a water bath which was surrounded by a heating coil. The temperature of the water bath was controlled by a temperature controller (METRAVI, DTC 200) with precision ±1 °C connected with the temperature sensor and the heating coil. The sensor (AE – WSα by Physical Acoustics Corporation) (frequency range ~ few kHz to 1 MHz) was placed on the top of the detector and the signals were stored in files using LabVIEW. The superheated emulsion was irradiated separately with ^{241}Am–Be (10 mCi) and ^{137}Cs (5 mCi) sources. It was already reported that R-134a becomes sensitive to gamma rays from ^{137}Cs at 38.5° ± 1.4 °C [10]. Therefore R-134a was irradiated to ^{241}Am–Be at 32 °C to measure the response for neutrons. To observe the response from gamma rays, R-134a was irradiated to ^{137}Cs at 50 °C which is above the gamma-ray sensitive temperature.

4. Results

The critical radius of the vapour bubble and the critical energy required for bubble nucleation has been calculated using NIST data [33] at the experimental temperatures. The critical radii are 20.09 nm and 8.07 nm and the critical energies are 2.87 keV and 0.34 keV at 32 °C and 50 °C temperatures respectively. The recorded acoustical signals were analysed by removing the signals due to the noise by eye selection [34]. The typical signals induced by neutrons and gamma rays in R-134a are displayed in Fig. 4 and a typical noise is shown in Fig. 5. A frequency analysis of the signals by using Fast Fourier Transformation (FFT) indicates the existence of several frequencies in the spectrum.

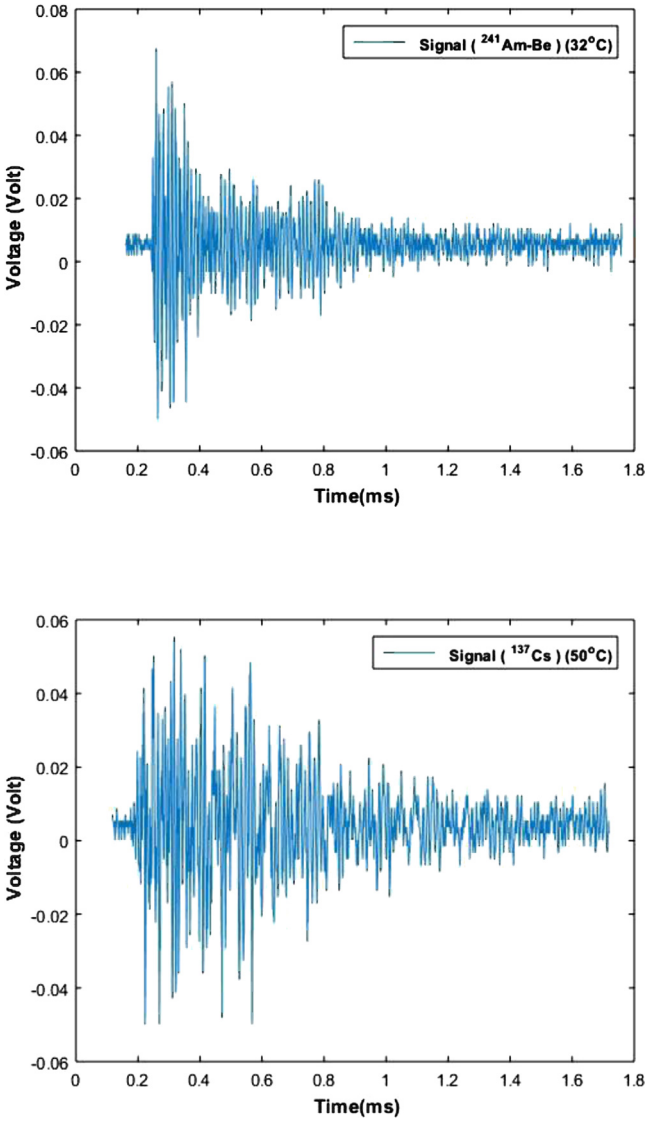

Fig. 4. Neutron and gamma ray induced typical signals and noise in R-134a SED.

The variable Pvar [35] which is proportional to the energy released during the bubble nucleation has been estimated. Other parameters like duration and number of peaks of the signal have also been studied. The duration of the signal is defined by considering the threshold voltage that eliminates the noise level as the reference. Number of peaks of the

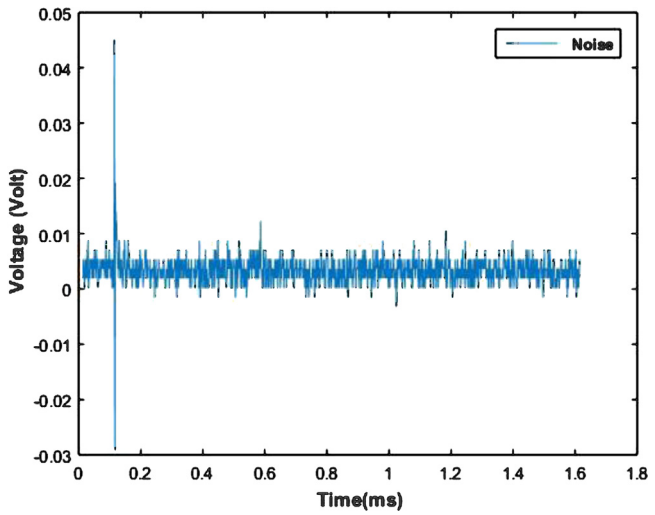

Fig. 5. Typical noise in R-134a SED.

signal is defined as the numbers of local maxima above the threshold voltage of the signal.

4.1. Frequency spectrum analysis of the signals

The FFT has been done on each collected signal to get information about the frequency content of the signal. The FFT spectrum of the typical neutron and gamma ray induced signals for R-134a are shown in Fig. 6. As observed in Fig. 6 the power spectrum is mostly limited within 150 kHz and the FFT spectrum for the neutron and gamma rays induced signals look different. The FFT spectrum of neutron induced signals shows that most of the peak frequencies are around 80 kHz. In the case of gamma ray induced signals, there are several frequencies in the FFT spectrum with a broad distribution between 50 and 100 kHz and a narrow distribution under 20 kHz. As discussed earlier, the frequency is inversely proportional to the size of the bubble and the low frequency appears at the larger size of the bubble. The radius of the growing bubble is found to be 31.91 μm at 80 kHz and 131.80 μm at 20 kHz as calculated using Eq. (4).

4.2. Pvar, duration and number of peaks of the signal

The observed distribution of the Pvar for the neutron and gamma ray induced signals are shown in Fig. 7. The distribution shows that the Pvar of the neutron induced signals lies within 1 V^2, but the Pvar of gamma rays with R-134a liquid is shifted towards higher values. The duration and number of peaks of the signals have been calculated from each collected signal and the distribution is displayed in Figs. 8 and 9. It is observed that the number of peaks and duration of gamma ray induced signals are higher than those from neutrons.

5. Discussion

The smaller droplet produces higher frequency and the frequency of emission decreases with the increase of bubble size. The localized high energy deposition plays an important role in the case of neutron induced or recoil nucleus induced bubble nucleation. The recoil nuclei from the neutrons with high LET deposit the whole energy within a shorter range and bubbles resulting from such high energy deposition may attain higher growth rate. The electron with lower stopping power deposits maximum energy mainly at the end of its track over a larger range [19] and the bubble may grow with lower rate. It is also possible to have several droplets along the path of the electron inside the emulsion [18]. Due to the possibility of merging of the nucleating bubbles

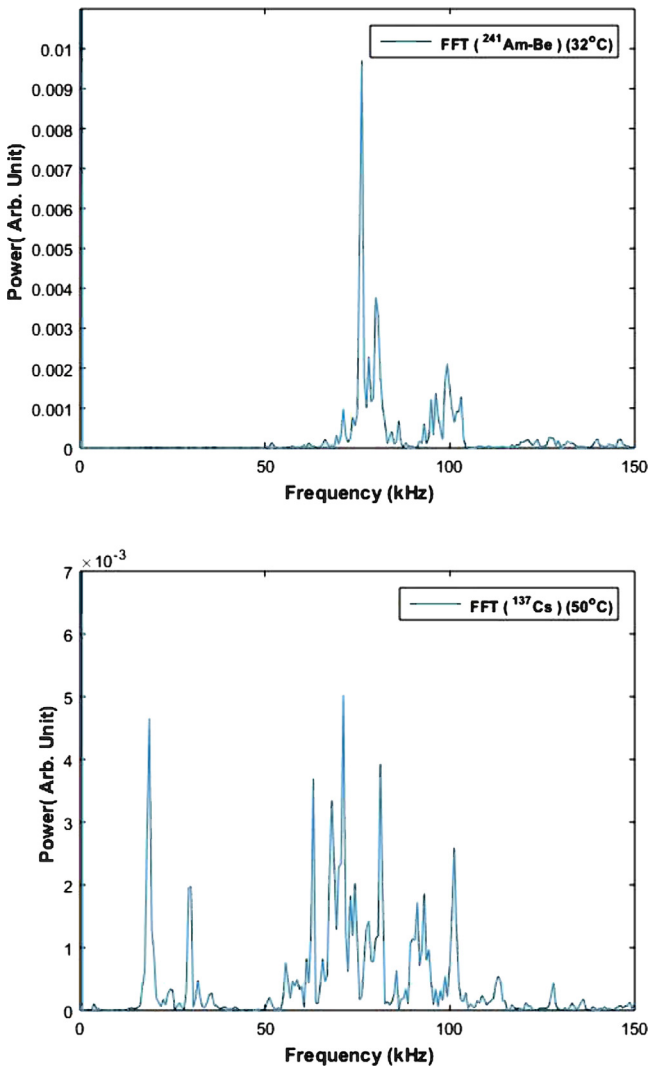

Fig. 6. FFT of neutron and gamma ray induced signals in R-134a SED.

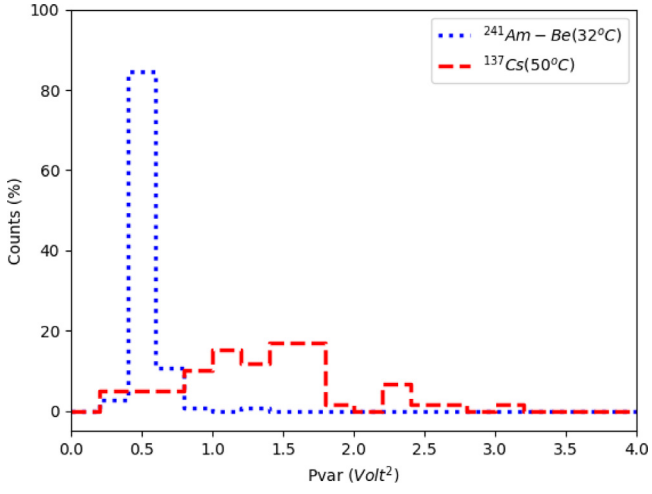

Fig. 7. The Pvar distribution of neutron and gamma induced nucleation signals.

along the extended path of the electrons which produce bubbles of various sizes and the lower growth rate of the bubbles from electrons, several frequencies in the FFT spectrum of gamma ray induced events are observed. On the other hand, the fast shock wave from the recoil

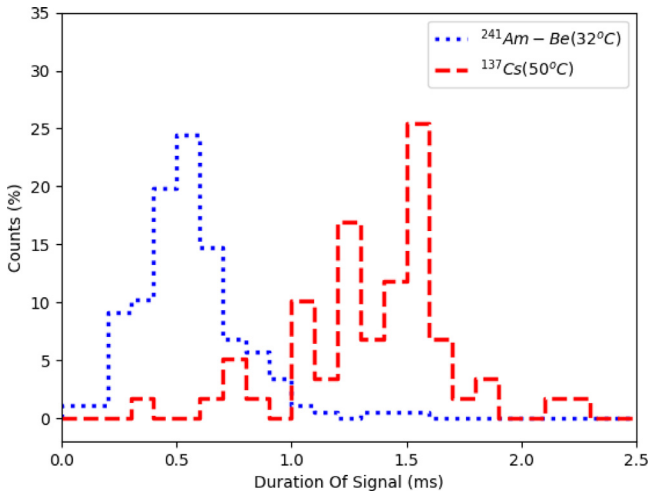

Fig. 8. Distribution of the duration of neutron and gamma induced nucleation signals.

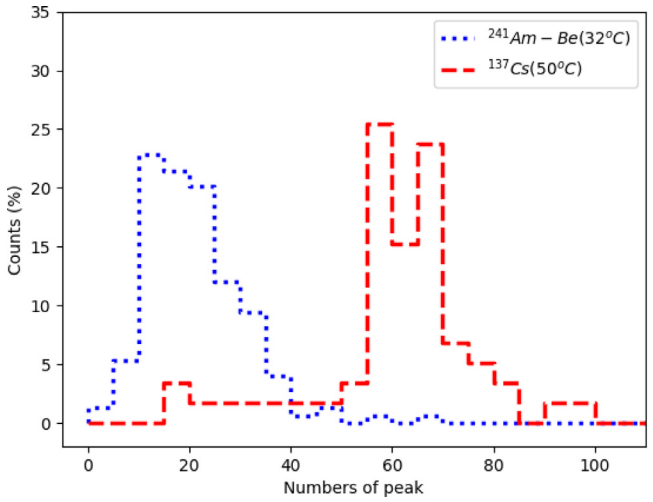

Fig. 9. Distribution of the numbers of peak of neutron and gamma induced nucleation signals.

nucleus would excite only high frequency components. The experiment has been done at a few other temperatures between 32 °C and 55 °C. There is no other low frequency peak in the FFT spectrum of the signals at high temperatures except near 20 kHz. Similarly, Figs. 7–9 show that the signals due to gamma ray induced events are predominantly of higher Pvar, duration and numbers of peaks compared to those of neutron induced events. The localized energy of the recoil nucleus produces a single nucleation but as explained before the electrons in the liquid may contribute multiple vapour embryos in the extended track, which merge into a larger single bubble and produce high Pvar, duration and number of peaks.

6. Conclusion

The FFT spectrum and distributions of Pvar, duration, number of peaks are studied using R-134a superheated emulsion irradiated with neutrons and gamma rays. Initially the tiny bubble oscillates with high frequencies but with time the bubble size increases and the bubble starts oscillating with low frequencies. The FFT spectrum shows that the gamma ray induced signals contain several frequencies which are absent in neutron induced signals. The Pvar, duration and number of peaks of the neutron induced signals are smaller than those of the gamma ray induced signals. The FFT spectrum, Pvar, duration and number of peaks are observed to be the efficient tools in the higher frequency region for the discrimination between the neutrons and gamma ray induced events in R134a superheated emulsion.

CRediT authorship contribution statement

Suraj Ali: Methodology, Investigation, Data analysis, Original draft preparation. **Mala Das:** Conceptualization, Methodology, Supervision, Validation, Reviewing and editing.

Declaration of competing interest

The authors declare that they have no known competing financial interests or personal relationships that could have appeared to influence the work reported in this paper.

Acknowledgements

The authors would like to thank Mr. Nilanjan Biswas, Ms Sunita Sahoo, APC Division, SINP and Mr. Sudipta Barman, Mechanical Workshop, SINP for the assistance during the experiment. The authors are thankful to Prof. Maitreyee Nandy, SINP and Health Physics Unit, Variable Energy Cyclotron Centre for providing ^{241}Am–Be source. The authors thank Prof. Pabitra Kumar Paul, Jadavpur University, Kolkata for valuable discussions and communications. The authors are grateful to CAPP - II project, SINP-DAE, India for the financial support.

References

[1] R.E. Apfel, Nucl. Instrum. Methods 162 (1979) 603–608.
[2] H. Ing, H.C. Birnboim, Nucl. Tracks Radiat. Meas. 8 (1984) 285–288.
[3] F. Seitz, Phys. Fluids 1 (1958) 2–13.
[4] Y. Sun, B. Chu, R. Apfel, J. Comput. Phys. 103 (1992) 116–125.
[5] M. Das, B.K. Chatterjee, B. Roy, S.C. Roy, Nucl. Instrum. Methods Phys. Res. A 452 (2000) 273–279.
[6] S.C. Roy, Radiat. Phys. Chem. 61 (2001) 271–281.
[7] F. d' Errico, Nucl. Instrum. Methods Phys. Res. B 184 (2001) 229–254.
[8] F. d'Errico, R. Nath, M. Lamba, S.K. Holland, Phys. Med. Biol. 43 (1998) 1147–1158.
[9] M. Das, B.K. Chatterjee, B. Roy, S.C. Roy, Radiat. Phys. Chem. 61 (2001) 447–448.
[10] S. Sahoo, S. Seth, M. Das, Nucl. Instrum. Methods Phys. Res. A 931 (2019) 44–51.
[11] M.W. Goodman, E. Witten, Phys. Rev. D 31 (12) (1985) 3059–3063.
[12] COUPP Collaboration, Phys. Rev. Lett. 106 (2) (2011) 021303.
[13] PICO Collaboration, Phys. Rev. Lett. 118 (25) (2017) 251301.
[14] SIMPLE Collaboration, Phys. Rev. D 89 (2014) 072013.
[15] A. Di Fulvio, J. Huang, L. Staib, F. d' Errico, Nucl. Instrum. Methods Phys. Res. A 784 (2015) 156–161.
[16] P.K. Mondal, S. Seth, M. das, P. Bhattacharjee, Nucl. Instrum. Methods Phys. Res. A 729 (2013) 182–187.
[17] M. Das, S. Seth, S. Saha, S. Bhattacharya, P. Bhattacharjee, Nucl. Instrum. Methods Phys. Res. A 622 (1) (2010) 196–199.
[18] S. Sahoo, M. Das, Radiat. Phys. Chem. 187 (2021) 109578.
[19] M. Das, R. Sarkar, P.K. Mondal, S. Saha, B.K. Chatterjee, S.C. Roy, Pramana 75 (2010) 675–682.
[20] P.K. Mondal, R. Sarkar, B.K. Chatterjee, Appl. Radiat. Isot. 90 (2014) 1–7.
[21] S. Seth, S. Sahoo, P. Bhattacharjee, M. Das, Phys. Rev. D 101 (10) (2020) 103005.
[22] N. Yu, N.S. Martynyuk, Smirnov, Sov. Phys. Acoust. 37 (1991) 376.
[23] H.Y. Kwak, S.D. Oh, C.H. Park, Int. Journ. Heat. Mass Transf. 38 (1995) 1709.
[24] L.K. Pan, C.-K.C. Wang, Nucl. Instrum. Methods Phys. Res. A 420 (1999) 345.
[25] M.C. Ghilea, D.D. Meyerhofer, T.C. Sangster, Nucl. Instrum. Methods Phys. Res. A 648 (2011) 210.
[26] L.W. Deitrich, T.J. Connolly, Nucl. Sci. Eng. 50 (1973) 273–282.
[27] Simple Collaboration, Nucl. Instrum. Method Phys. Res. A 863 (2017) 62–73.
[28] L. Rayleigh, Phil. Mag. 34 (1917) 94.
[29] M.S. Plesset, S.A. Zwick, J. Appl. Phys. 25 (1954) 493.
[30] M. Minnaert, Phil. Mag. 16 (1933) 235.
[31] A.J. Robinson, R.L. Judd, Int. J. Heat Mass Transfer 47 (2004) 5101–5113.
[32] B. Roy, B.K. Chatterjee, S.C. Roy, Radiat. Meas. 29 (1998) 173.
[33] E.W. Lemmon, M.L. Huber, M.O. McLinden, NIST standard reference database 23: Reference fluid thermodynamic and transport properties-REFPROP, version 9.0, 2010, National Institute of Standards and Technology, Standard Reference Data Program, Gaithersburg, MD.
[34] S. Seth, M. Das, Nucl. Instrum. Methods Phys. Res. A 837 (2016) 92–98.
[35] PICASSO Collaboration, Phys. Lett. B 682 (2) (2009) 185–192.

The Study of the Frequency of Bubble Oscillation in R-12 Superheated Emulsion for Neutron -Gamma Discrimination

Suraj Ali, Mala Das, and Pabitra Kumar Paul

1 Introduction

The superheated liquid maintains its liquid state at a temperature above its boiling point and it is a metastable state of the liquid. It moves to the stable (vapour) state after the formation of a critical size bubble by the energy deposition of energetic radiation or particle. The vapour bubble expands very rapidly and emits an acoustic pulse which can be detected by an active device like a microphone, piezoelectric transducer, etc. A superheated emulsion detector (SED) consists of a large number of superheated liquid drops of micron radius in a viscoelastic gel [1] or soft polymer [2]. This type of detector is useful in the detection of neutrons [3–6], gamma-rays [7, 8], and other charged particles [9, 10]. The customized SED is extensively used in the detection of the WIMP (Weakly Interacting Massive Particle), a favoured candidate of cold dark matter [11, 12]. The WIMP and neutron both initiate nucleation by the elastic collision with the nuclei of the detector material after satisfying the bubble nucleation conditions [13]. The threshold energy of such a detector depends on the operating temperature and pressure of the detector and the type of liquid used in the detector. Neutrons may initiate nucleation at high threshold energy or low operating temperature of the detector while the detector is insensitive to gamma-

S. Ali · M. Das (✉)
Saha Institute of Nuclear Physics, 1/AF Bidhannagar, Kolkata 700064, India
e-mail: mala.das@saha.ac.in

S. Ali
e-mail: suraj.ali@muralidhargirlscollege.ac.in

S. Ali · P. K. Paul
Department of Physics, Jadavpur University, 188 Raja S. C. Mallick Rd, Kolkata 700032, India
e-mail: pabitrak.pal@jadavpuruniversity.in

S. Ali
Muralidhar Girls' College, P411/14 Gariahat Road, Kolkata 700029, India

R. N. Patra (ed.), *Advanced Radiation Detector and Instrumentation in Nuclear and Particle Physics*, Springer Proceedings in Physics 282,
https://doi.org/10.1007/978-3-031-19268-5_4

rays. It becomes sensitive to gamma-rays above some specific operating temperature and it was found that the sensitivity starts at 41.9 °C [14], 45 °C [15], and 38.5 °C [16] for R-12 (CCl_2F_2; $b.p. = -29.8$ °C), R-114 ($C_2Cl_2F_4$; $b.p. = 3.7$ °C) and R-134a ($C_2H_2F_4$; $b.p. = -26.3$ °C) liquid SEDs respectively. The gamma-rays are the dominant background in the WIMPs detection experiments at the low threshold energy of the detector. It is therefore important to discriminate the gamma-ray to use this low threshold detector in the detection of neutron or WIMP in presence of gamma-ray background. Das et al. [17] have studied the neutrons and gamma-rays-induced pulses from the nucleation of R-114 SED and discriminated them using the maximum amplitude and power of the pulses. Mondal et al. [18] observed a significant difference between amplitude, power, and frequencies of the neutrons and gamma-rays-induced pulses using R-12 liquid in the audio frequency region (20 Hz to 20 kHz). Felizardo et al. [19] and Barnabe-Heider et al. [20] found the fundamental harmonic of neutron-induced events at a frequency between 0.45–0.75 kHz and 20–40 kHz using R-115 and R-610 liquid detectors. In the present work, we have tried to discriminate neutrons and gamma-rays-induced events from R-12 SED using Pvar and F.F. distributions in the high-frequency region. This high-frequency pulse is produced at the very early stage of the nucleation and carries the information about the value of Linear Energy Transfer (LET) of the nucleating particle [21].

2 Condition of Nucleation

The bubble nucleates after forming a bubble of critical radius (R_c) [22] represented by Eq. (1) and the embryo larger than or equal to R_c grows to visible vapour bubbles whereas the embryo smaller than R_c collapses back to the liquid state.

$$R_c = \frac{2\sigma(T)}{(P_v - P_l)} \tag{1}$$

To form a bubble of critical radius the energetic particle should deposit energy along the effective path length (L_{eff}) and the energy must be greater than or equal to the critical energy ($E_c(T)$). $E_c(T)$ can be expressed by Eq. (2) [23] and its variation at different temperatures is shown in Fig. 1,

$$E_c = 4\pi R_c^2 \left(\sigma - T\frac{\partial\sigma}{\partial T}\right) + \frac{4\pi}{3} R_c^3 \rho_v (h_v - h_l) - \frac{4\pi}{3} R_c^3 (P_v - P_l) \tag{2}$$

where $\sigma(T)$ is the liquid-vapour interfacial tension at temperature T, P_v and P_l are the vapour and liquid pressure, h_v and h_l are the specific enthalpies of the vapour bubble and liquid respectively and ρ_v is the vapour density. The effective path length can be written as bR_c, where b is the nucleation parameter.

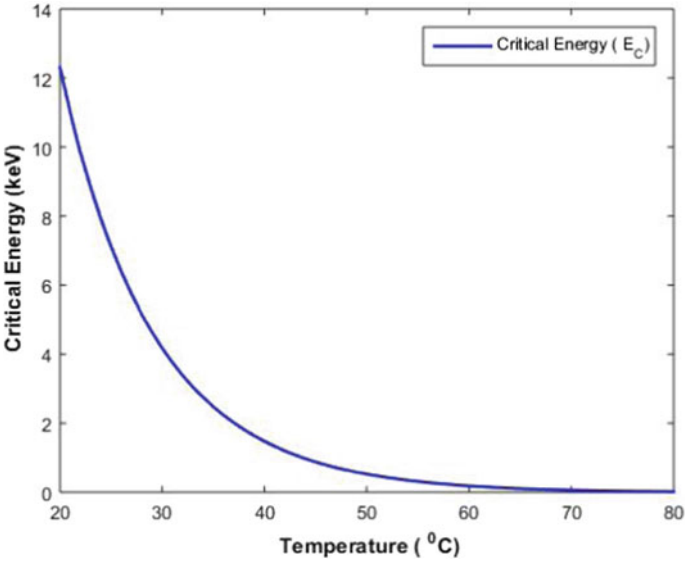

Fig. 1 The variation of critical energy for bubble formation as a function of temperature

3 Present Experiment and Analysis

The SED was fabricated using superheated R-12 liquid and aquasonic gel matrix. The experiments have been performed with the fabricated SED, one in the presence of a neutron source ($^{241}Am - Be$) of activity 10 mCi with average and maximum neutron energy of 4.2 MeV and 11 MeV respectively. Another in the presence of a gamma-ray source (^{137}Cs) of activity 5 mCi with gamma-ray energy of 0.662 MeV. The experiment with a neutron and gamma-ray source was performed at 35 °C and 55 °C respectively. The temperature of the experiment was controlled and measured using a temperature sensor and a controller (METRAVI, DTC 200) with precision ±1 °C. The nucleated acoustical pulses were collected using an AE sensor (AE - WSα by Physical Acoustics Corporation) placed on the top of the detector. The LabView hardware and software were used to store the pulses into data files. At the beginning of the analysis, the noises were rejected by visual selection [24] and only the traces decaying in nature were considered as actual bubble nucleated pulses. First, the pulses were analysed in the time domain and the Pvar variable was collected from each pulse. The Pvar variable is the summation of the square of the amplitude of the signal which is proportional to the energy deposited by the energetic particle. The fast Fourier transformation (FFT) was done for the collected pulses. In the FFT spectrum, the frequency with maximum power is defined as the fundamental frequency (F.F.). Discrimination can be quantified by the percentage of discrimination and it has been calculated by subtracting the overlapping area of F.F. distribution of neutron and gamma-rays-induced pulses, from the total area of each F.F. distribution.

4 Result and Discussions

The Pvar distributions in Fig. 2 show that the neutrons and gamma-rays-induced pulses are merged. The distribution of F.F. variable corresponding to neutrons and gamma-rays-induced signals is presented in Fig. 3. The distribution shows that the F.F. of the pulses from gamma-rays is lower than those of the neutrons and allows discrimination of 83.47% of neutrons from gamma-rays. A possible explanation is that Pvar has been calculated by summing the square of the voltages over the total time span of the signal so here both the amplitude and time information is present but the F.F. only contains the frequency or time information of the pulses. The neutron-induced pulses have low time span and high amplitude and gamma-rays-induced pulses have high time span and low amplitude as a result both the pulses have the same Pvar value. The F.F. value discriminates between the neutrons and gamma-rays-induced pulses as the recoil nucleus from neutrons deposits the whole energy within the critical radius due to its higher LET and lower ranges and hence produces the high-frequency pulses. On the other hand, the gamma-rays-induced pulses are predicted to grow at a slower rate due to the energy deposition over an extended track of the electrons and produce low-frequency pulses.

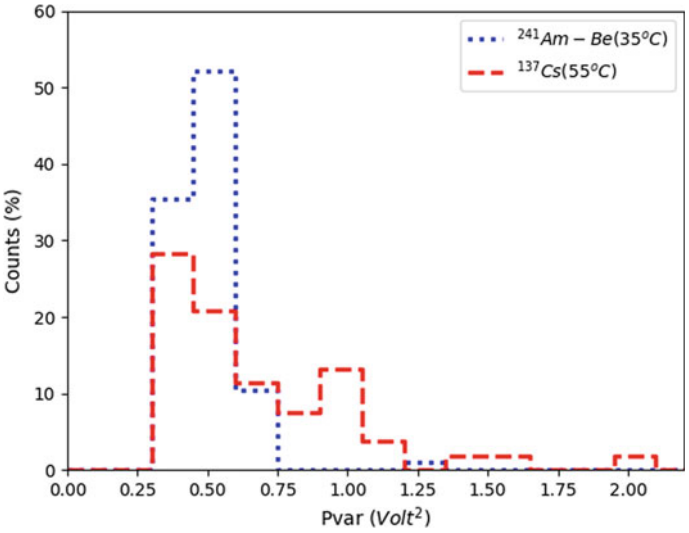

Fig. 2 The distribution of Pvar of the neutrons and gamma-rays-induced acoustical pulses

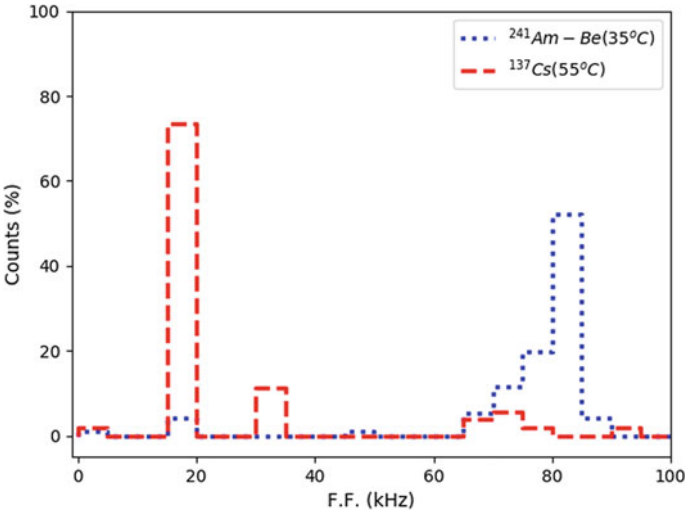

Fig. 3 The distribution of F.F. of the neutrons and gamma-rays-induced acoustical pulses

5 Conclusion

In this work, we have studied the frequency spectrum of the bubble nucleated pulses from neutrons and gamma-rays in R-12 SED. Although Pvar parameters of both types of signals are almost the same, the F.F. parameter significantly discriminates the neutrons-induced pluses from the gamma-rays-induced pulses.

Acknowledgements The authors would like to thank Mr. Nilanjan Biswas, Dr. Sunita Sahoo, SINP, and Mr. Sudipta Barman, Mechanical Workshop, SINP for the assistance during the experiment. The authors are thankful to Prof. Maitreyee Nandy, SINP and Health Physics Unit, Variable Energy Cyclotron Centre for providing $^{241}Am - Be$ source. The authors are grateful to CAPP - II project, SINP-DAE for the financial support.

References

1. R.E. Apfel, The superheated drop detector. Nucl. Instrum. Methods **162**, 603–608 (1979)
2. H. Ing, H.C. Birnboim, A bubble-damage polymer detector for neutrons. Nucl. Tracks Radiat. Meas. **8**, 285–288 (1984)
3. R.E. Apfel, B.T. Chu, J. Mengel, Superheated drop nucleation for neutron detection. Appl. Sci. Res. **38**, 117–122 (1982)
4. B. Mukherjee, D. Rybka, D. Makowski, T. Lipka, S. Simrock, Radiation measurement in the environment of FLASH using passive dosimeters. Meas. Sci. Technol. **18**, 2387 (2007)
5. P.K. Mondal, B.K. Chatterjee, Characteristics of acoustic emissions during nucleation of superheated droplets. Phys. Lett. A **375**, 237–244 (2011)
6. F. d'Errico, Radiation dosimetry and spectrometry with superheated emulsions. Nucl. Instrum. Methods Phys. Res. B **184**, 229–254 (2001)

7. F. d'Errico, R. Nath, R. Nolte, A model for photon detection and dosimetry with superheated emulsions. Med. Phys. **27**, 401–409 (200)
8. B. Roy, M. Das, S.C. Roy, B.K. Chatterjee, Threshold temperature for γ-ray detection in superheated drop detector. Radiat. Phys. Chem. **61**, 509–510 (2001)
9. S.L. Guo et al., High energy heavy ion tracks in bubble detectors. Radiat. Meas. **31**, 167–172 (1999)
10. S. Tsuda, T. Sawamura, A. Homma, M. Narita, Pressure dependence of neutron detection sensitivity in a superheated drop detector. Radiat. Prot. Dosim. **87**, 87–92 (2000)
11. E. Behnke et al., Improved limits on spin-dependent WIMP-proton interactions from a two liter CF_3I bubble chamber. Phys. Rev. Lett. **106**, 021303 (2011)
12. M. Felizardo et al., First results of the phase II SIMPLE dark matter search. Phys. Rev. Lett. **105**, 211301 (2010)
13. C. Amole et al., Dark matter search results from the PICO-60 C_3F_8 bubble chamber. Phys. Rev. Lett. **118**, 251301 (2017)
14. R. Sarkar, P.K. Mondal, B.K. Chatterjee, The gamma ray detection threshold temperature of different superheated droplet detectors. Appl. Radiat. Isot. **139**, 127–130 (2018)
15. M. Das, B. Roy, B.K. Chatterjee, S.C. Roy, Use of basic principle of nucleation in determining temperature-threshold neutron energy relationship in superheated emulsions. Radiat. Phys. Chem. **66**, 323–328 (2003)
16. S. Sahoo, S. Seth, M. Das, The threshold of gamma-ray induced bubble nucleation in superheated emulsion. Nucl. Instrum. Methods Phys. Res. A **931**, 44–51 (2019)
17. M. Das, S. Seth, S. Saha, S. Bhattacharya, P. Bhattacharjee, Neutron-gamma discrimination by pulse analysis with superheated drop detector. Nucl. Instrum. Methods Phys. Res. A **622**, 196–199 (2010)
18. P.K. Mondal, S. Seth, M. Das, P. Bhattacharjee, Study of low frequency acoustic signals from superheated droplet detector. Nucl. Instrum. Methods Phys. Res. A **729**, 182–187 (2013)
19. M. Felizardo et al., The SIMPLE phase II dark matter search. Phys. Rev. D **89**, 072013 (2014)
20. M. Barnabé-Heider et al., Response of superheated droplet detectors of the PICASSO dark matter search experiment. Nucl. Instrum. Methods Phys. Res. A **555**, 184–204 (2005)
21. S. Ali, M. Das, Discrimination of neutron and gamma ray induced nucleation events at high frequency in R134a superheated emulsion. Nucl. Instrum. Methods Phys. Res. A **1025**, 166186 (2022)
22. F. Seitz, On the theory of the bubble chamber. Phys. Fluids **1**, 1–13 (1958)
23. A.G. Tenner, Nucleation in bubble chambers. Nucl. Instrum. Methods **22**, 1–42 (1963)
24. S. Seth, M. Das, Radiation linear energy transfer and drop size dependence of the low frequency signal from tiny superheated droplets. Nucl. Instrum. Methods Phys. Res. A **837**, 92–98 (2016)